UNIVERSITY OF CALGARY

Estimation of Reservoir Heterogeneity from the Depositional Environment in Reservoir Characterization of a CHOPS Field

by

Mahbub Alam

A THESIS
SUBMITTED TO THE FACULTY OF GRADUATE STUDIES IN PARTIAL FULFILMENT OF THE REQUIREMENTS FOR THE DEGREE OF MASTER OF SCIENCE

DEPARTMENT OF GEOSCIENCE

CALGARY, ALBERTA
APRIL, 2012

THE UNIVERSITY OF CALGARY
FACULTY OF GRADUATE STUDIES

The undersigned certify that they have read, and recommended to the Faculty of Graduate Studies for acceptance the thesis entitled "Estimation of Reservoir Heterogeneity from the Depositional Environment in Reservoir Characterization of a CHOPS Field" submitted by Mahbub Alam in partial fulfillment of the requirements for the degree of Master of Science.

Supervisor: Dr. Laurence R. Lines
Department of Geoscience

Dr. Steve Hubbard
Department of Geoscience

Dr. Brij Maini
Department of Chemical and Petroleum Engineeering

Date: March 26, 2012

ABSTRACT

The major challenge in reservoir characterization is to estimate the effective porosity and the permeability of the reservoir due to reservoir heterogeneity. Often the vertical and the horizontal permeability are not considered separately in 3D geo-cellular models and in the reservoir simulations. Conventional reservoir modeling extrapolates all of the small-scale data to full-field scale data without considering the impact of the small-scale geological details, and builds inherent errors into the reservoir predictions as a consequence of ignoring the reservoir heterogeneity. Practically most reservoirs are geologically complex and heterogeneous and that greatly influences reservoir performance.

A case study is taken from a Cold Heavy Oil Production with Sands (CHOPS) field. A unique method of reservoir heterogeneity estimation has been introduced to illustrate the complex reservoir heterogeneity honouring all of the small-scale geological details in the 3D geological model. This detailed near wellbore modeling can provide the realistic quantitative volumetric assumption of the production prediction and improve the Enhanced Oil Recovery (EOR) processes.

ACKNOWLEDGEMENTS

I am very thankful to my supervisor, Dr. Laurence R Lines, whose encouragement, guidance and support from the initial to the final level enabled me to complete this thesis. I am ever grateful to Joan Embleton, the Manager of the CHORUS integrated science research consortium for her continuous feedback with the data, software, and creating the research project opportunities with the CHORUS team and her editing with the manuscripts.

Special thanks to Dr. Steve Hubbard for his time and patience, and going through the whole thesis word by word. I gratefully acknowledge his valuable advice.

I am indebted to my many friends for providing enthusiastic help to improve my model for the research. I am especially grateful to Les Dabek of Geomodeling Technology Inc., John Zhao and Laurence Jayawardane of Schlumberger, and Boyd McIntyre of Equal Energy.

I would like to thank the CHORUS grad student team members for their kind assistance with giving advice, helping with various applications and the terrific general team support. Special thanks to Xianfeng Zhang, Fereidoon Vasheghani, Carmen Dumitrescu, Hossein Agharbarati, Amir Shamsa and Latif Ibna-Hamid.

Last but not the least, I gratefully acknowledge the valuable time of Mahadia Ibrahim for her patience on reading the manuscript and critics to improve the writings.

I offer my regards and blessings to all of those who supported me in any respect during the completion of the thesis.

Thank you so much;

Mahbub Alam

DEDICATION

To my amazing wife Nasreen and wonderful daughters Raisa and Ryeen.

TABLE OF CONTENTS

LIST OF TABLES AND APPENDICES

Tables:

Appendices:

Appendix VI: Up-scaled Results from SBED showing the porosity and the directional permeability distribution for all the wells in the reservoir intervals.

Appendix VII: SBED Input: Analytical data from the core plugs of the offset wells in the table were used in the Facies Templates of SBED for the Reservoir Wells.

Appendix VIII: Near Wellbore Images of the Individual Wells.

Appendix IX: The parameters used in the calculation of the Original Oil in Place (OOIP) and Recoverable Oil for the production history matching from the Primate Pool.

LIST OF FIGURES

GLOSSARY OF TERMS

This glossary of terms describes the context and meaning to expressions used in this thesis.

3D	Three Dimensions.
4D	Four Dimensions.
AVO	Amplitude Versus Offset.
API	American Petroleum Institute for expressing units.
CDP	Common Depth Point represents the midpoint between a source and the receiver.
CHOPS	Cold Heavy Oil Production with Sands
cm-level	Centimeter Scale
EOR	Enhanced Oil Recovery
G Elev	Ground Elevation
G&G	Geology and Geophysics
K	Permeability
Kx / Kxx	Horizontal Permeability in X direction
Ky / Kyy	Horizontal Permeability in Y direction
Kz / Kzz	Vertical Permeability in Z direction
KB	Kelly Bushing
mD	**Mili Darcy**
m-level	Meter Scale
MMSTB	Million Standard Barrels
NTG	Net To Gross
Perm	Permeability
Phi /	Indicates Porosity
POM	Process Oriented Modeling
Por	Porosity
RF	Recovery Factor
OOIP	Original Oil In Place
Sw	Water Saturation
UWI	Unique Well Identifier

Vp	P-wave velocity.
Vp/Vs	Ratio of P-wave velocity to S-wave velocity.
Vs	S-wave velocity.
Vsh	Shale Volume

INTRODUCTION

1.1 Over View

Reservoir characterization of a Cold Heavy Oil Production with Sands (CHOPS) field is unique due to the distinct nature of its production mechanism. In the reservoir characterization process, reservoir heterogeneity associated with reservoir properties is the most challenging factor in reservoir simulation. The architectural complexities of the depositional bodies are commonly associated with the heterolithic facies (Ruvo et al, 2008). The heterogeneity is controlled by many factors, such as lateral and vertical extent of the beds, geometry of the sandstone bodies, mudstone and other low-permeability baffles. Reservoir fluid flow is also controlled by the vertical and lateral distribution of the facies and their inter-bedded characteristics (Weber, 1986; Knox & Barton, 1999). The dimensions of the heterogeneity may range in size from micrometers over kilometers.

The objective of this study was reservoir characterization by quantitative estimation of reservoir heterogeneity associated with depositional environment to be used for the infill drilling and enhanced oil recovery (EOR) from a CHOPS pool. The study was conducted by finding the production footprints of the current production wells and by estimating the directional permeabilities barriers in the 3D geo-cellular model as reservoir heterogeneity in the reservoir characterization processes. Reservoir heterogeneity was found to be the major issue in the evaluation and production history matching of the pool. Flow simulation and reservoir performance estimations are directly dependant on the geological model of the reservoir. Building a realistic 3D geo-cellular model in estimation of the reservoir heterogeneity was the key factor in the evaluation of the reservoir performances and in planning for the EOR strategy. In this study, a 3D geo-cellular model was built using an unique high resolution near wellbore model to estimate reservoir permeability barriers. The emphasis was put on the facies distribution, sedimentary structures of the known depositional environment and high-resolution (cm-level) up-scaling of the geological model. In this study, 4D seismic data has been used for determining the lateral extent of the reservoir and finding the production footprints of the CHOPS reservoir. The vertical facies distribution of the reservoir has been analyzed from

wireline logs and offset core data. All the integrated results along with the detailed near wellbore heterogeneity imaging allowed for proper evaluation of the reservoir performance and practically impact the EOR processes through additional drilling opportunities.

In this thesis, Chapter 1 describes the introduction and objectives of the study, the stratigraphy of the study area, related work and software uses. Chapter 2 highlights the methodology of the work including the time lapse 3D seismic, wire-line logs, offset core data and the petrophysical interpretations. Chapter 3 focuses on the 3D geo-cellular modeling and includes the conventional model and the high resolution new model along with the production history matching. Chapter 4 is the discussion including the results, data analyses and limitations of the study. Chapter 5 reveals the conclusion of the study including future outlook.

1.2 Study Area

The study area is located close to the border of Alberta and Saskatchewan, about 50 kilometers south of the Lloydminster area in Saskatchewan (Figure 1-1). A case study is taken from a pool of the Primate Heavy Oil Field of Saskatchewan that comprises 10 cold heavy oil producing wells (Table 1-1). The wells are located along the intersection of the Township 37 and Range 27 of the West 3rd Meridian known as South Mannville Pool of the Primate Field in Saskatchewan (Figure 1-2).

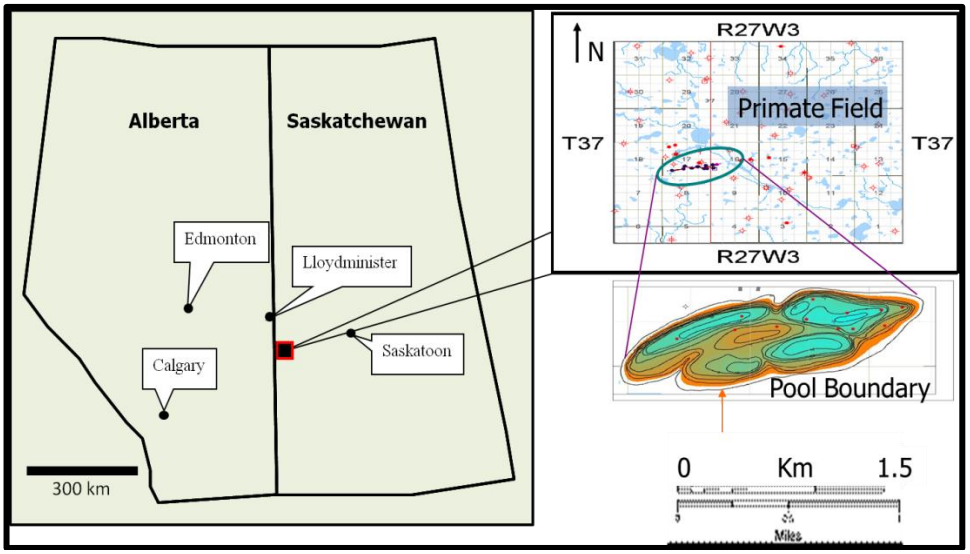

Figure 1-1: Location map of the Primate South Mannville pool in Saskatchewan.

The pool was discovered in 2005 and is currently producing from unconsolidated McLaren and Waseca sandstones units of the Upper Mannville Group of the Early Cretaceous age and is situated approximately 770 meters in average below the surface. At the Primate South Mannville Pool, in west-central Saskatchewan, the McLaren-Waseca formation is a heavy-oil bearing formation believed to be within a northwest southeast trending channel facies inferred from the seismic and log data analysis (Figure 2-6). This channel sand acts as a reservoir for oil with stratigraphic trapping caused by porosity pinch-out when surrounded by fine-grained non-marine to marginal marine deposits in the non-channel facies inferred from the model (Figures 2-6 and 3-3). The channel gross sand as observed on well logs attains a maximum thickness of about 17 meters and 8 meters minimum thickness with an average of 11 meters (Table 3-1). Net oil pay thickness is as much as 14 meters maximum, 4 meters minimum with an average of 8 meters in 10 wells. The reservoir has excellent porosity of up to 36 percent with a pool-weighted average of 32 percent. Pool boundaries are defined by a 3D seismic survey in 2004-2005 (Figure 2-4). Prolific wells with peak production rates well over 100 bpd with low water cut of about 20% (Figure 3-21). The Primate oil field is characterized from its production footprint as a foamy oil field whereby the expansion of gas is believed to be a major oil recovery driver. The pool's estimated OOIP (Original Oil in Place) is roughly 17 MMSTB estimated by the operating oil company. Current cumulative production is 1.23 MMSTB (until July 2009) yielding a 7.2 percent recovery factor (RF).

Table 1-1: List of the Wells studied for the Primate pool. The well names are shown in different format sometimes for different reasons as shown in Figure 1-2.

Well_Name	UWI	Surface X	Surface Y	Bottom X	Bottom Y	Status	G Elev	KB	Total Depth
1110617	111061703727W300	580408.90	5781118.17	580408.90	5781118.17	Oil	730.20	734.30	823.20
1110717	111071703727W300	580853.59	5781094.37	580853.59	5781094.37	Oil	731.50	735.20	829.00
1110817	111081703727W300	581127.67	5781157.53	581127.67	5781157.53	Oil	731.70	735.70	812.00
1210416	121041603727W300	581412.92	5781012.97	581377.55	5781042.30	Oil	731.10	734.90	810.10
1210516	121051603727W300	581353.52	5781190.19	581353.52	5781190.19	Oil	731.70	735.90	737.00
1310117	131011703727W300	581070.02	5781006.56	581070.02	5781006.56	Oil	731.70	735.70	798.80
1410117	141011703727W300	581170.52	5781008.00	581170.52	5781008.00	Oil	731.70	735.30	808.60
1410217	141021703727W300	580656.74	5781022.99	580656.74	5781022.99	Oil	730.10	734.00	804.00
1410317	141031703727W300	580364.08	5780987.53	580364.08	5780987.53	Oil	732.70	736.60	820.00
1410417	141041703727W300	579975.08	5780899.60	579975.08	5780899.60	Oil	735.20	739.10	825.00

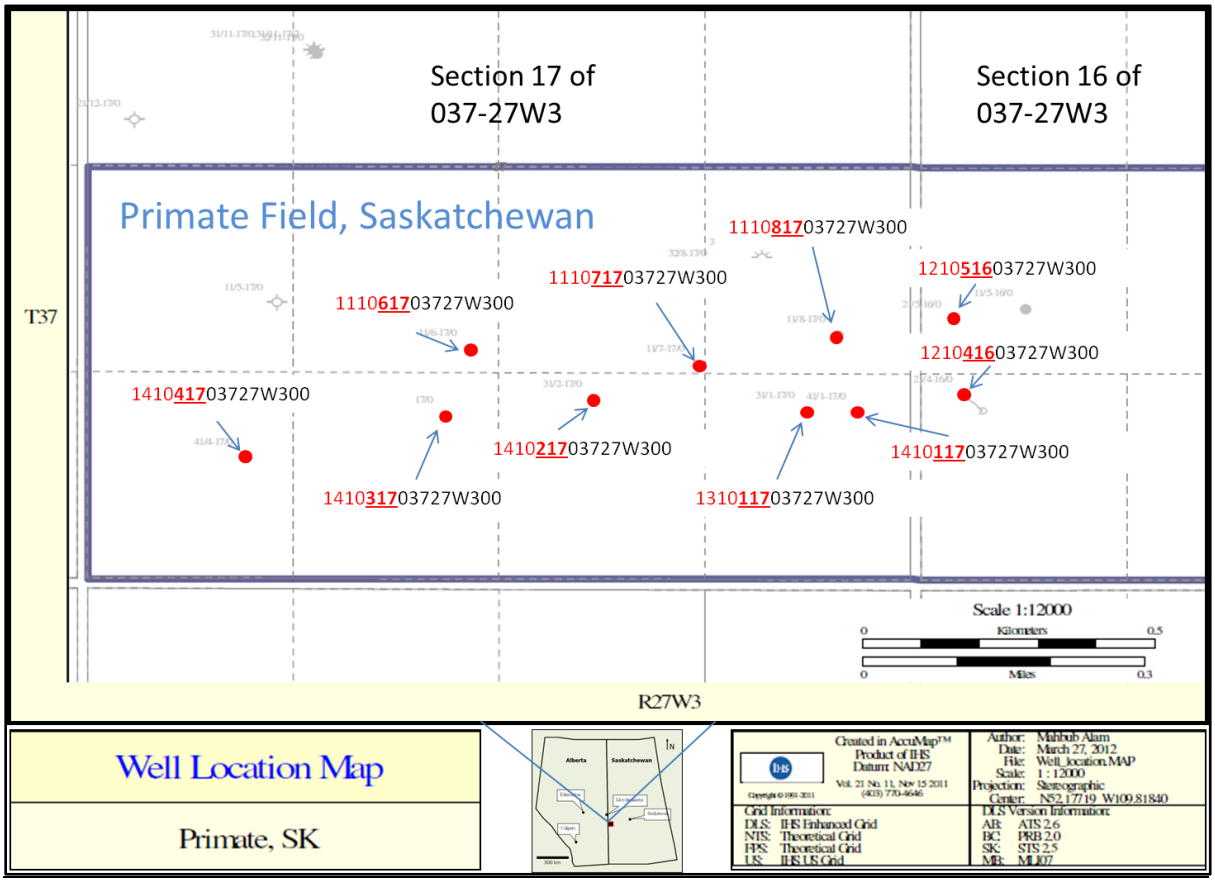

Figure 1-2: Location map of the studied wells in the Primate pool in Saskatchewan.

1.3 CHOPS Mechanism

The simultaneous extraction of the oil and sand during the cold production processes of heavy oil generates some high permeability channels termed "wormholes" (Lines et al., 2008). The development of wormholes causes the reservoir pressure drop to the bubble point, causing in a dissolved-gas within the live heavy oil to come out of solution to form the foamy oil. The foamy oil could fill the depressurized drainage regions as the production footprints around the borehole, which leads to the fluid phase changes with gas bubbles in these regions. The viscosity and specific gravity of heavy oil restrict the gas bubbles from separating into a single phase resulting in what is known as foamy oil. This process increases the fluid volume within the reservoir, forcing the grains to separate, and providing pressure to sustain the high production rates (Chen et al., 2004).

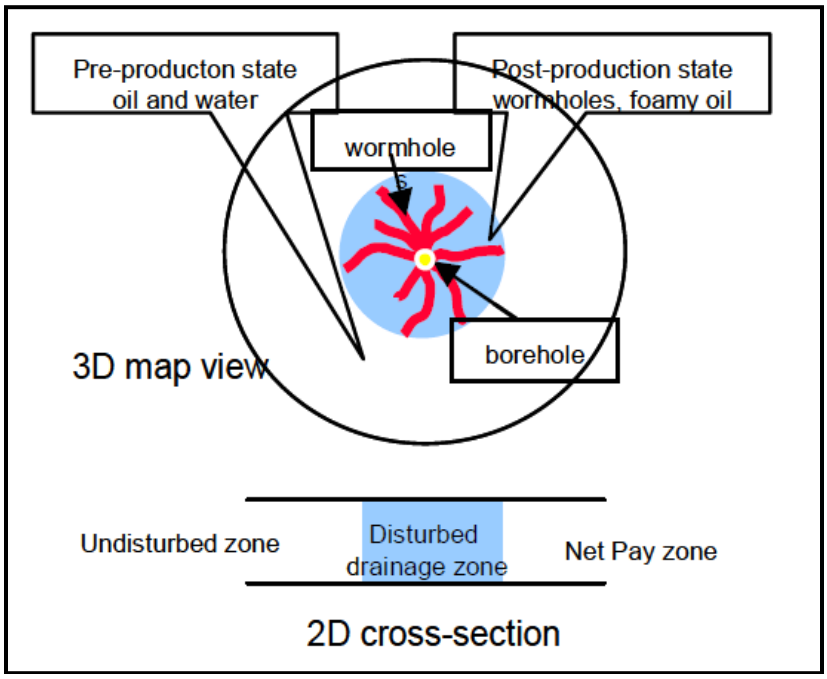

Figure 1-3: Simplified CHOPS drainage model and wormholes (Chen et al., 2004).

Wormholes are believed to grow in unconsolidated, clean sand layers within the net pay zone, along the highest pressure gradient between the borehole and the tip of the wormhole (Figure 1-3). Usually, they can grow to a distance of up to 150 m or more away from the original wells, and form horizontal high permeability channels with the connecting wells in the reservoirs (Sawatzky et al, 2002). The new EOR drilling location should avoid this area of influence or production footprints of a CHOPS field.

1.4 Geology and Stratigraphic Settings

The geology of the study area is subject to detail investigation. The geology of the Upper Mannville and the Lower Mannville differs by different authors in different literatures. The study area is part of the Upper Mannville sequence, which is Albian in age and was deposited in a prograding deltaic environment in the foreland basin, from the sediment source in the Cordillera to the west (Keith et al, 1988). The Mannville Group is a siliciclastic assemblage of sands and shales with minor coals and carbonates, which was deposited in the broad Western Canada Basin and occurred during the Clearwater transgressive-regressive cycle of the Cretaceous Boreal Sea

(Caldwell, 1984). A schematic paleogeopgraphy of the Mannville at the Aptian-Albian boundary is shown (Figure 1-4) to illustrate the basin outline and the paleo-topography of the high areas with inferred fluvial drainage systems (Benns et. al., 1988). The main Upper Mannville reservoirs are located in the incised valley fills and are yet to be distinguished from others through detailed exploration strategies. Deschamps et al., 2008 studied the Regional and local facies distribution and sequence boundary of the Upper Mannville based on the analysis of log stacking pattern, core descriptions, and on the regional facies transition pattern; and their schematic cross-section of the incised valley fills are illustrated in Figure 1-5.

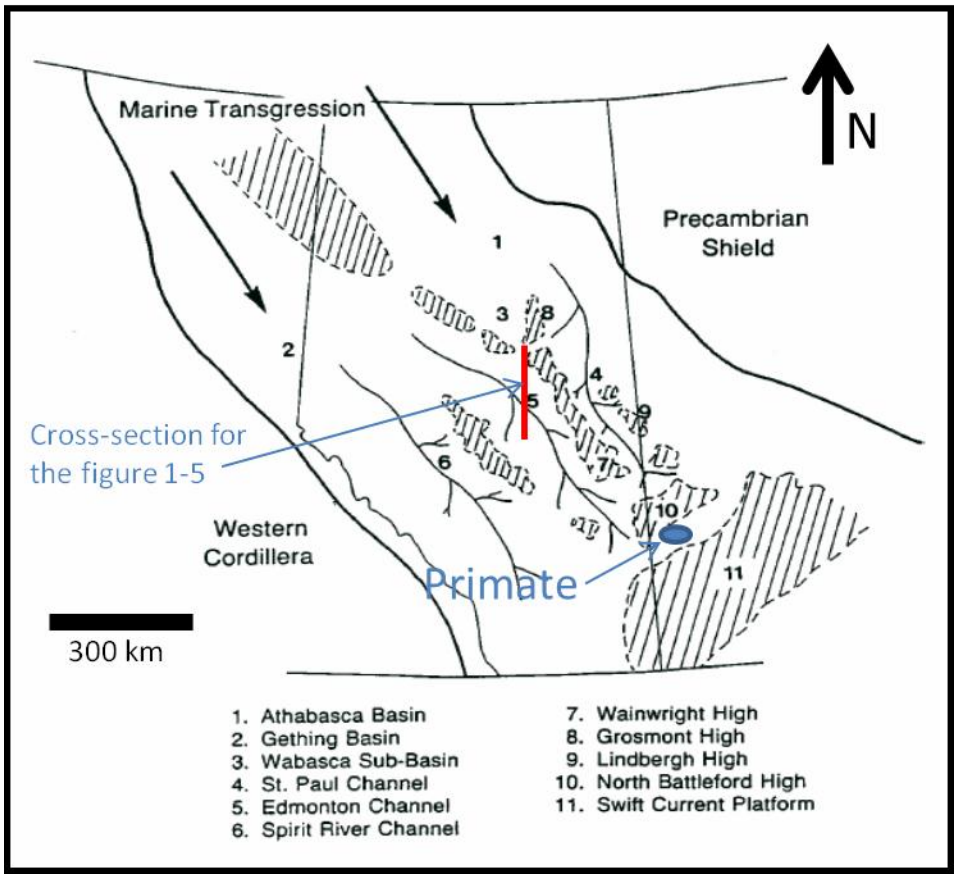

Figure 1-4: Schematic Mannville paleogeography at the Aptian-Albian boundary showing the basin outline and the topographically high areas with inferred fluvial drainage (Benns et. al., 1988).

The Upper Mannville sediments (McLaren and Waseca) have been locally re-worked by the fluvial or tidal channels. The overall settings of the Mannville were interpreted to be transgressional from the northwest with counter-progradational from the southeast in the Lower Mannville and from the southwest and northeast in the Upper Mannville, where each Mannville

member began with a transgressive facies and ended with a regressive facies (Christopher, 2002). The bedding cycle typically includes coal-capped, upward-coarsening units that are graded from the basal shale through sandy mudstone to sandstone and upward-fining units that are graded from the basal sandstone to mudstone and shale for the Mannville Group.

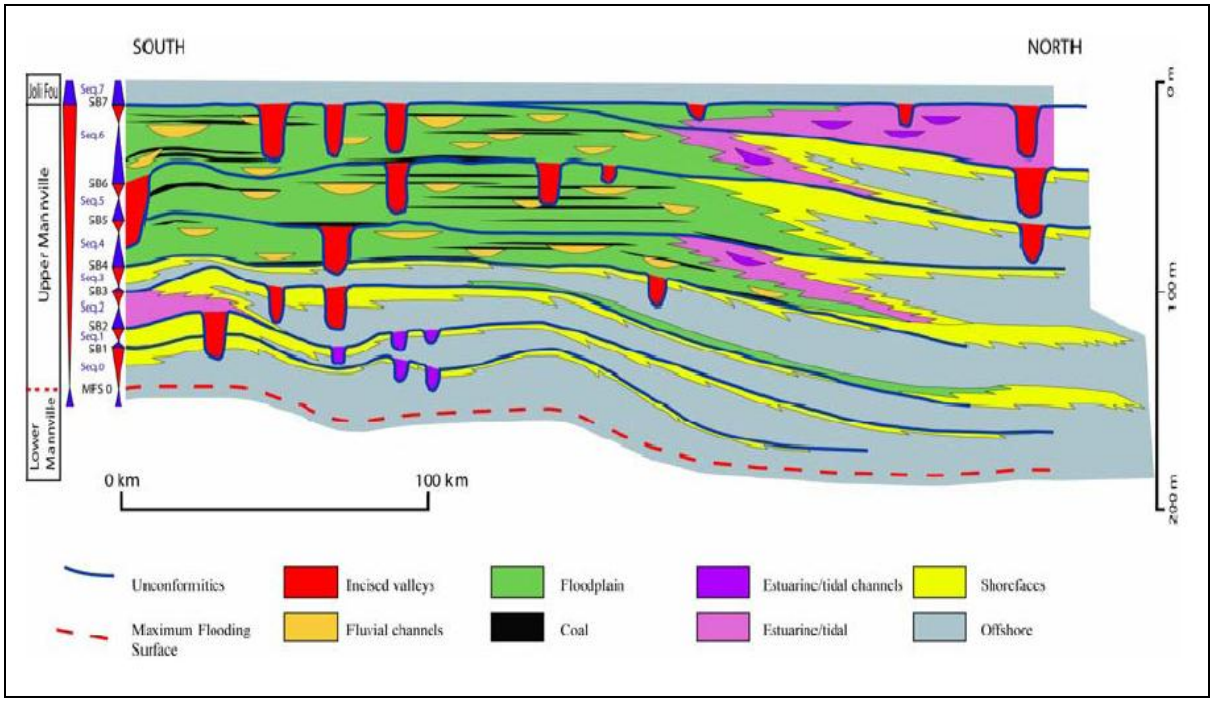

Figure 1-5: North-South Stratigraphic scheme and facies of the Upper Mannville (Deschamps et al., 2008), the location is shown in the figure 1-4.

The Mannville terminology (Figure 1-6) in the Lloydminster region was first developed by Nauss (1945) and subsequently adapted by Wickenden (1948), Ambler (1951), Kent (1959), Fuglem (1970), Vigrass (1977), and Putnam (1980) (McNeil et. al., 2004). Christopher (2002) utilized terminology from Lloydmister and integrated it with that of southern Saskatchewan (Prince, 1963; Maycock, 1967; Christopher, 1974) (OFR 1988-1). The Pense Formation of southern Saskatchewan includes the McLaren and Colony members (Figure 1-7) and integrated with the underlying Mannville units from Dina to the Waseca of the Cantuar Formation. , from the oldest to the youngest: Dina, Cummings, Lloydminster, Rex, General Petroleums (GP), Sparky, Waseca, McLaren and Colony. Lloydminster stratigraphy with local subdivision is applied to the Fort Kent Thermal Project area (Figure 1-8) and the relationship between Fort Kent stratigraphy and that of Lloydminster Stratigraphy has not been formally established

(Mathison, J. E., 1988). Major stratigraphic divisions at Fort Kent (equivalent to formations in the Lloydminster area) are referred to as formations and are similar to that described by Chistopher (2002) used for the south Saskatchewan (Figure 1-6). Local subdivisions of these Upper Waseca and Lower McLaren units are referred to as subunits (Figure 1-9). Reservoir sands at this current study occur in the Lower Waseca, Upper Waseca and Lower McLaren subunits.

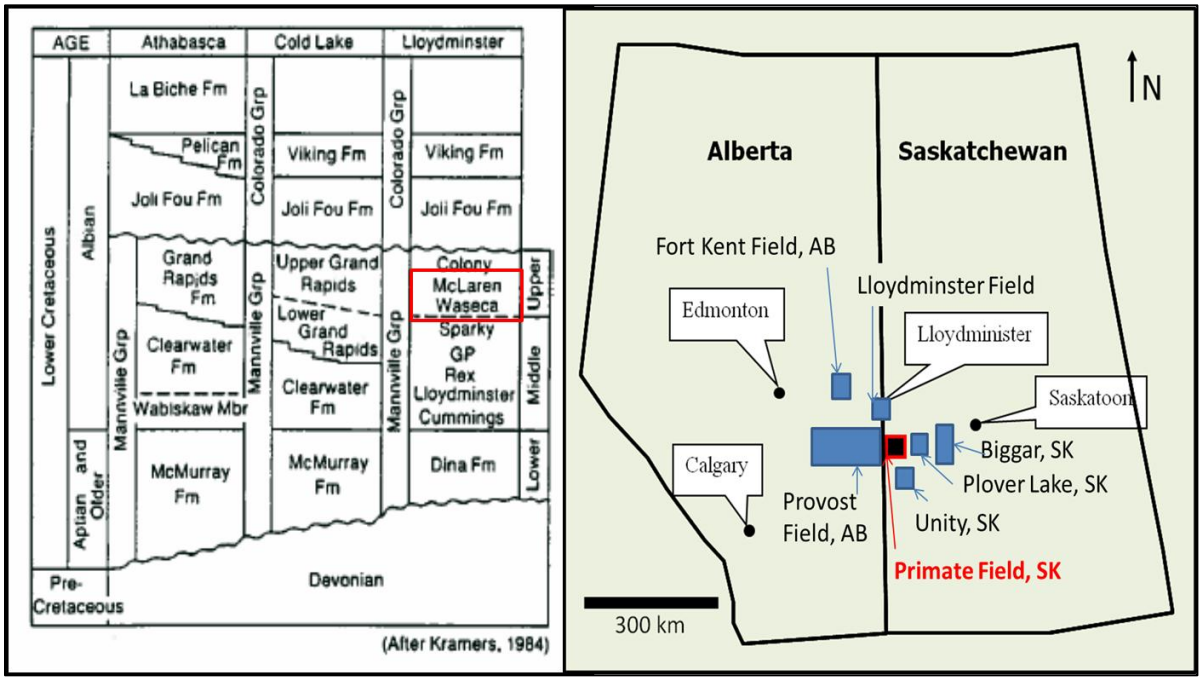

Figure 1-6: Stratigraphic Succession of Lower Cretaceous Mannville over east-central and northern Alberta (after Kramers, 1984). A schematic location map is at the right.

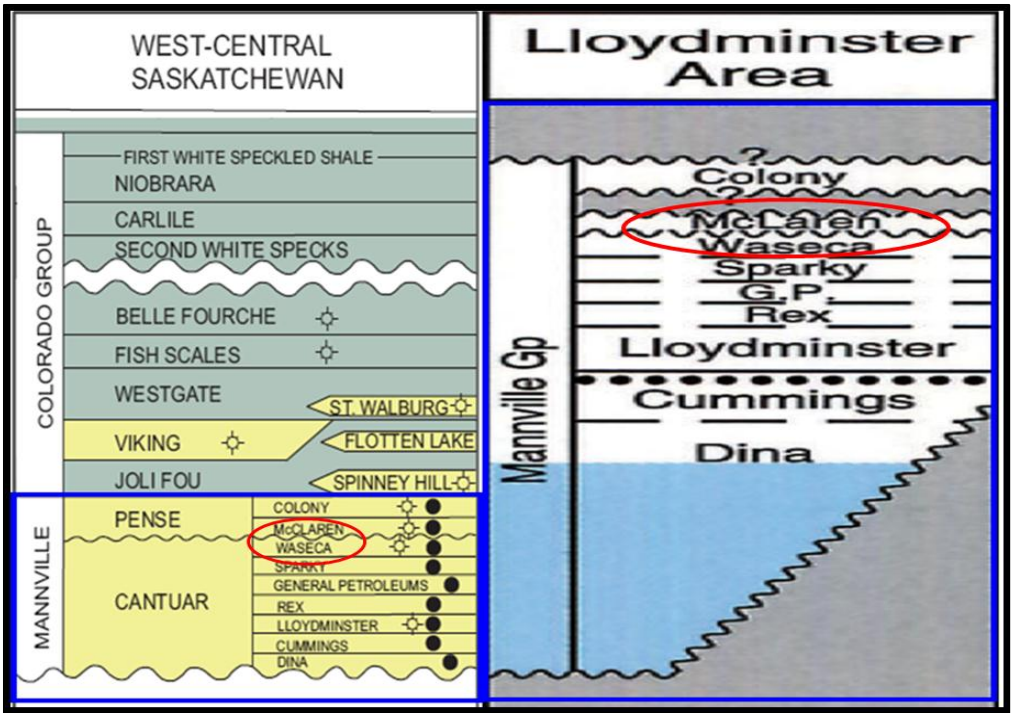

Figure 1-7: Comparison of Mannville Stratigraphy between Lloydminster area and West-Central Saskatchewan (Source: Alberta Geological Survey- Open File Report. OFR 1988-1, revised Jan 11, 2011).

The stratigraphy of this pool is scarcely investigated in the literature and not as much if any at all has been done to relate these oil producing zones to the overall development of the well-studied Mannville Group. The nearest relatively better studied areas (Figure 1-8) are the Lloydminster Heavy Oil Field or the Kent Field to the North, the Provost Field to the West, the Unity Field to the south, and the Plover Lake and the Biggar Field to the east. The northern and western parts are in Alberta and the eastern and southern parts are in Saskatchewan. The geological succession and the stratigraphic nomenclature for this study follow the stratigraphic nomenclature system of Kramer (1984), as Christopher (2002) utilized the latter in combination with the Lloydminster's area and the west-central Saskatchewan's succession (Figure 1-6 and Figure 1-7).

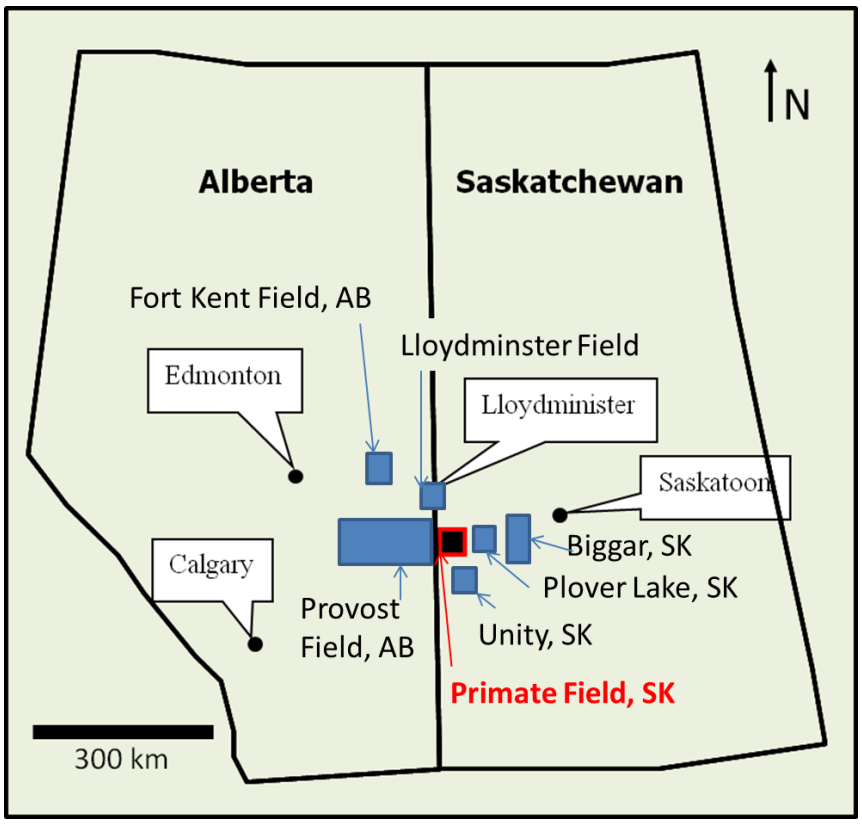

Figure 1-8: Schematic location map of the neighboring comparatively better studied areas / Fields.

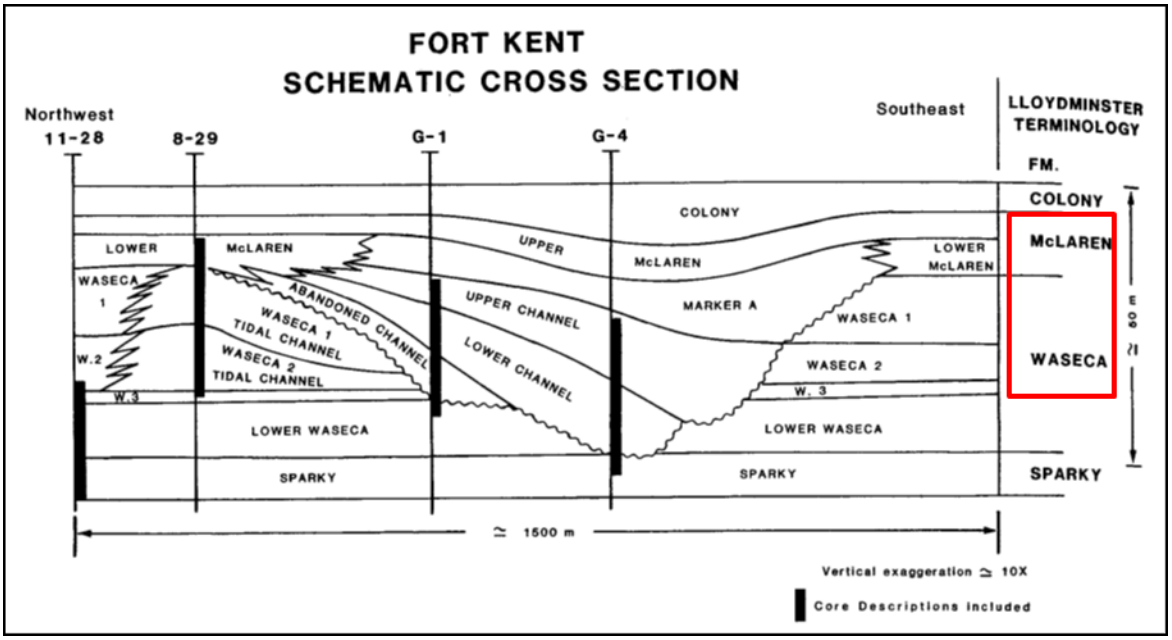

Figure 1-9: Schematic cross-section of the Fort Kent project analog to the Primate Field (from Mathison, J. E., 1988).

1.5 RELEVANT STUDIES

Reservoir modeling is an integrated approach to geophysical, geological and reservoir engineering data. Each of these divisions has a more detailed working system and unique approach in their respective areas. Reservoir property evaluations from seismic data, especially on porosity and permeability in contrast to seismic wave velocities (Vp, Vs), amplitude anomaly and acoustic impedance analysis and interpretation, were demonstrated by many authors. Lines et al., (2002, 2005, 2008) showed the robustness of Vp/Vs ratio mapping and concluded that the measured Vp and Vs decreased dramatically with increasing porosity. Generally the effects of reservoir porosity on Vs are larger than that on Vp. The formation of foamy oil results in the higher gas saturation in the reservoir, and this could also affect seismic velocity (Toksoz et al., 1976; Watson et al., 2002; Nur et al., 1984). Lines and Daley (2006) concluded that individual wormhole mapping is not possible by normal seismic frequencies; rather their influences near a producing well could be estimated for cold production. Time lapse 3D seismic data also reveals the production footprints or wormhole influenced area. Cross-well seismic data can provide better information about the reservoir attributes in terms of resolution and Lines et al. (2005) showed a classic comparison of the multi-scale resolution limits in Figure 1-10.

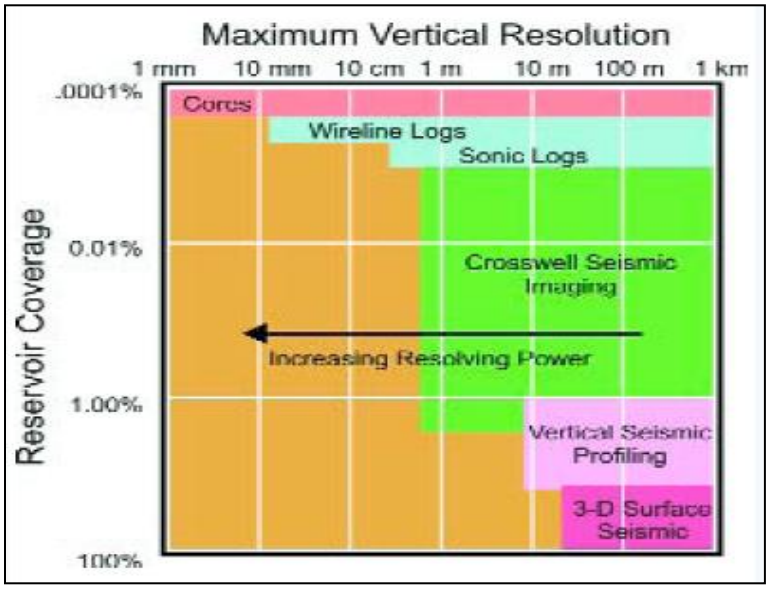

Figure 1-10: Harris's (2002) diagram shows the reservoir resolution and coverage (from Lines et al., 2005).

The depositional environment is the key in finding the major reservoir components, such as porosity and permeability distribution in the geological facies. Many experiments have been done on sedimentation using heterogeneous mixtures of particles carried by flowing water and have shown that the strata and sedimentary layers produced are generally distinct from one another (Visher, 1965). Hydraulic conditions necessary for sediment transport during transgression or regression were also analysed in the laboratory and published in many previous studies (Middleton 1984, Reinek & Singh 1980, Miall 1977, 1978, 1985). The relationships are expressed on various current velocities versus grain sizes diagrams indicating that large-scale unidirectional current structures (dune-scale cross-bedding) do not form at grains sizes below very fine sand-size, below about 100 microns. On the other hand, ripple-sized structures do not form at grain sizes above very coarse sand-size, about 0.8mm or so. These relationships are based on flume experiments carried out many years ago and were discussed thoroughly by Reineck and Singh (1980), Middleton (1984) and other sedimentary text books. These types of detailed work were never incorporated in the reservoir simulation stage due to computational complexities, and software and hardware limitations. Now, with the technological advancement and higher capabilities of computer software, these types of detailed high resolution works in the reservoir flow simulations and 3D geo-cellular modeling can finally be achieved.

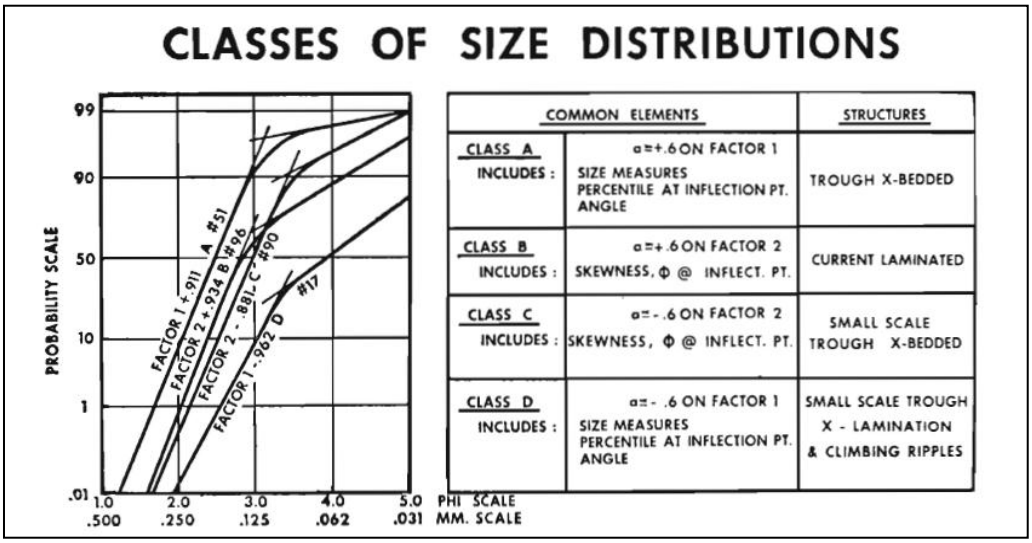

Figure 1-11: Four classes of size distributions are illustrated along with the limits for factor loadings for each class together with the sedimentary structure, and the principal elements that are included in that factor (Visher, 1965).

Detailed outcrop studies by Visher (1965) on fluvial deposits revealed a systematic vertical variation in grain size, sedimentary structures, bedding characteristics, and morphology of sedimentary units. The frequency of an ideal sequence (Figure 1-11) was developed and suggested a common process in the deposition of many fluvial sands. The sequence had been found in both recent and ancient fluvial deposits. Flume and river studies have demonstrated that the specific sedimentary structures are directly related to the sediment transport and the dynamics of open-channel flow (Figure 1-12). The grain size distribution of the fluvial sands of the study area suggested an upward decrease in energy observed the fining upward sequence. Both the grain size mean and maximum size decrease upwards and the sediments are progressively more poorly sorted upwards (Figure 1-13). These changes are directly related to variation in the type of the sedimentary structures.

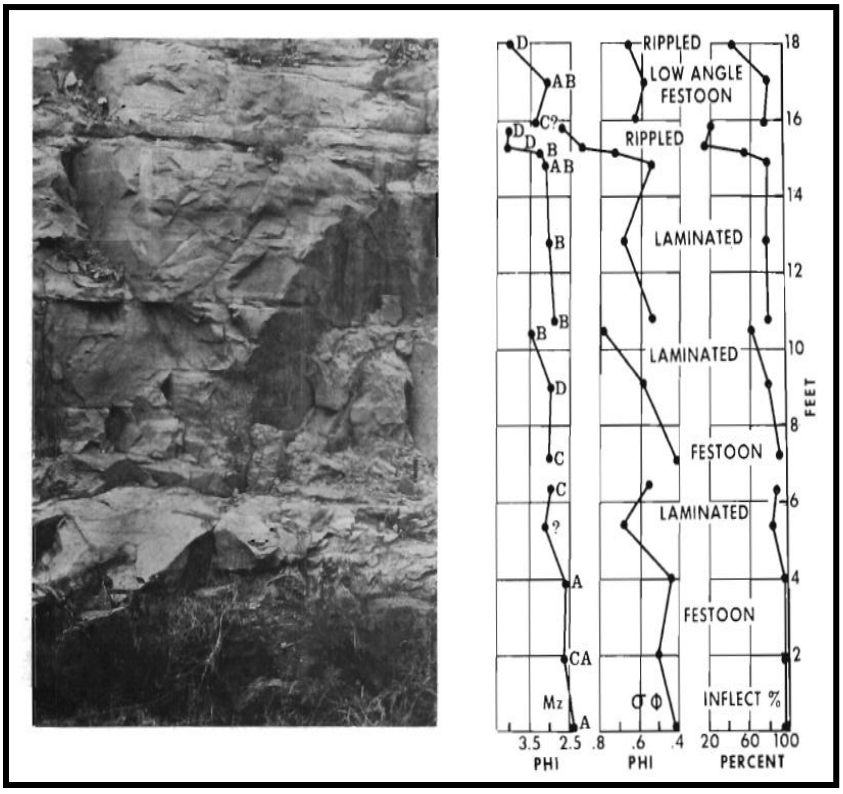

Figure 1-12: Relation of textural changes to outcrop features showing the vertical size data include mean size (Mz), sorting (σ_1 ϕ), and percent deposited by traction (inflect. %) (Visher, 1965).

Allen (1970) worked on the secondary flow and transverse changes of water depth in curved stream channels and developed a quantitative, partly empirical model to describe the way the lithology varies vertically in deposits accumulated through processes of lateral deposition. He also found that the grain size decreases upward in a lateral deposit and the sedimentary structures change from those denoting large stream powers upward which is an indication of low energy. The model also showed that the proportion of flat-bedded sand-grade material in a lateral accretion deposit was essentially independent of the stream power, and controlled by the channel curvature and sinuosity. The predictions of the model compared satisfactorily with the characteristics of selected coarse members in fining-upwards cycles of fluvial origin.

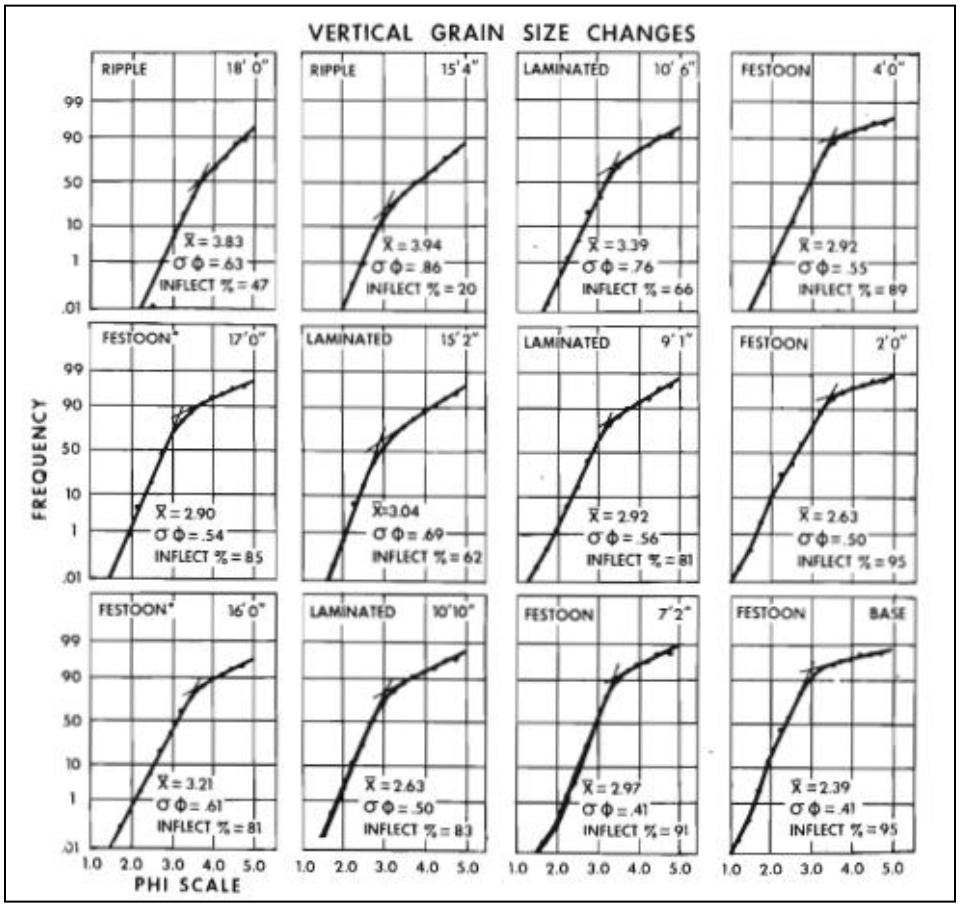

Figure 1-13: Size distribution curves for the previous section and each column represents a different depositional unit where sedimentary structure and height above base is listed at the top of each graph (Visher, 1965).

The major reservoir attributes, such as porosity and permeability are directly controlled by the geological facies distribution in the reservoir. Traditionally the works on finding facies distribution and the reservoir attributes are mainly derived from geostatistical analysis. Two original bases of geostatistics are the variogram model and the Kriging methodology, which were both initiated by the work of Daniel Krige (1951) and built up by Georges Matheron (1973). Stochastic simulation was introduced by Matheron (1973) and Journel (1974) to correct for the smoothing effects and other artifacts of Kriging and allowed the reproduction of spatial variance predicted by the variogram model. Different algorithms were developed including Sequential Simulation (Journel, 1986; Goovaerts, 1997; Chiles and Delfiner, 1999) and became the workhorse for many current geostatistical applications. Stochastic simulation provides the capability to generate multiple equiprobable realizations to the idea of assessing spatial uncertainty (Journel 2002). Training images and multiple point statistics methods remained largely untried until developments in computational capacity and multiple point scanning techniques took place (Strebelle, 2002). The purpose of every reservoir model is to provide reliable predictions of reservoir performance. The model with a more accurate description of the driving mechanisms will provide a more realistic estimation.

The SBED™ (Sedimentary Bed) modeling approach focused on generating a 3D sub-seismic-scale (cell dimension = millimeter to meter) petrophysical models to improve the accuracy and reduce the uncertainty in flow simulation studies. It enabled modelling of small-scale bedding structures that can impact fluid distribution significantly. The software's built-in upscaling functions integrate all small-scaled effects into large-scale reservoir models (Figure 1-14) and decrease the uncertainty in the reservoir predictions (Pickup, 2000).

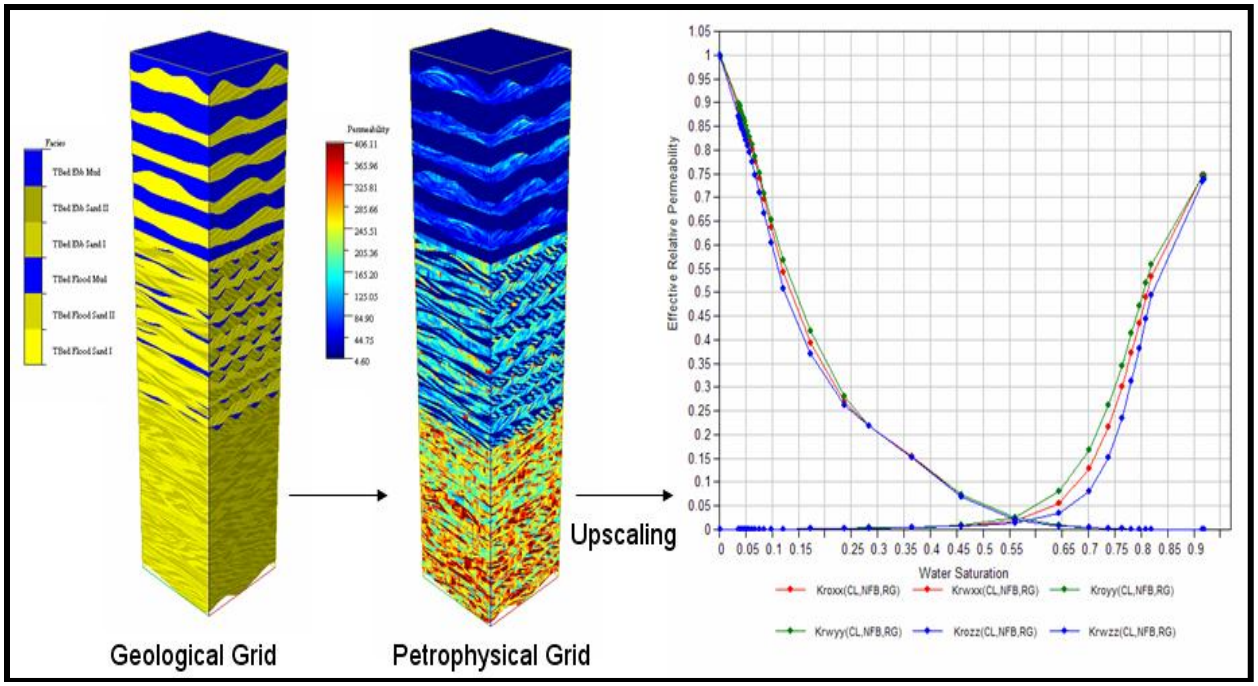

Figure 1-14: SBED model is showing the upscaling from wellbore to reservoir levels and the data integrity (SBED Manual, 2010).

Worthington (2008) evaluated a shaly reservoir using shale volume fraction (Vsh) in the determination of effective porosity from well logs and also applied the estimation of Vsh away from cored intervals. The results from density, density-neutron and sonic logs were found demonstrably improved and consistent across different tool types with substantial reductions in uncertainty.

Bauer et. al., 2009 showed a reservoir horizon slice map where sedimentary facies in response to the API units of Gamma-ray has been shown for lateral facies distribution (Figure 1-15). Numerous publications are available on reservoir characterization and reservoir heterogeneity along with geological modeling, but no published literature has been found on quantitative volumetric estimation of sub-seismic reservoir heterogeneity based on the sedimentary facies and directional permeability (Kx, Ky, Kz) for the fluvial environment. An integrated approach of reservoir modeling was done for a deep water turbidite reservoir by Ruvo et. al. (2008).

The most recent work on "Rock physics and seismic methods for characterizing the heterogeneity of oil sands reservoirs in the Western Canadian Sedimentary Basin" was conducted by Yong Xu (2012), where litho-facies (Figure 1-16) were categorized by gamma ray log and correlated with seismic attributes. The reservoir properties were estimated based on the conventional geostatistical distribution. Yong Xu's (2012) high resolution seismic contribution and the current study's high resolution near borehole facies model with cm-level features could make a complete realistic geological model on reservoir heterogeneity estimation in reservoir characterization of a heavy oil field.

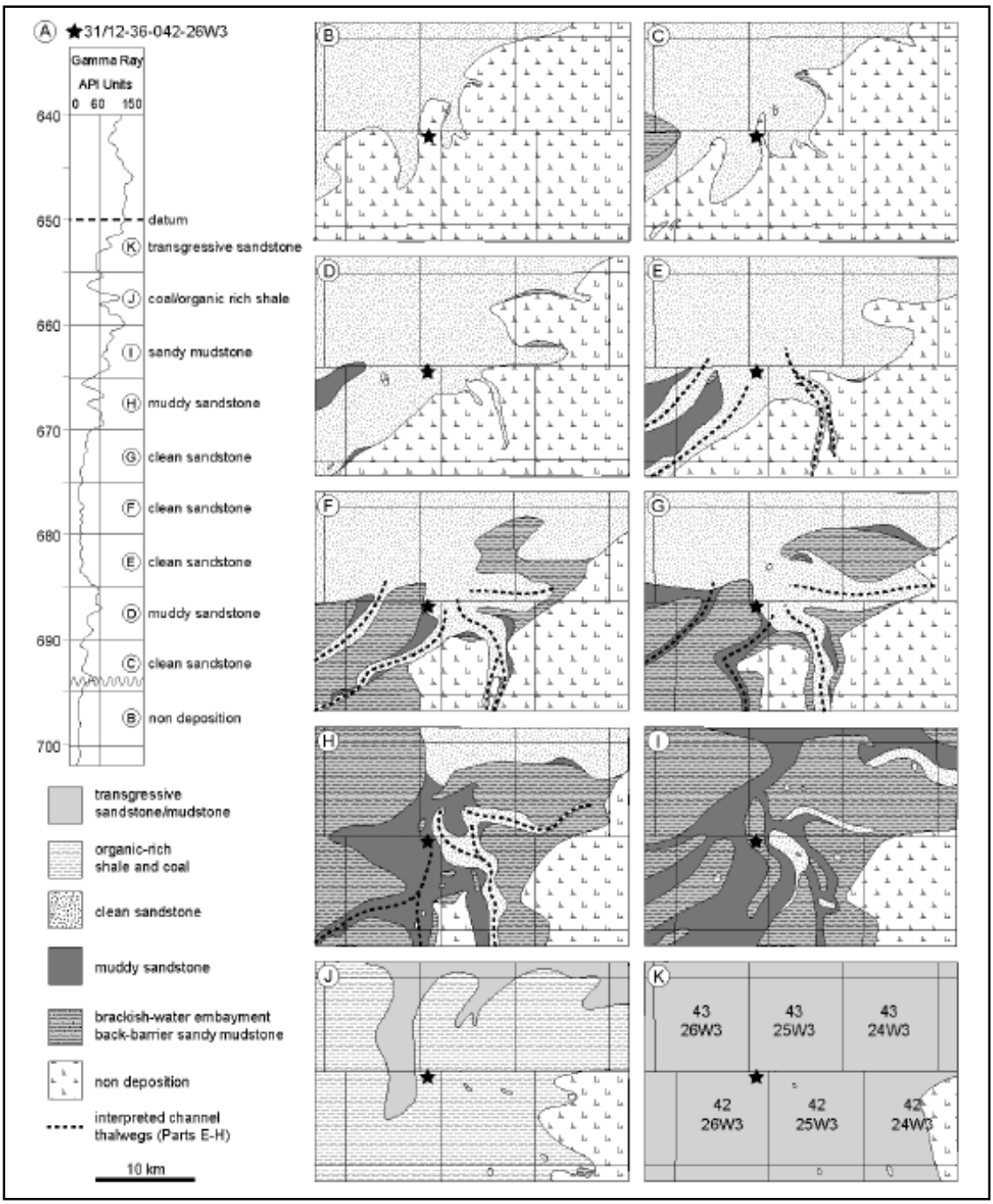

Figure 1-15: Reservoir horizon slice map is showing the relationship of Gamma-ray log and the sedimentary facies (Bauer et. al., 2009).

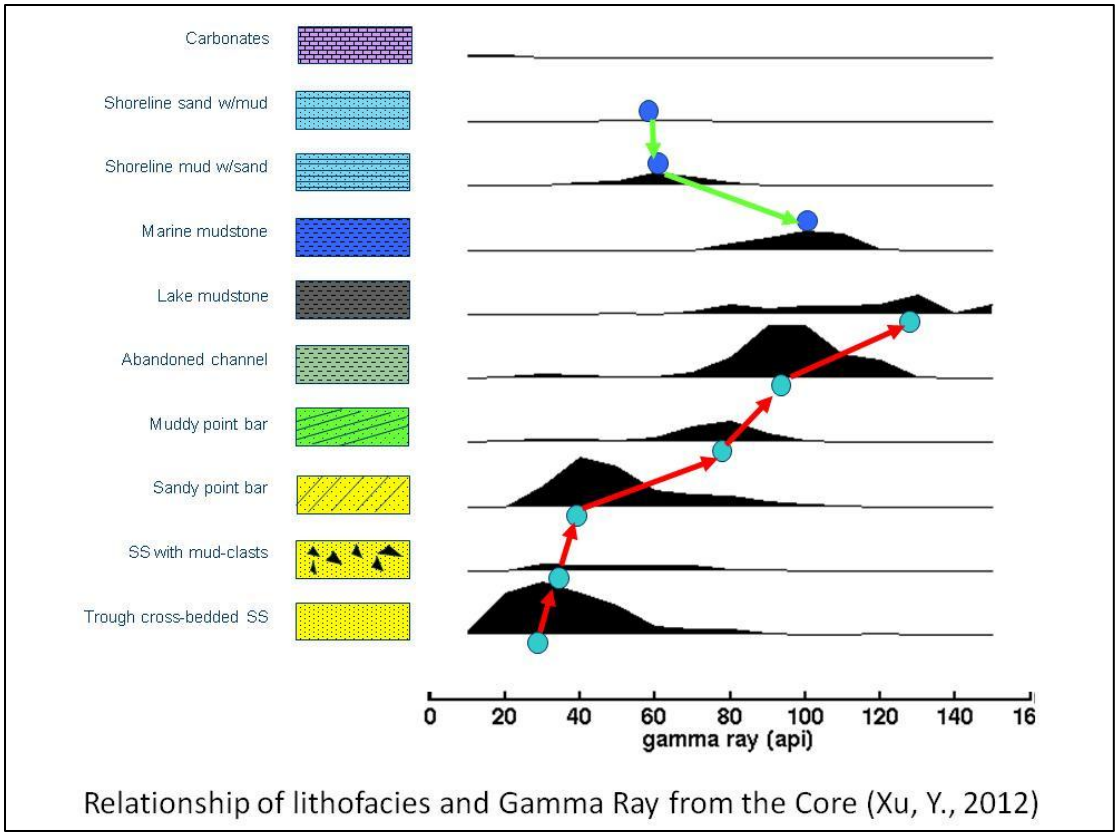

Figure 1-16: Relationship of sedimentary facies and the gamma ray is shown by Yong Xu (2012).

1.6 DATA AND THE SOFTWARE USED

The data used in this research study were provided via the Consortium for Heavy Oil Research by University Scientists (CHORUS) from Enterra Energy Inc. (currently named as Equal Energy Inc.) for the reservoir characterization study of the South Mannville Pool, Primate Field, Saskatchewan. Equal Energy provided 4D seismic data that comprised a 3D base seismic survey acquired in 2004 and the monitor seismic survey data acquired in 2009. Well data includes wire-line logging data from 10 producing wells from the Primate Field. Wireline log data includes Gamma Ray, Spontaneous Potential, Resistivity, Neutron and Density curves. There was no core data from this field. Offset Core data from the neighbouring field 'Provost' (Figure 1-17) of the same depositional environment was also provided by Equal Energy and the study was conducted at the ERCB Core Research Center, Calgary. Twenty core plugs were taken

for the laboratory petrophysical analysis from the three offset cores. The maximum 13 core plugs were taken from one offset well 00/14-29-037-01W4.

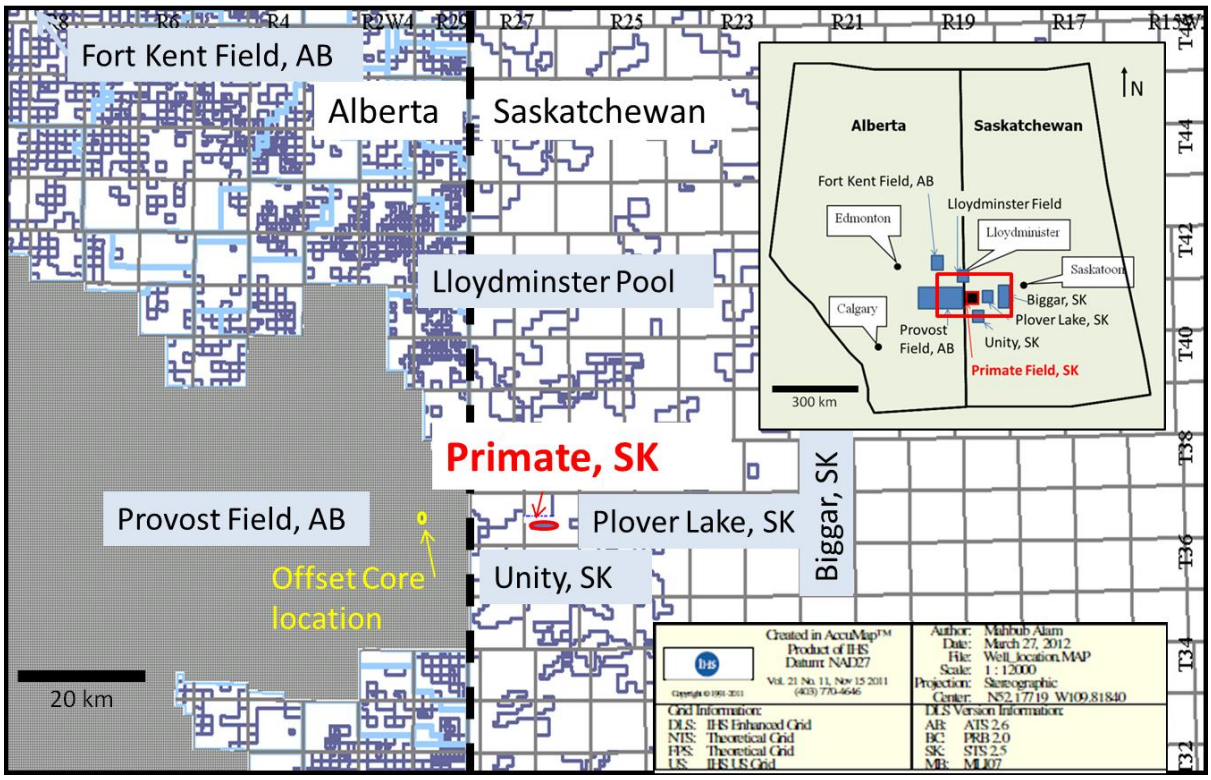

Figure 1-17: Showing the offset core location compare to the Primate pool.

Seismic data were analysed using Kingdom Suite, Hampson-Russell Suite, Reservoir Attributes and Petrel. Log data were analysed by using Power Log Suite and Petrel. The geological facies interpretation was input and up-scaled by SBED software. The ultimate 3D geo-cellular modeling for the Reservoir Characterization was completed within Schlumberger's Petrel software. Reservoir volumetric calculation and history matching was conducted using Excel software, including in-built modules. GeoScout software was used to correlate wells contouring maps and to access the well and production database. A flow diagram is given in the Figure 1-18.

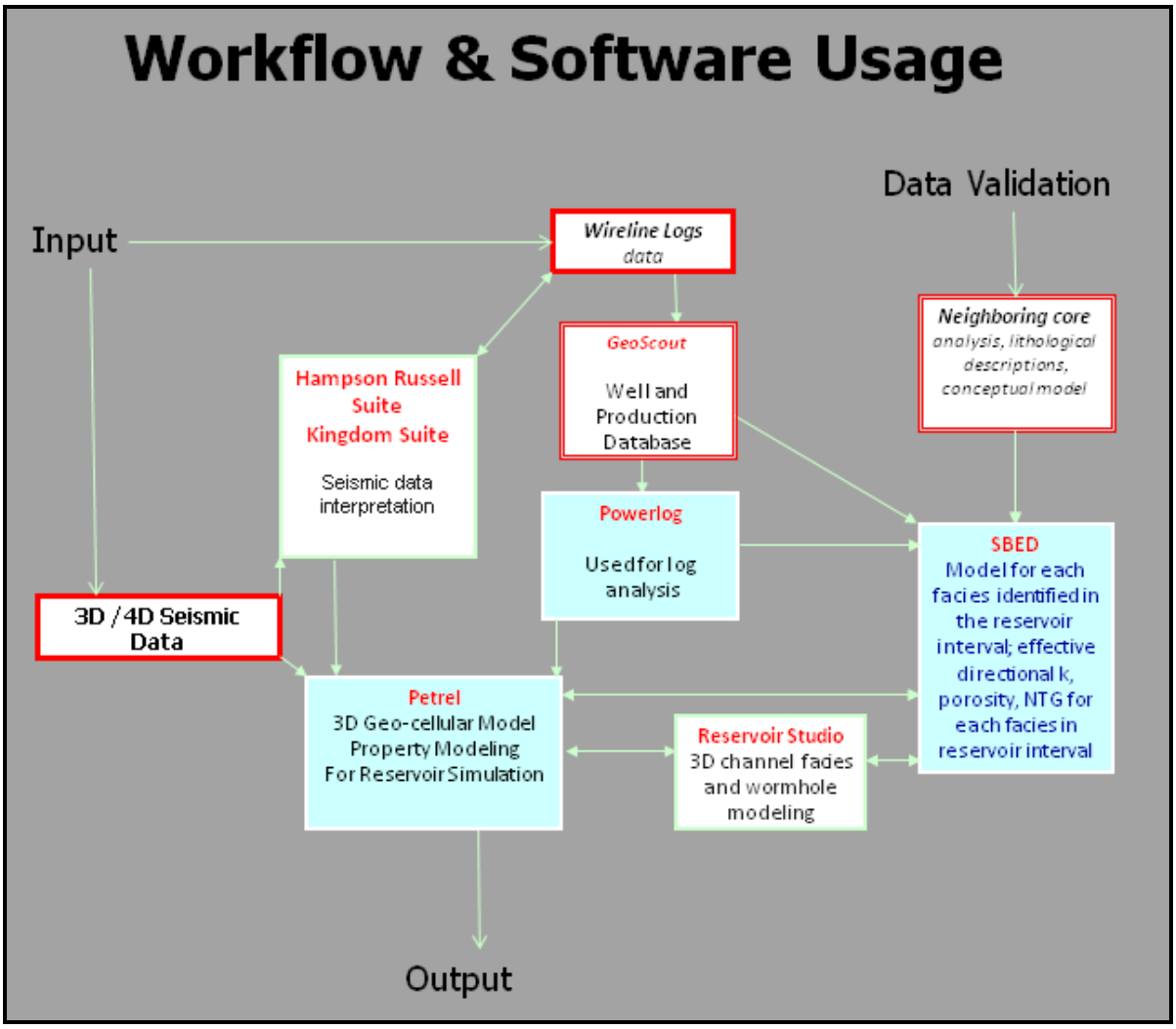

Figure 1-18: Showing the workflow and the software used in the study.

METHODS OF STUDY

The thesis followed an integrated approach (Figure 2-1), including time lapse 3D seismic interpretation, wireline log interpretation, offset core analysis and petrophysical interpretation for geological facies estimation and reservoir property evaluation using 3D geo-cellular model. All aspects are examined, correlated and shown in a 3D geo-cellular model for the visualization and determination of the infill or prospective additional drilling location(s) for the enhanced oil recovery. Reservoir heterogeneity is estimated quantitatively to evaluate the reservoir performances and production history matching in a realistic cutting edge manner maintaining the vertically high resolution of cm-level sedimentary features.

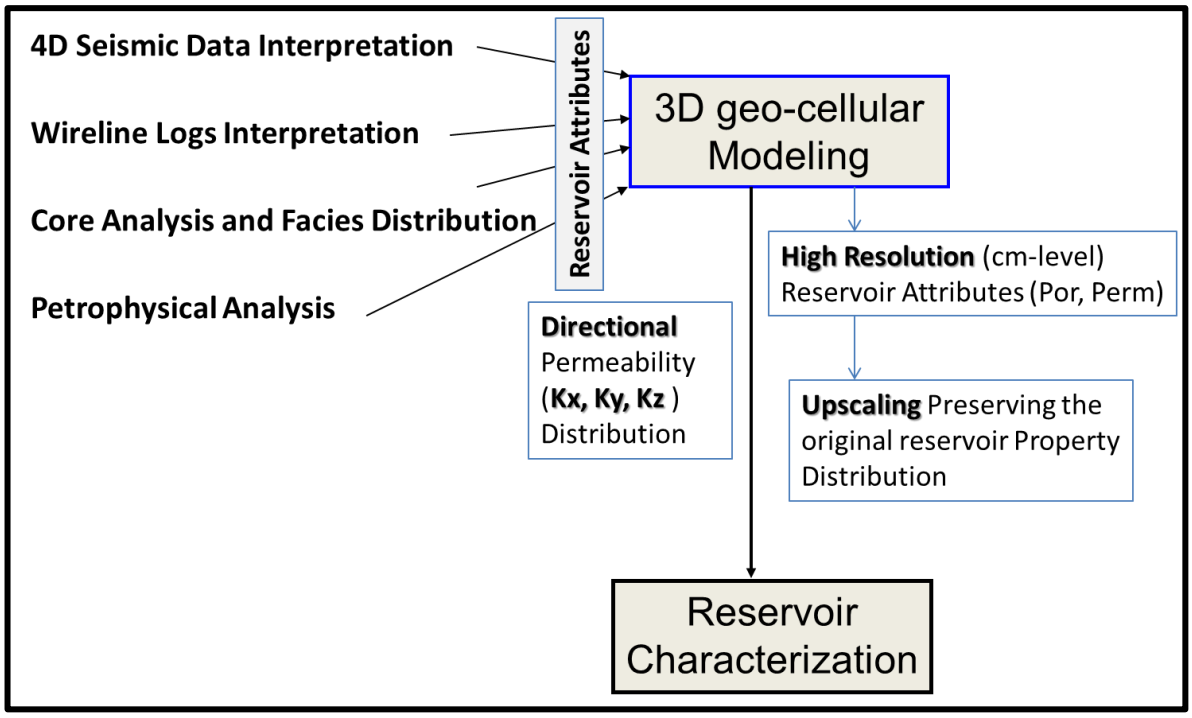

Figure 2-1: Work Flow of the integrated approach of 3D Geo-cellular Model for Reservoir Characterization based on the available data.

2.1 4D Seismic Interpretation

Reservoir boundary or the lateral extension of the heavy oil producing horizon was determined from the amplitude anomaly of the seismic interpretation and the production footprints of the CHOPS field, recorded from the time-lapse 3D seismic data sets acquired in the

year 2004 (base) and 2009 (monitor). Lithological discriminations of sand and shale in seismic data were obtained from the AVO inversion (Vp/Vs) and were compared with the geological facies distribution in the model.

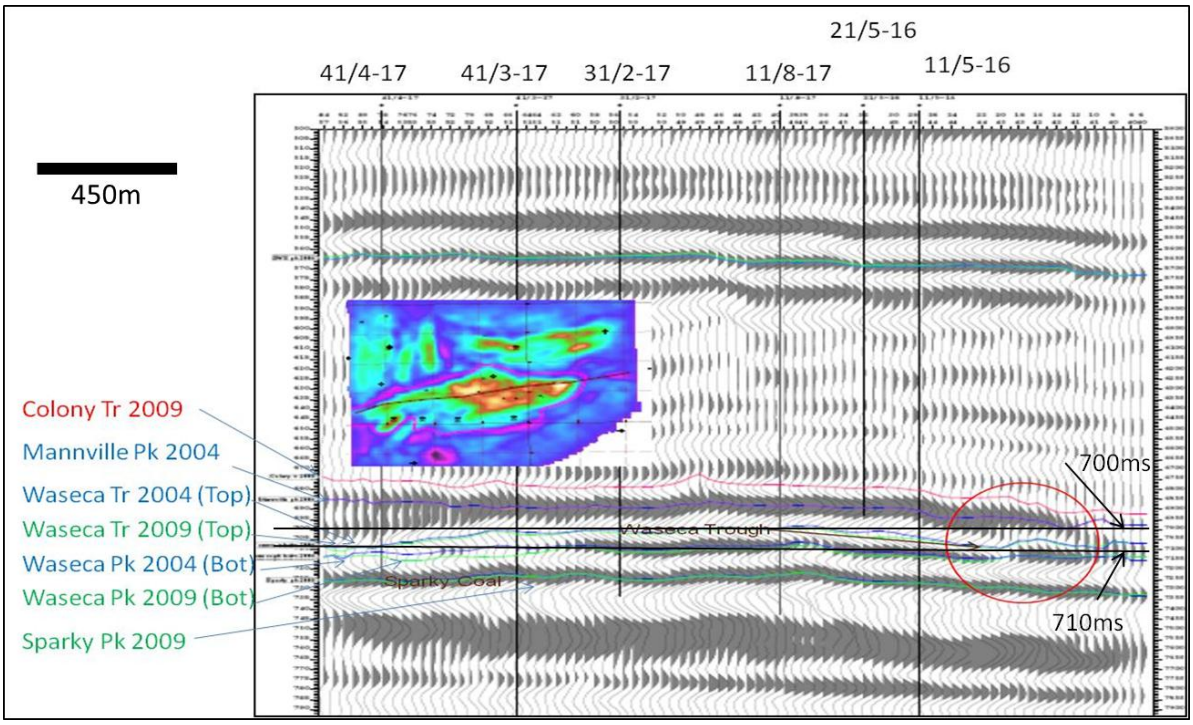

Figure 2-2: East-West Cross section (2009) of the Primate Pool showing the amplitude anomaly of the top of Waseca formation and the edge of the boundary. Light blue and the green line are representing the tops picked from 2004 and 2009 survey respectively.

The base 3D seismic survey was acquired in the year 2004 using the Aram 24 instrument with a spread of East-West receiver line of 200 meters spacing and a North-South source (explosives) line of 120 meters spacing. Shot intervals were 180 meters and the receiver intervals were 50 meters with a 2 milliseconds sample rate and 106 maximum fold. The monitor 3D survey was conducted in the year 2009 and maintaining the same acquisition parameters with some extra shots in the survey. The data were processed by CGG Veritas using the bin size of 30m x 30m.

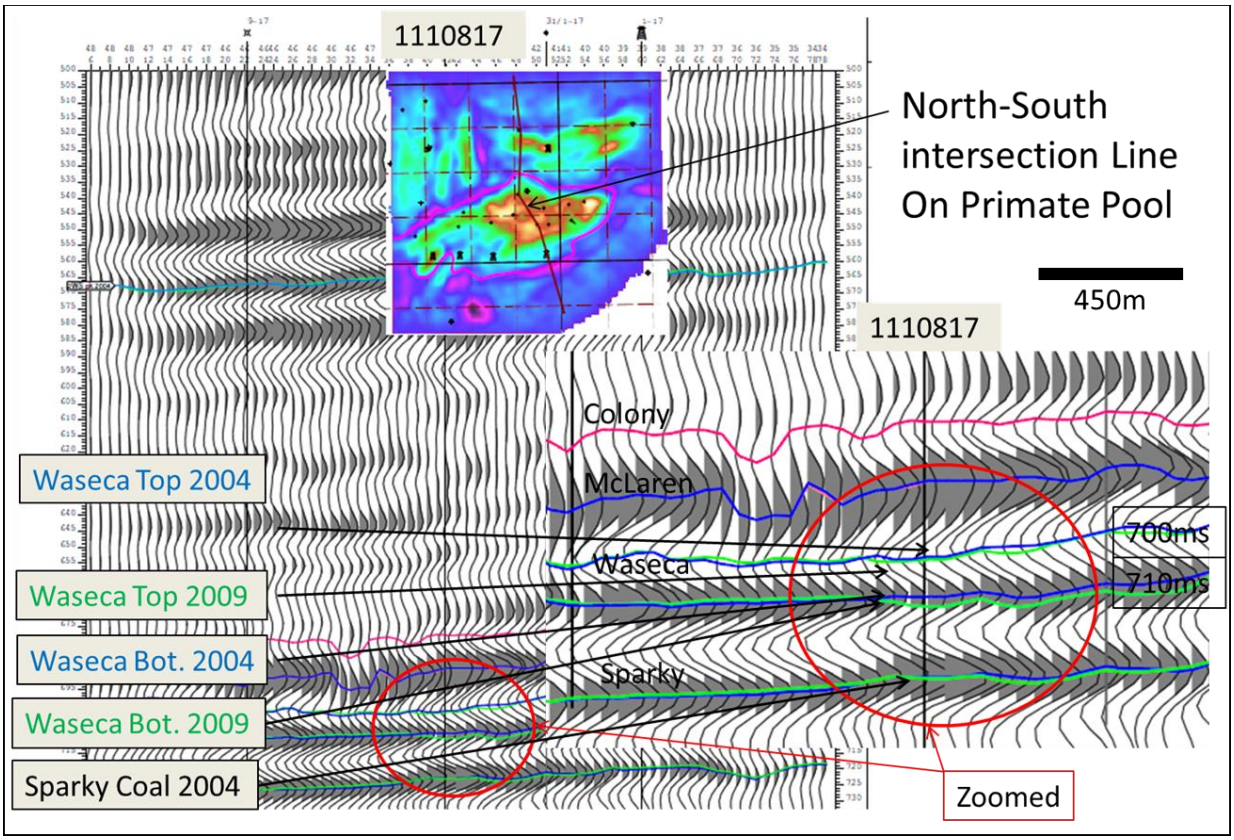

Figure 2-3: North-South Cross section of the Primate Pool showing the amplitude anomaly of the top of Waseca formation (blue line) and the edge of the boundary.

The seismic images of the study area did not reveal any clear trend of the subsurface channel systems; details of their extent and lithology are unclear, especially using these mega-bin datasets. Seismic attributes, such as stack amplitude and instantaneous attributes were analyzed and compared with well data to predict lithology and the reservoir lateral extension (Figures 2-2 and 2-3). Reservoir boundaries extracted from the amplitude anomalies of the both surveys were compared and are shown in Figure 2-4. This map suggests that the current and past high amplitude edges are very close to the same position. The difference between the two surveys is the production footprint of the CHOPS field.

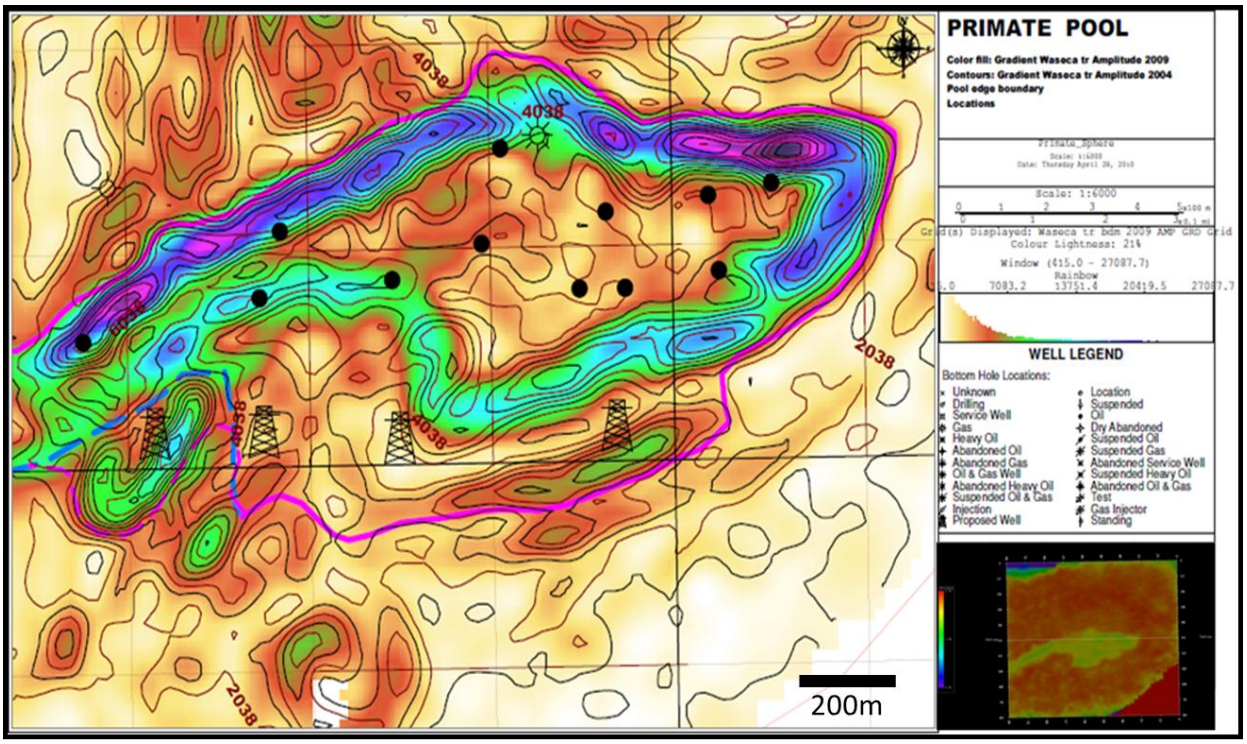

Figure 2-4: The map shows the trough amplitude gradient of the 2004 base survey as the contours and the 2009 as the color fill at 700ms.

Model based (blocky) amplitude inversions were conducted using the Hampson-Russell Suite software STRATA. The linear relationship between the P-impedance and both the S-impedance and density (Figure 2-5) in simultaneous inversion allowed an estimation of the S-impedance (Castagnas Equation in HRS) to derive Vp/Vs ratio volumes (Aki and Richards, 1980 modifications in HRS). A time slice at 700 milliseconds of the Vp/Vs map (Figure 2-6) shows the distribution of the sand and shaly part of the reservoir. In finding the lateral lithological variation of the sand and shale, the Vp/Vs ratio map was used to compare the facies or geological data. Vp/Vs ratio is a good lithology discriminator to separate the sand and shale in the reservoir (Lines et.al., 2004). Lower value represents the sand and the higher value of the Vp/Vs is shaly. The Vp value does not differ much in the sand and shale, whereas the Vs in the porous media is high, consequently reducing the ratio low for the sand.

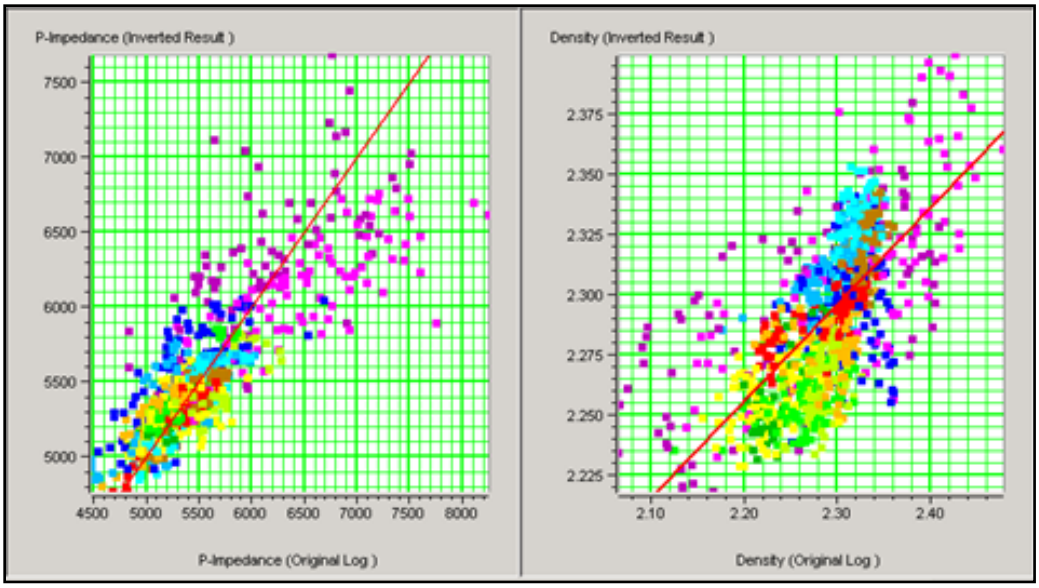

Figure 2-5: The linear relationship of the P-impedance and the density derived from the Primate Pool seismic and the log data.

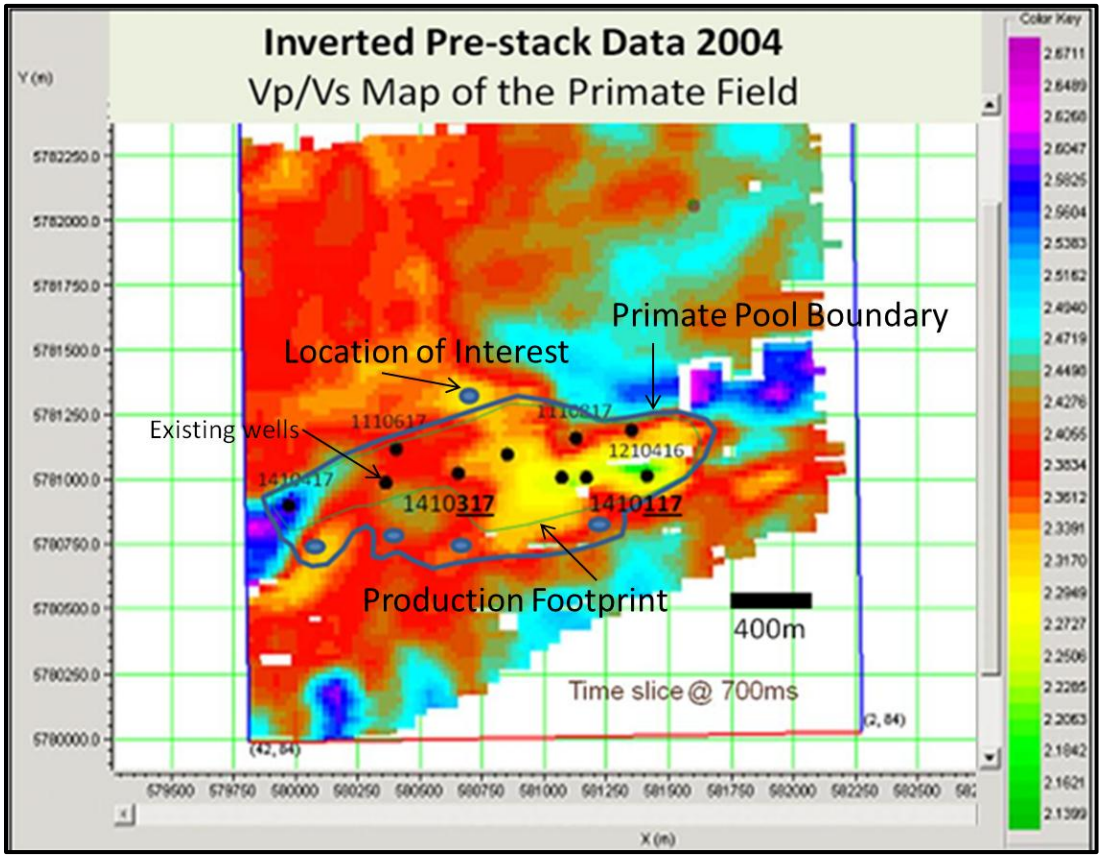

Figure 2-6: Vp/Vs distribution map over the Primate Pool at 700ms depth (upper part of the reservoir). Yellow is showing the low Vp/Vs ratio as reservoir rocks / sand against the high value red/ blue as shale.

2.2 Wire-line Log Interpretation

In the study area, the Primate Pool has only the conventional wireline logs such as Gamma, Neutron, Density and Electrical logs. For the near wellbore imaging FMI (Formation Microscanner Imaging^{TM} Schlumberger) or dip-meter log data in replacement of the core descriptions is of paramount importance, which unfortunately was not available for this study. The oil producing formation of this pool is Waseca and amalgamated McLaren-Waseca channel sands. A net pay zone was calculated based on the GR less than 30 API, density porosity was more than 30% and resistivity over 10 ohmm from the top of McLaren to the base of Waseca (Figure 2-7). There are many impermeable barriers of the shale layers, and shalyness in laminar forms is common in the producing zones, which are not noticeable on the normal log displays. However, bigger heterogeneous barriers which are clearly noticeable on the conventional logs (Figure 2-7) are not even considered in the conventional reserve calculation as heterogeneities. In terms of reservoir quality assessment, a shale volume calculation scheme was taken to categorize the detailed facies in the reservoir zone. This will provide a better and higher resolution near wellbore images.

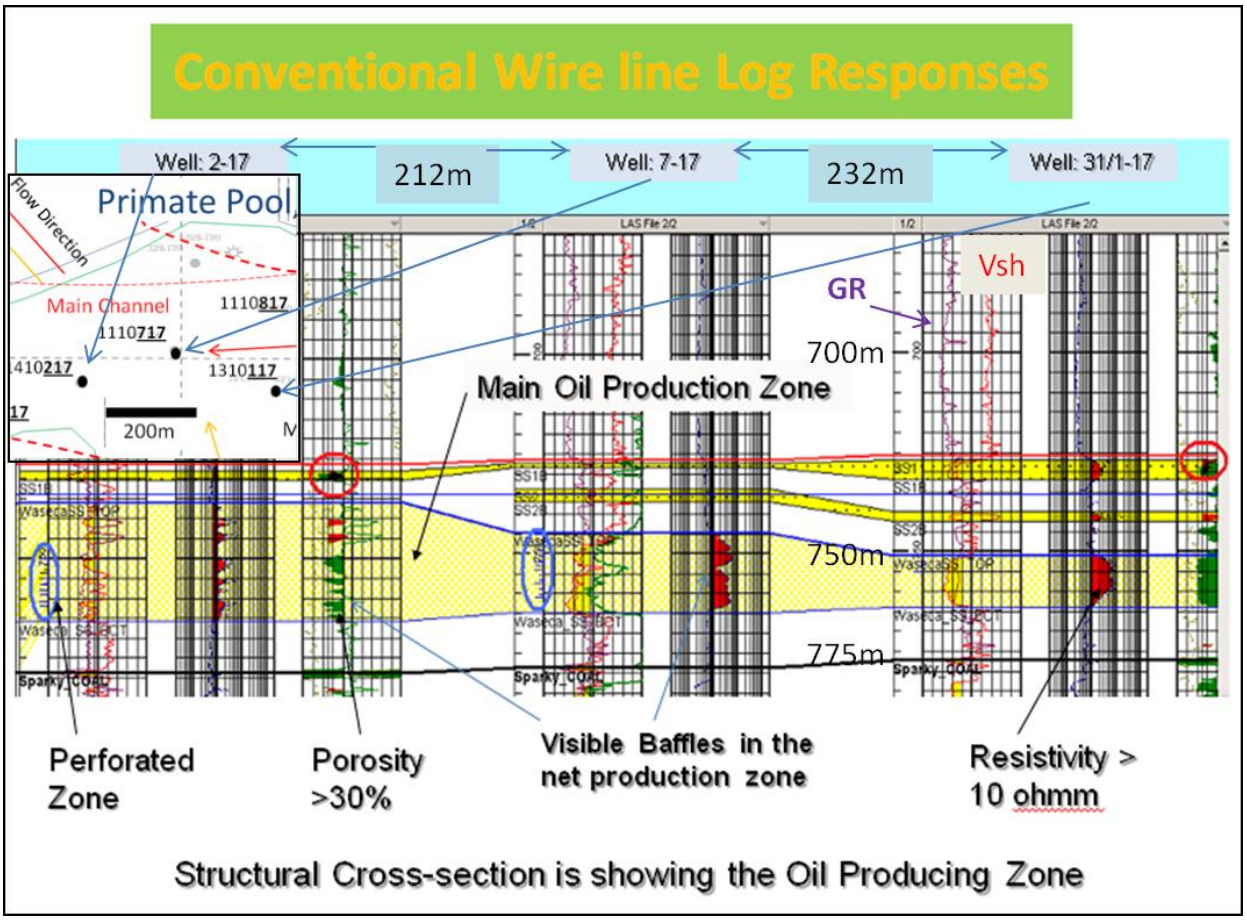

Figure 2-7: Conventional Wireline Logs show the main production zone with different reservoir attributes, such as lithology, porosity and formation resistivity.

The most commonly used logs included Gamma Ray (GR) and Neutron-Density (Porosity) logs, for electro-facies analysis, and compared with the electric log i.e., resistivity. In reservoir rock type characterizations, quantification of the shale abundance was needed to reveal the lithological variation and finding the depositional energy condition for a known depositional environment. The Shale Volume (V_{SH}) was determined using a GR log and Neutron-Density log separately and the average value was used in facies classification. The data and the results were compared to Thomas-Steiber's (1975) cross plots. Two cross plots such as Neutron versus Density (Figure 2-8) and Porosity versus Shale Volume (Figure 2-9) were used to determine the degree of shalyness of the reservoir. The results also confirm the presence of laminated shale beds in the reservoir which are considered as permeable barriers. Based on the average shale volume (V_{SH}) factor, a 'Rule' based log facies classification has been established (Table 2-1). The derived log facies have been plotted in the individual wells and vertically stacked for correlation.

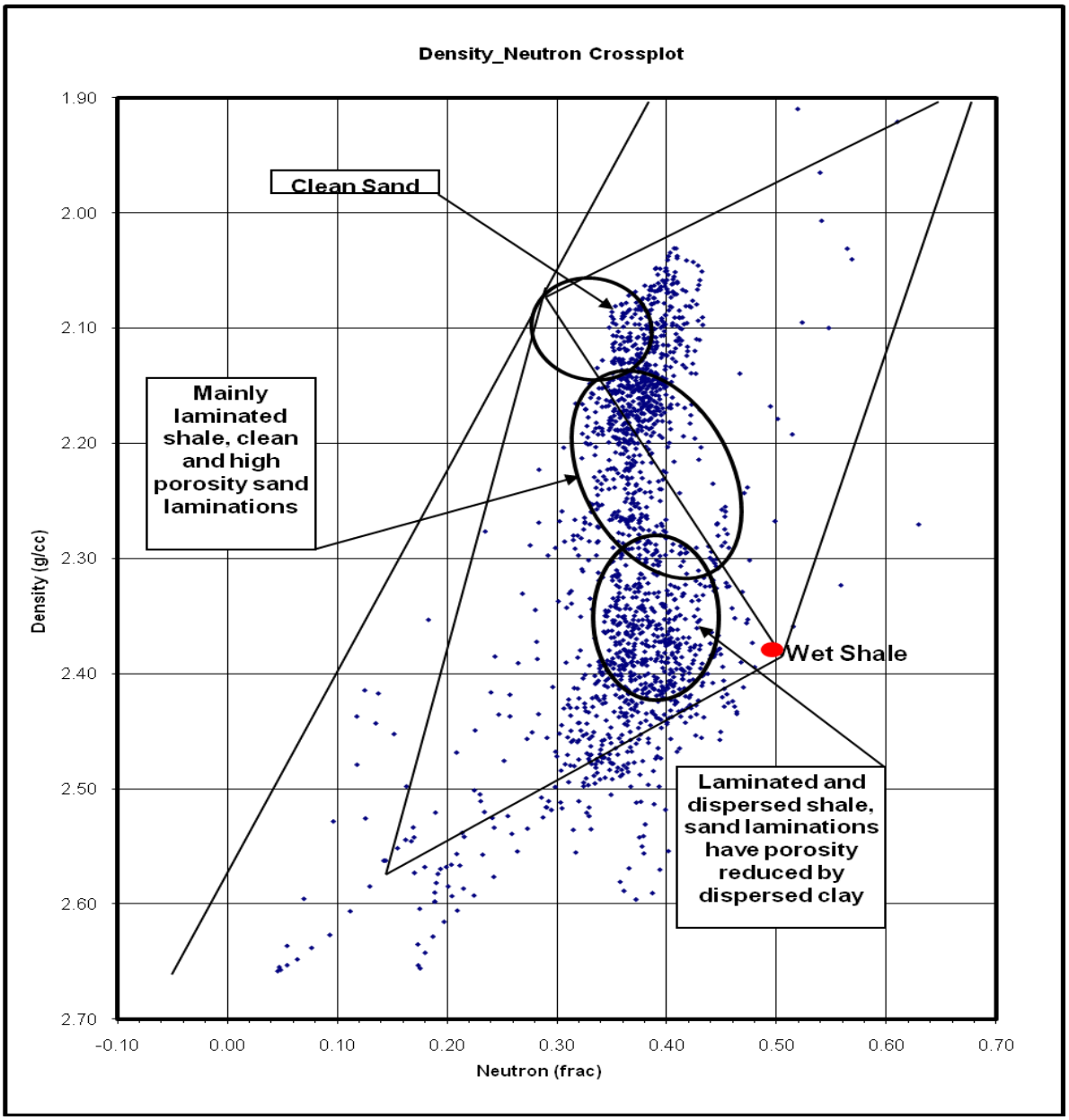

Figure 2-8: Neutron-Density Cross-plot showing the distribution of laminated shale in the sandstone reservoir of the Primate pool.

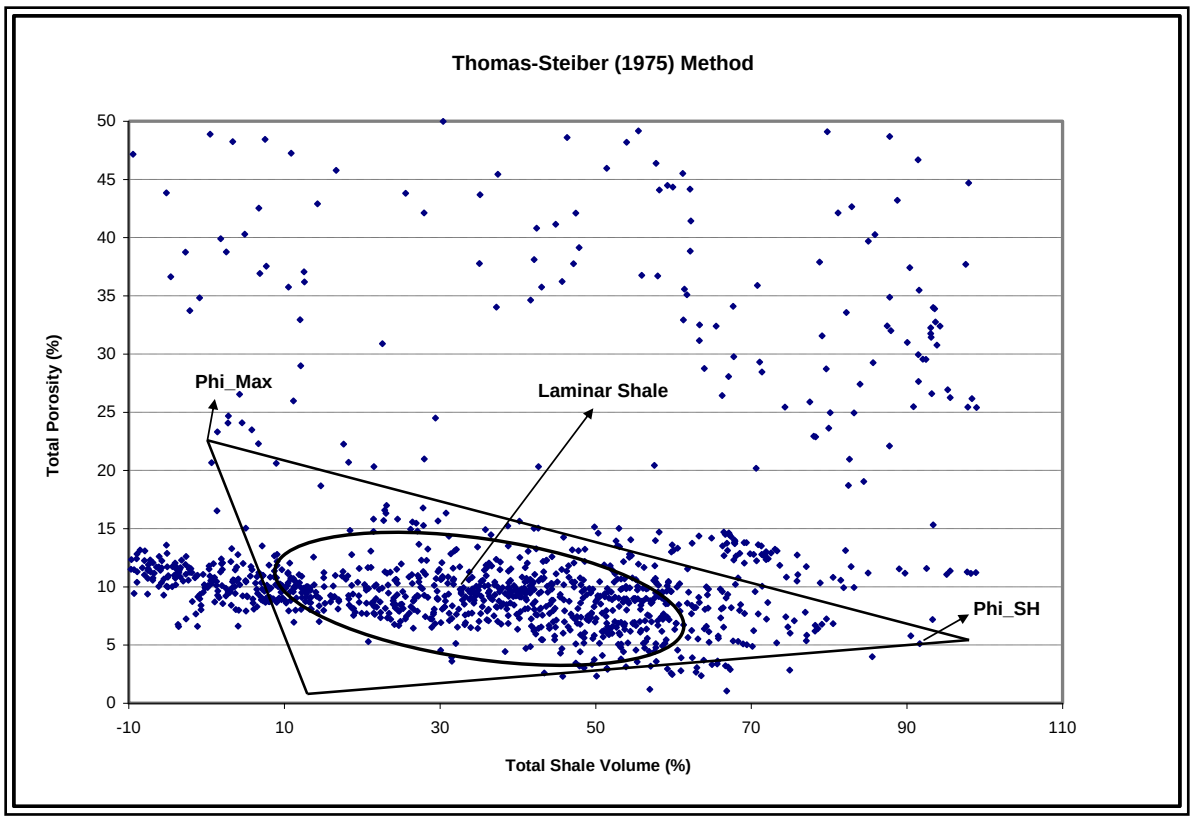

Figure 2-9: Thomas-Steiber's Cross-plot of the total shale volume and total porosity also confirms the distribution of laminated shale in the reservoir of the Primate pool.

2.2.1 Shale Volume Calculation

Gamma Ray (GR) data have been normalized for all the wells by using a normalization factor of ~1 since all the wells data are very similar in acquisition nature coincidentally. This normalization factor depends on the instrument calibration, logging environment, hole conditions etc. The data were found to be consistent among the wells. Some data were in decimal or in percentage value and were converted accordingly in the calculations.

Shale volume (V_{SH1}) was calculated by using the following formula from gamma ray logs:

$$I_{sh} = \frac{\gamma_{\log} - \gamma_{Min}}{\gamma_{Max} - \gamma_{Min}} \qquad V_{sh1} = 0.083(2^{3.7(I_{sh})} - 1)$$

For Tertiary and younger age, the above formula was used by Thomas-Steiber (1975) and cross referenced with Larionov (1969).

Where, I_{sh} is the estimated Shale Volume, V_{sh1} is the estimated Shale Volume after compaction correction, $\gamma_{\log}$ is the GR log reading, γ_{Min} is the clean sand section reading and γ_{Max} is the 100% shale section reading.

Another method was also used to calculate Shale Volume (V_{SH2}) as follows for the Neutron-Density data:

$$V_{sh2} = \frac{\phi_D - \phi_N}{(\phi_D)_{SH} - (\phi_N)_{SH}}$$

Where, ϕ_D is the Log Density-porosity and ϕ_N is the Log Neutron-porosity. $(\phi_D)_{SH}$ and $(\phi_N)_{SH}$ are the 'Wet Shale Point's density-porosity and neutron-porosity values respectively.

A 'Wet Shale point' was picked based on the high gamma and neutron value. In this case the values of $(\phi_D)_{SH}$ and $(\phi_N)_{SH}$ are 22% and 49% respectively for the above calculation.

Averaging the shale volume obtained from the above GR log and the Porosity logs, the final shale volume factor was derived and used in the facies classification.

$$V_{SH} = (V_{sh1} + V_{sh2}) / 2$$

2.2.2 Rule Based Facies Classification

A 'Rule' based log classification scheme was established to categorize the log facies based on the average Shale Volume (V_{SH}) factors obtained from the individual wells. The values are given in the Table 2-1 as the facies were classified.

The log-derived facies were plotted on the individual wells and correlated geo-statistically over the pool (Figure 2-10).

Table 2-1: Rule based log facies classification based on Shale Volume (V_{SH}) factor.

Rule based Facies Classification

Facies Template	V_{SH} (%)		Facies Type
• Facies A	00 – 20	Sand	Tabular Massive Sand
• Facies B	20 – 30		Trough Cross-bedded Sand
• Facies C	30 – 50	Silt	Planner bedded Sand with Shale
• Facies D	50 – 60		Lenticular Bedding
• Facies E	60 – 70		Low angled Ripples with Parallel bedding
• Facies F	70 – 80	Shale	Bioturbated Shale
• Facies G	80 – 100		Laminated Shale

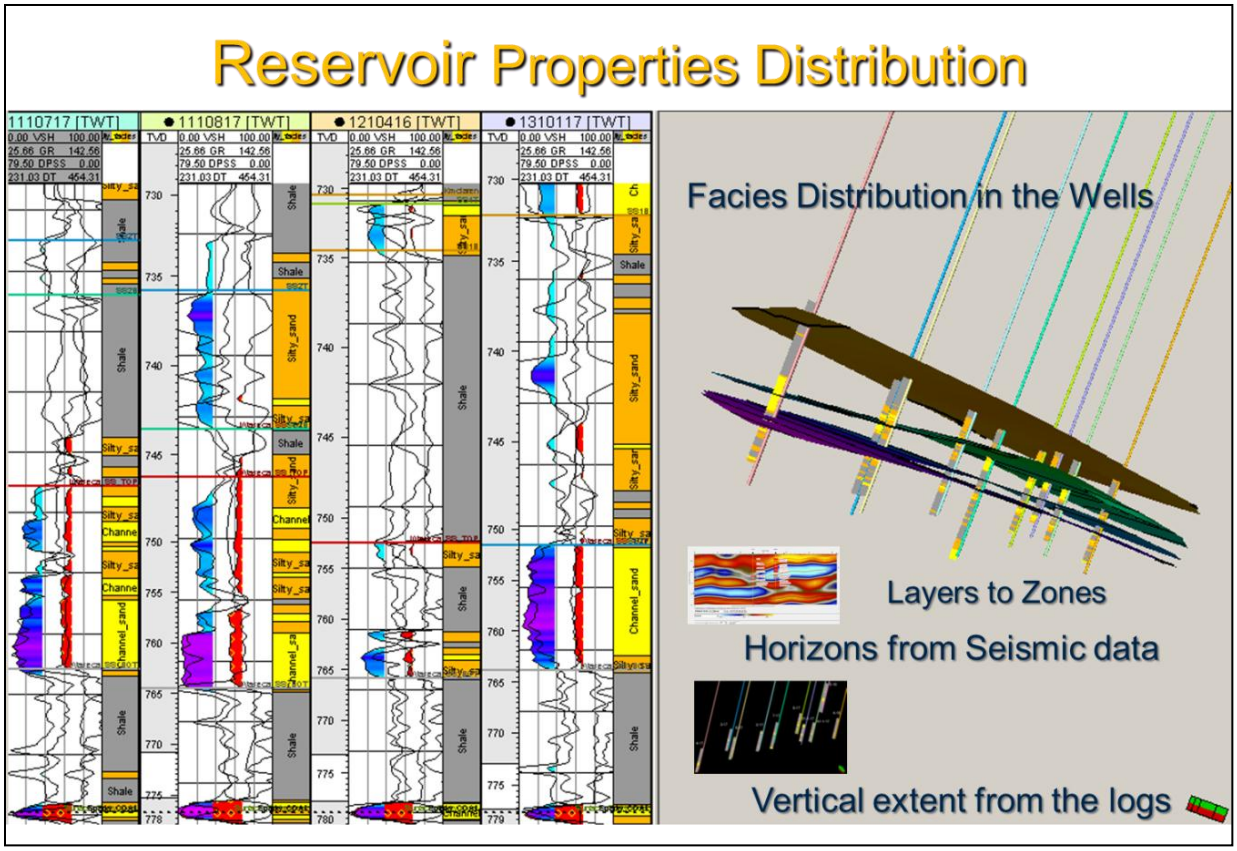

Figure 2-10: Estimated log-facies for the individual well that reflects the pool facies distribution.

2.3 Core Analysis

Three offset cores of the neighbouring wells (Figure 2-11) were examined to validate the similar types of data for the Primate pool (Figure 2-12 and 2-13). Petrophysical properties from the well logs and the cores were correlated for reservoir properties evaluation and used in the 3D geo-cellular model for the flow simulations. Individual core descriptions are shown in the Appendix I and the log responses including the shale volume factors (Figure 2-14) related to the detail sedimentary facies (Figure 2-15) of the core sections were analysed and compared with the other wells those that have no cores.

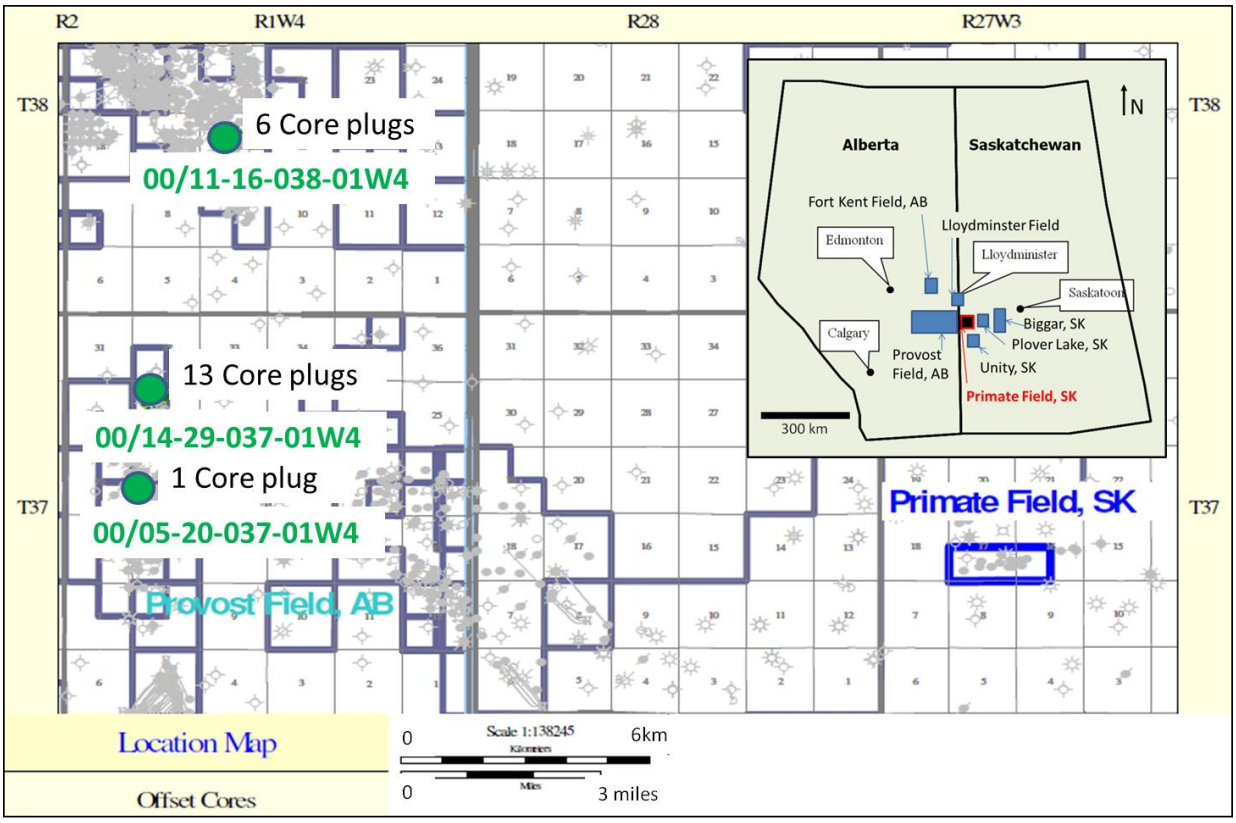

Figure 2-11: Location map of three offset cores from the Provost Field of the same depositional environment (Source: AccuMap).

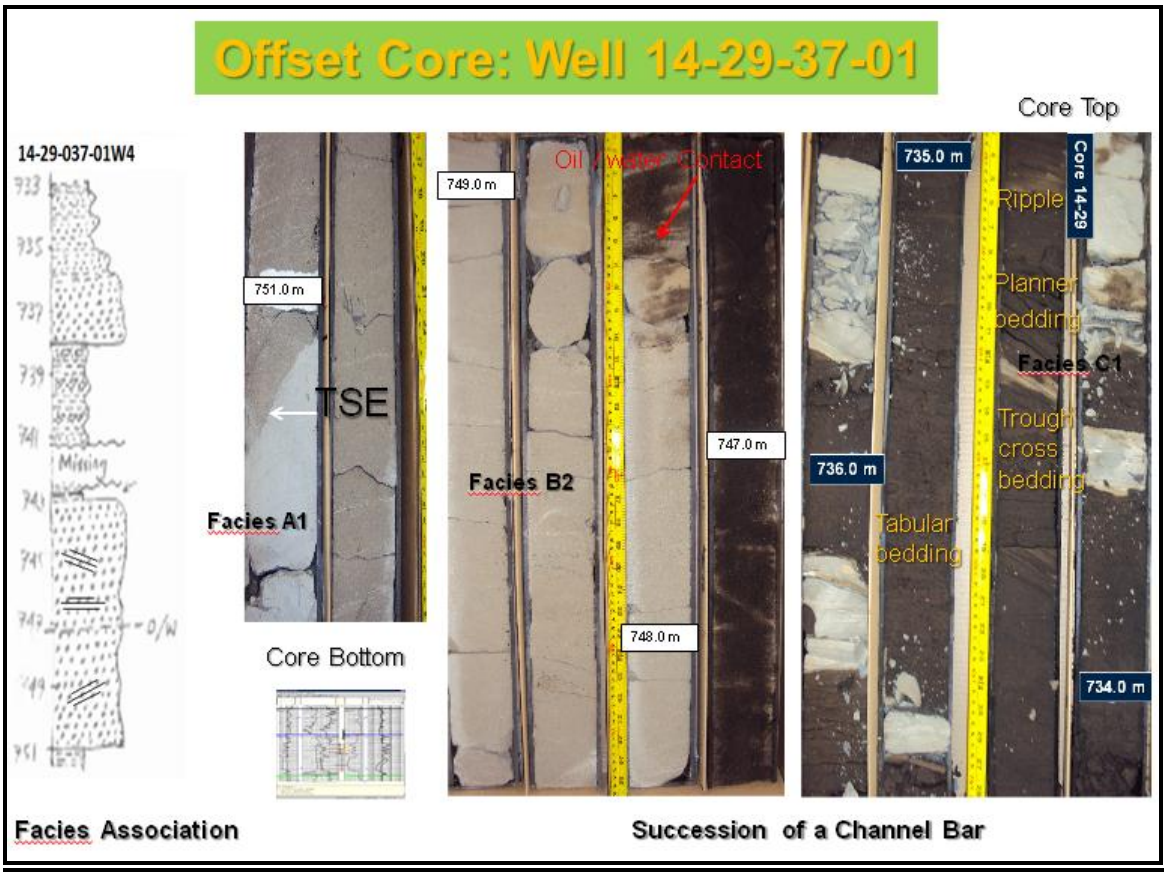

Figure 2-12: Core picture of the offset well 14-29-37-1 (McLaren/Waseca formation).

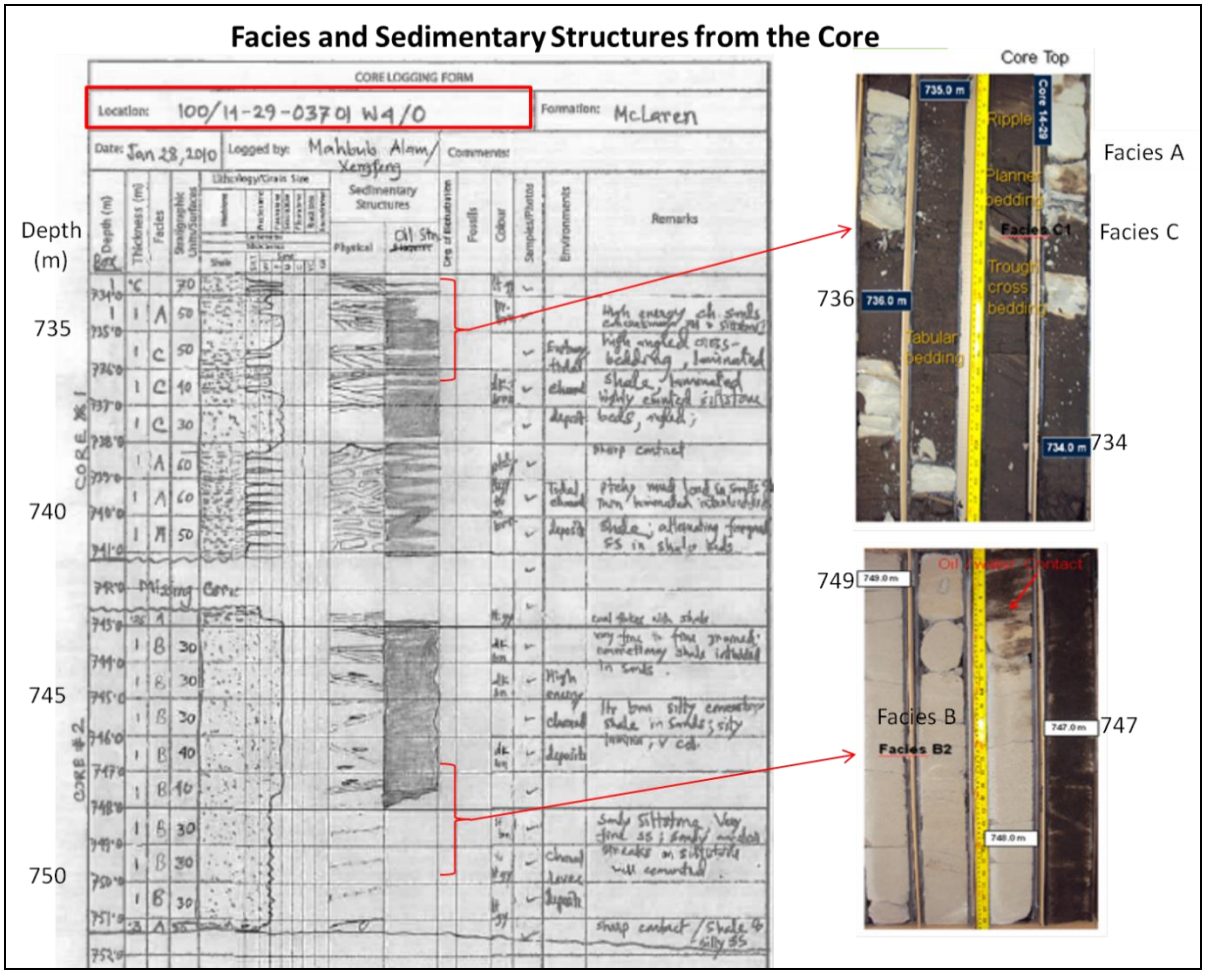

Figure 2-13: Facies association and related sedimentary structures from the core description of the offset well 14-29.

A total of seven sedimentary facies were found in three facies associations interpreted from the three offset cores. The facies are: (A) lowermost massive sand; (B) trough cross-bedded sand; (C) planner bedded sand; (D) lenticular bedding with less shaley silt; (E) low angle ripples with more shaley silt; and (F) bioturbated shale; and (G) the upper most laminated shale (Figure 2-12 and Appendices I, II and III). Based on the known fluvial environment, the facies were categorized in associations. Facies associations are: 1) Cross-bedded very fine sand and silt with laminated (flat and very low angle) shale, 2) Massive or tabular bedded sand, trough cross-bedded sand with low-angle small-scale cross-beds for planner and ripple together, and 3) Alteration of the ripple cross bedding (low energy) and flat regular parallel bedding of shale and silt. The depositional sequences had been identified as a facies association and are based on the detail observations and genetic classification; seven SBED templates (Table 2-1, Figure 3-10)

have been constructed for the further analyses and correlation. The genetic classification in the facies association were found as channel deposits as sand, marginal channel as shaley sand or silt, and the non-channel deposits as shale (Table 2-1, Figure 3-15). These templates will represent the reservoir attributes of the facies, such as directional permeabilities consistent with the laboratory core analysis data.

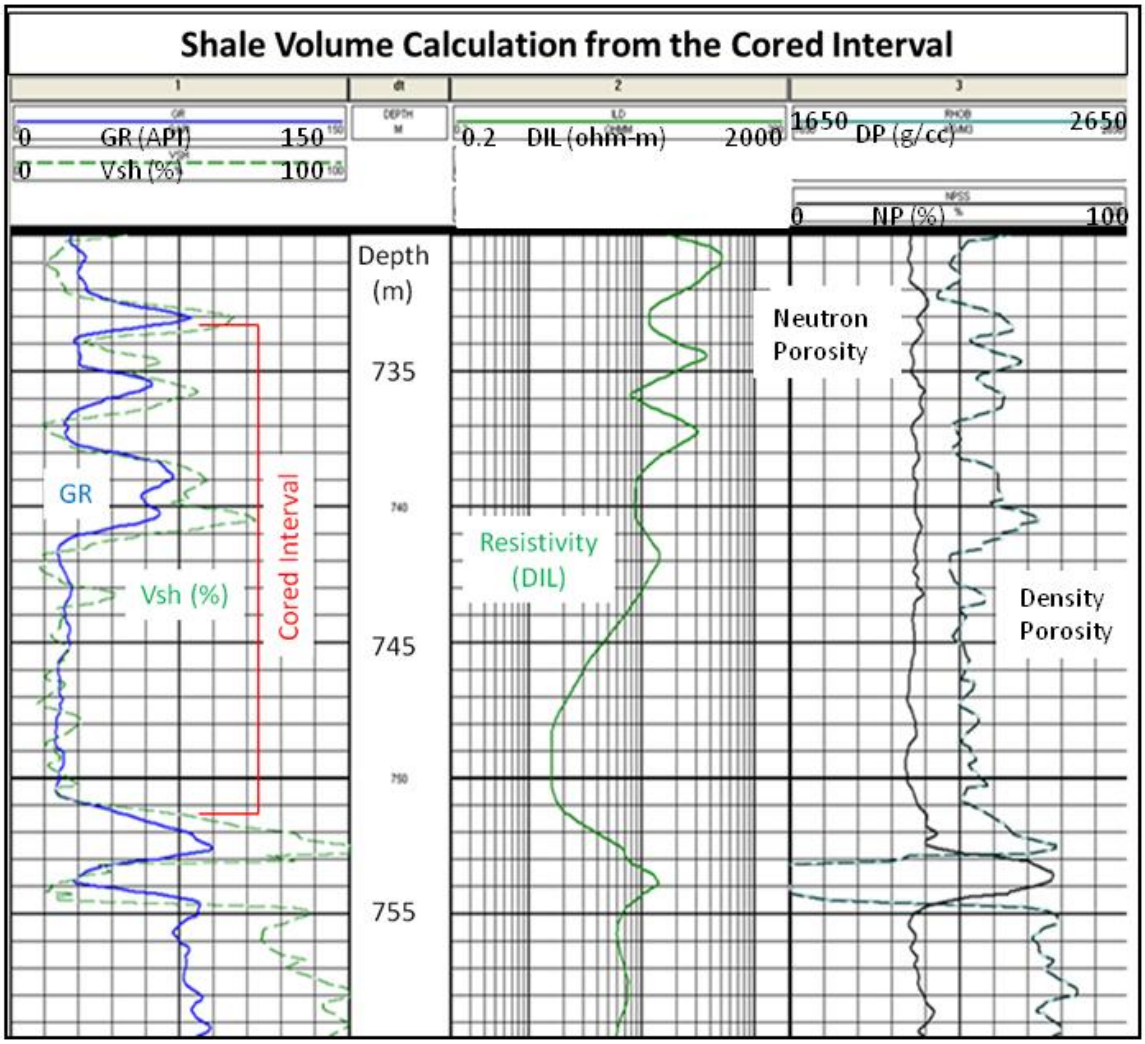

Figure 2-14: Shale Volume Curve from GR, Density Porosity and Neutron Porosity Logs along with Resistivity curve on the cored interval of the reservoir.

The known depositional environments of the channel sands were well recognized in the core and consistent with Vsh interpretation for the current study. The characteristic features of a channel point bar, i.e., fining upward sequence and the repetition of facies association at the vertical stacking in the core and Vsh curve are the indicatives of the lateral accretion within a

point bar. Tidal influence within the meandering fluvial system produces sandstone and mudstone couplets on the lateral accretion surfaces and was also seen in the cores.

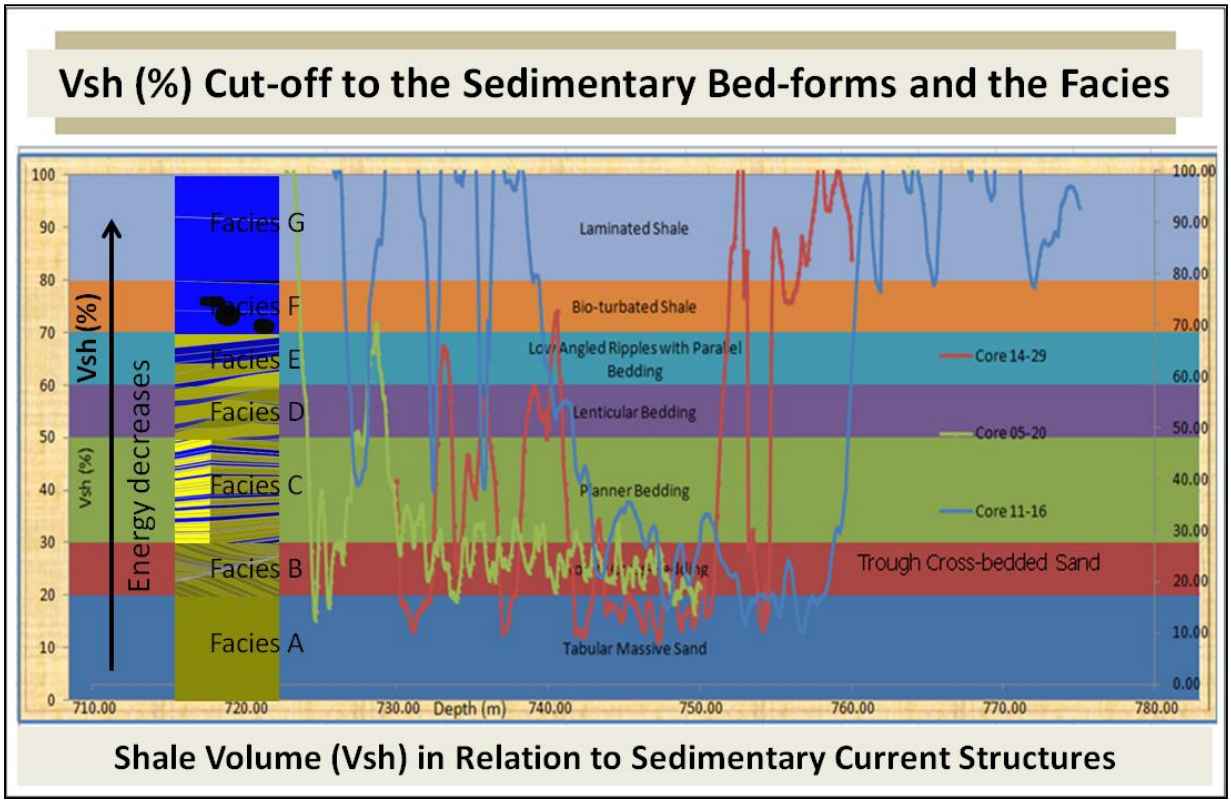

Figure 2-15: Shale Volumes from three cores (red, blue and green) are plotted against the reservoir depth intervals and Sedimentary facies based on the cut off values from the rule based facies classification is showing the relationship of the Sedimentary facies to the Shale Volume factors.

Core descriptions of the same members from the neighbouring field indicate that the channel deposits are well laminated, ripple cross laminated, very fine to fine grained sand with thin interbedded shale, and the intra-clast horizons are common as described by Kramers et. al.,(1993). The Waseca formation is generally found to be composed of fine to very fine grained well-sorted sand with sideritic and large intraclasts lie at the base of the grey shale as found by Davies et al., 2001. A large portion of the shaly Lower McLaren regional strata have been described by Mathison (1988) and bioturbated shales at the base of the Upper McLaren overlie the Lower McLaren regionally. Considering the geology of the pool, especially the tidal estuary channel deposit with the fluvial incised valley deposit, clay and laminated shale have major roles in the reservoir quality and pool characterization. The fining-upward sequence and the porosity

pinched out along with lateral distribution of the reservoir rocks demand a more detailed and more improved 3D geological modeling for the reservoir characterization, especially with the reservoir core data.

2.4 Petrophysical Data Analysis

Reservoir properties, such as shale volume (Vcl), total porosity (Phit), water saturation (Sw) and permeability (Perm) were derived from the three offset cores and wireline log data using the following petrophysical methods:

- Vcl: Neutron-Density
- Phit: Neutron-Density crossplot
- Sw: Modified Simondoux
- Perm: Coates FF

Table 2-2: Porosity and permeability results derived from the petrophysical interpretation of the offset core data.

Lithology	POROSITY(v/v)		LN (PERM) (lnMD)	
	MEAN	STDEV	MEAN	STDEV
SHALE	0.056	0.097	-2.47	0.13
SILT	0.043	0.02	5.263	0.878
FINESAND	0.275	0.033	8.515	0.819

The results (Table 2-2) of the offset core data were compared with the Primate Pool data and were used in the 3D geo-cellular model for the property modeling. One of the petrophysical interpretations of the core (well 14-29-037-01W4) is shown in Figure (2-16).

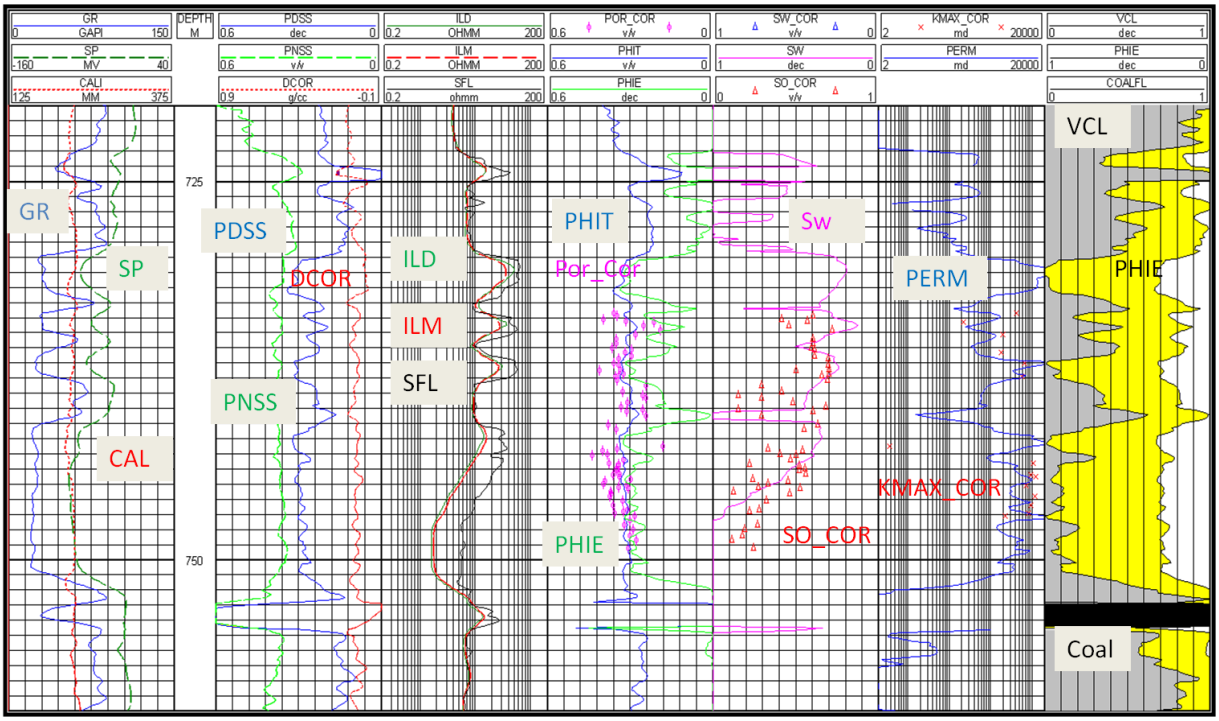

Figure 2-16: The curves of the petrophysical interpretation for the well 14-29-037-01W4.

The Simandoux equation was modified in 1969 by Bardon and Pied, as shown below:

$$S_W = \left[\sqrt{\left(\frac{F R_w}{R_t}\right) + V_{sh}\left(\frac{F R_w}{2R_{sh}}\right)}\right] - V_{sh}\left(\frac{F R_w}{2R_{sh}}\right)$$

where:

S_w = water saturation
F = formation factor
R_w = formation water resistivity
R_t = true resistivity
R_{sh} = resistivity of adjacent shale
V_{sh} = volume of shale

The Free Fluid Model (FF) of Coates (1999) is based on the relationship between porosity and water saturation data. The input data for direct PERM determination on core samples are from the laboratory core analysis data.

3D GEOCELLULAR MODELLING

Production footprints in a 3D geo-cellular model integrated the seismic, geological and petrophysical data and helps to better understand the reservoir and reduce risk and uncertainties. A complete 3D geo-cellular model is useful to aid in the decision for future infill development drilling and to maximize the production including the introduction of new technology for EOR. A 3D geo-cellular model is a significant tool for reservoir simulation and convenient for the iterative history matching process. Knowing the production footprints and the reservoir properties in the development field helps to maximize the recovery factor and improve the reservoir characterization process. This research aims at a better understanding of the reservoir properties distribution and tries to properly evaluate the practical scenario to realistically enhance the production from the heavy oil fields. The work flow of 3D Geo-cellular modeling is shown in Figure (3-1). A conventional 3D geo-cellular model is built for the Primate pool first; and using the novel approach of determination of sedimentary facies structures from the logs, the detailed high vertical resolution of the wells have been incorporated into the model to look at the influence of the reservoir heterogeneity due to the depositional pattern and facies distribution.

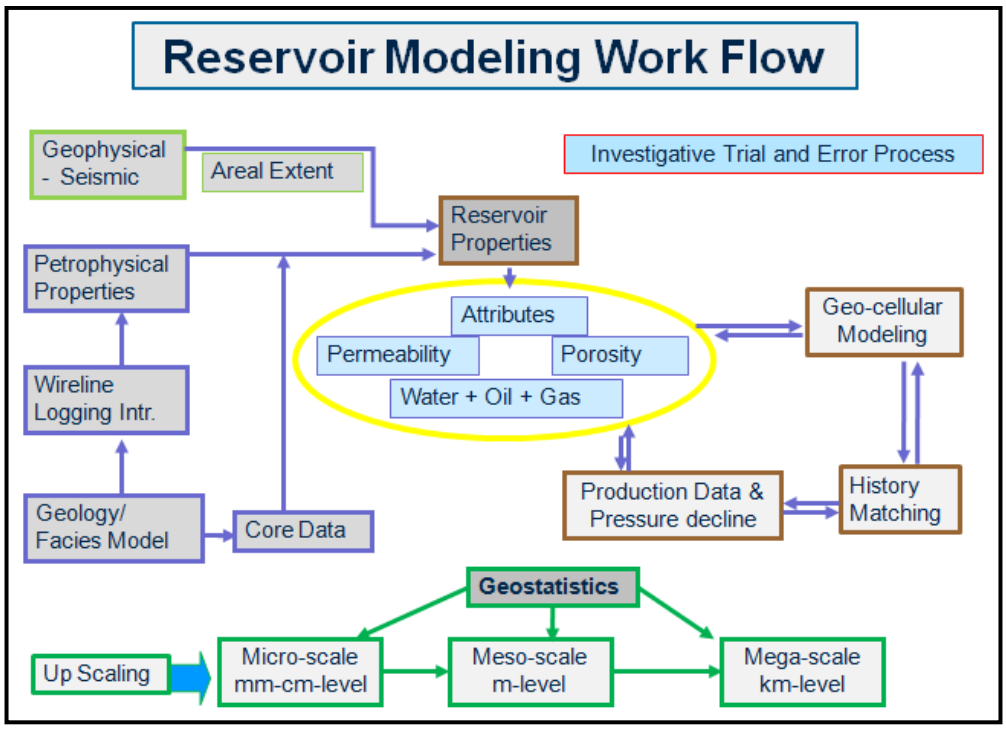

Figure 3-1: Showing the 3D geo-cellular modeling workflow integrating seismic, geological and reservoir engineering attributes and their relationships with geostatistics.

3.1 Conventional 3D Geo-cellular Model

The 3D geo-cellular model (Figure 3-2 and 3-3) was created by making the cell-grids of 10mX10mX1m in the 3D geological model of the Primate Pool. A total of 1.6 million cells constitute the 3D geo-cellular model. This is a static model aiming to run the reservoir simulation of all the well logs available, and the production data combined with all of the G&G aspects. The 3D geological model was constructed based on the seismic data for the lateral extension of the pool area and the production footprints of the drainage area. The vertical extension or net-pay thicknesses of the reservoir were extracted from the wireline log data. The reservoir properties were incorporated from petrophysical interpretation of the logs and core data. A part of the history matching of the production data were carried out to validate the 3D geological model and to compare the wormhole affected area to the 4D production footprints. The primary target is to locate the infill or additional drilling location avoiding the wormhole drainage area for the enhanced oil recovery (EOR).

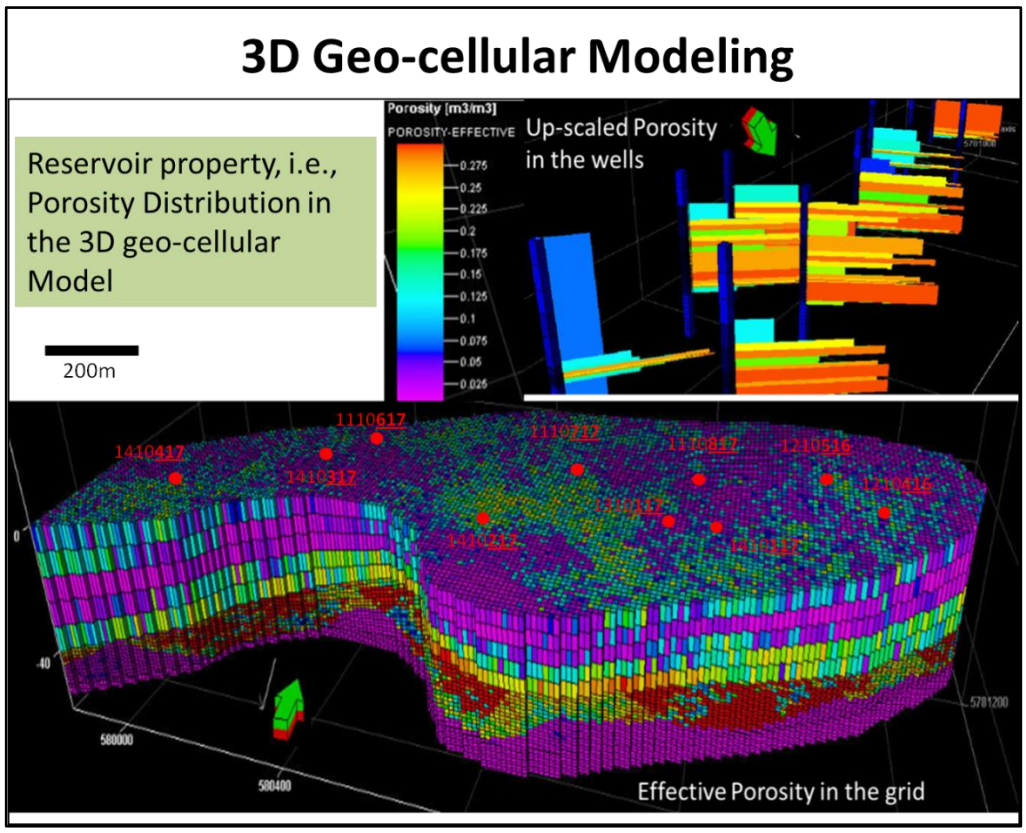

Figure 3-2: 3D geo-cellular model / Static Model for the Primate Pool.

In 3D geological model building process, seismic data and well log data were input and calibrated using 'Petrel' software. The seismic data were converted from time domain to depth domain, wire line log data were up-scaled (Figure 3-3 and 3-4) and different geo-statistical parameters were used to guide the facies that based on the environment of deposition, i.e., tidally influenced fluvial channel as Christopher (2001) described. This is mainly an object-based geological model honouring the well log data over the seismic data due to the resolution constraint. The Sequential Indicator Simulation (SIS) algorithm (a built-in module in the modeling software) was used in the facies modeling that estimates the facies probability using the up-scaled cells and its variogram information. Based on the seismic data, the channel trend (Figure 3-6) was inferred mainly east-west with three major incised channels flowing from south to due north direction. May be this is same incised channel changed its course through time. This interpretation may vary and was done for this model based on the available data and log data has been respected over seismic. The length of the major channel was calculated based on the pool long axis of about 1600 meters and the width from the seismic inferred about 500 meters for the calculation in petrel.

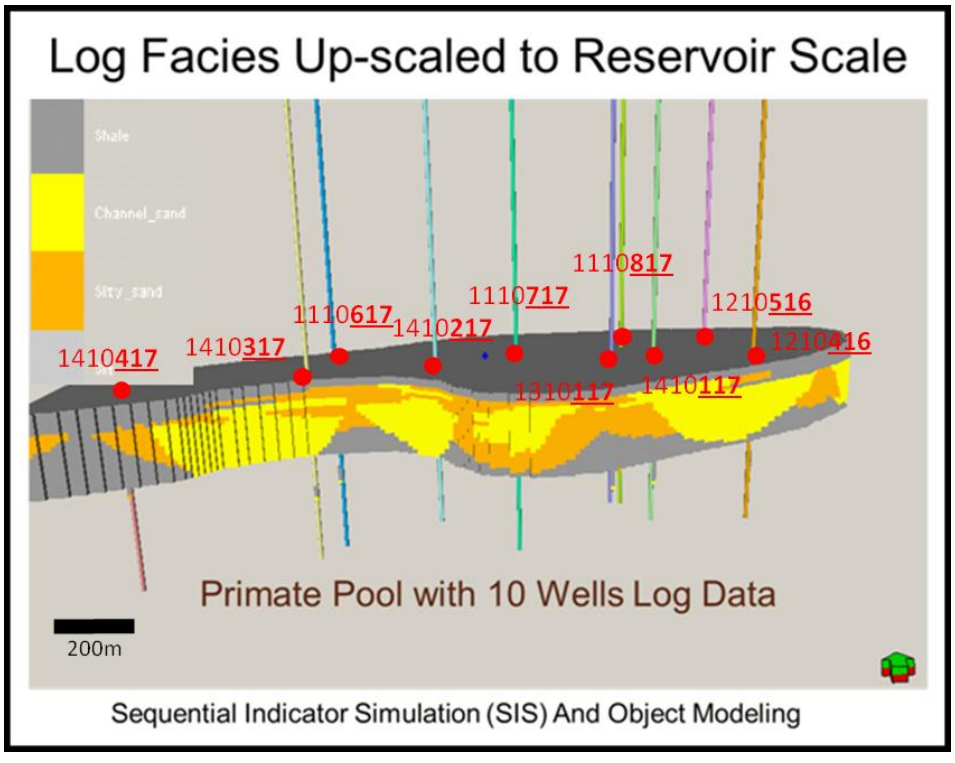

Figure 3-3: The complex channel system in the 3D geological model.

Different petrophysical properties i.e., porosity (Por), permeability (Perm), water saturation (Sw) obtained from the offset core plugs were incorporated into the model (Figure 3-5), then compared with the facies distribution in the model. The reservoir seismic boundary was extended further to explore the new drilling location using Petrel in-built geostatistical 'averaging neighbouring cell's method (Figure 3-9). Sparky coal is the bottom layer of the reservoir Waseca formation and was considered as datum for the stratigraphical correlation in this study. Sparky coal was detected both in seismic and wireline logs very clearly. Based on the structural configuration of the underlying Sparky Coal (Figure 3-7 and 3-8) and the facies distribution in the reservoir, the new prospective area out of the production influence was chosen for enhance oil recovery (EOR). Few snapshots of the conventional 3D model of the Primate pool is shown as a visual display in Figure 3-9 and the qualitative estimation of the reservoir parameters will be used in reservoir simulator for the evaluation of reservoir performances.

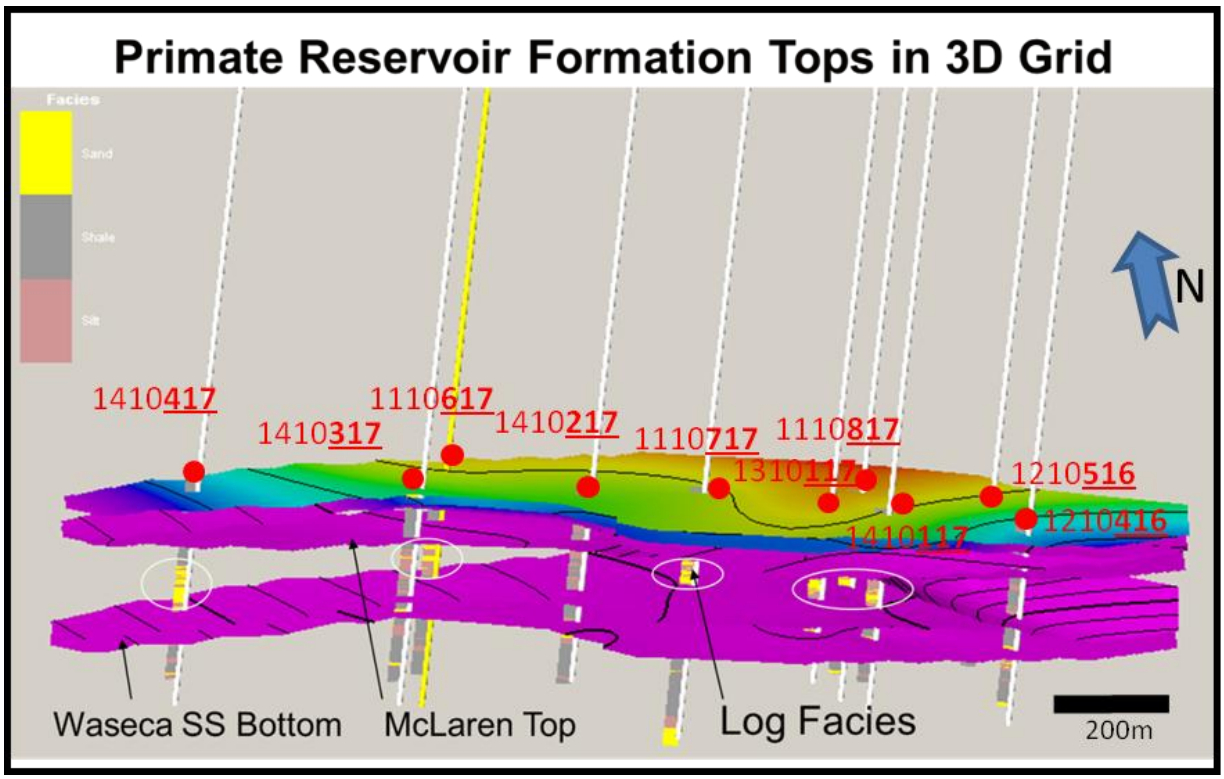

Figure 3-4: Log facies for upscale to represent the pool in the 3D model. The colored top is the McLaren top followed by Waseca top and the bottom.

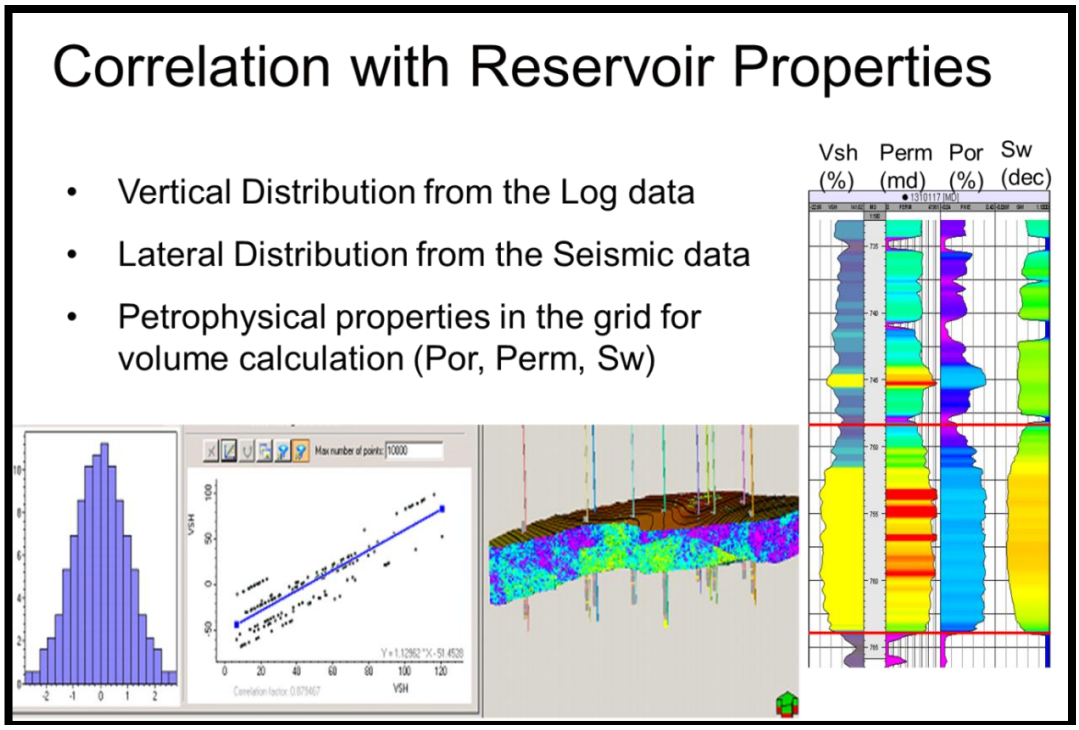

Figure 3-5: Geo-cellular model for the reservoir properties to run the simulation and estimation of the reservoir prospect.

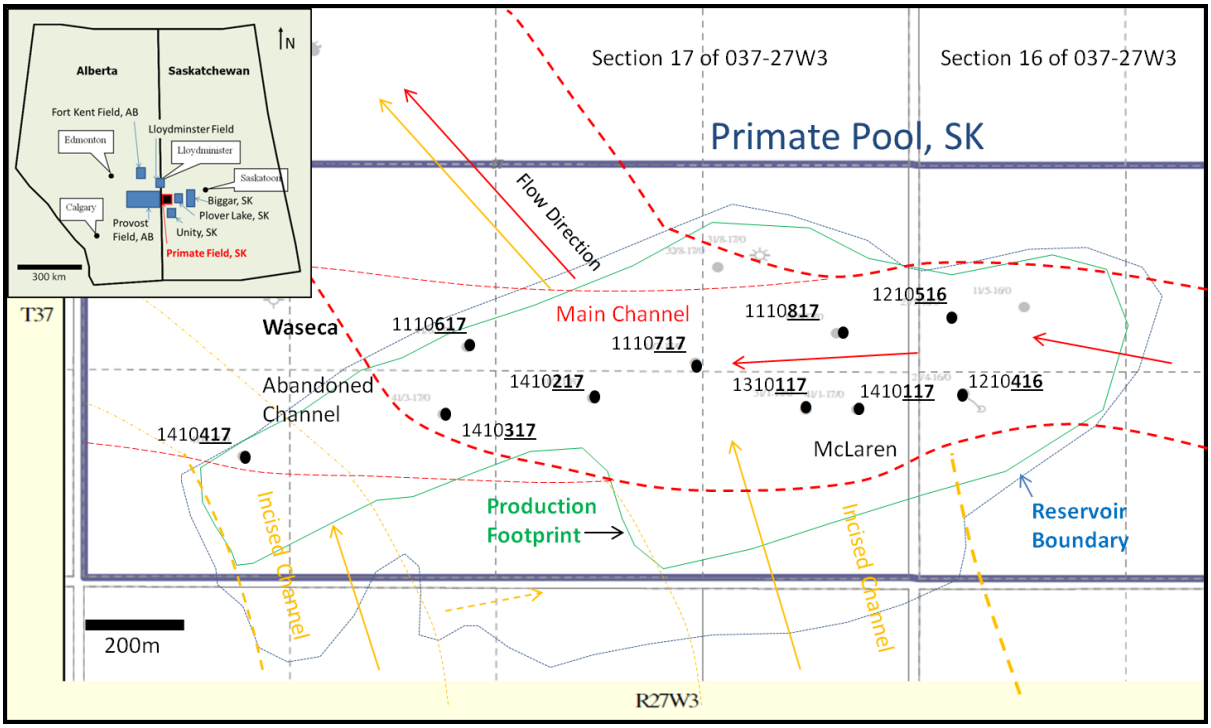

Figure 3-6: Reservoir seismic boundary extended further to explore the sub seismic extension of the reservoir that based on the reservoir properties and production footprint.

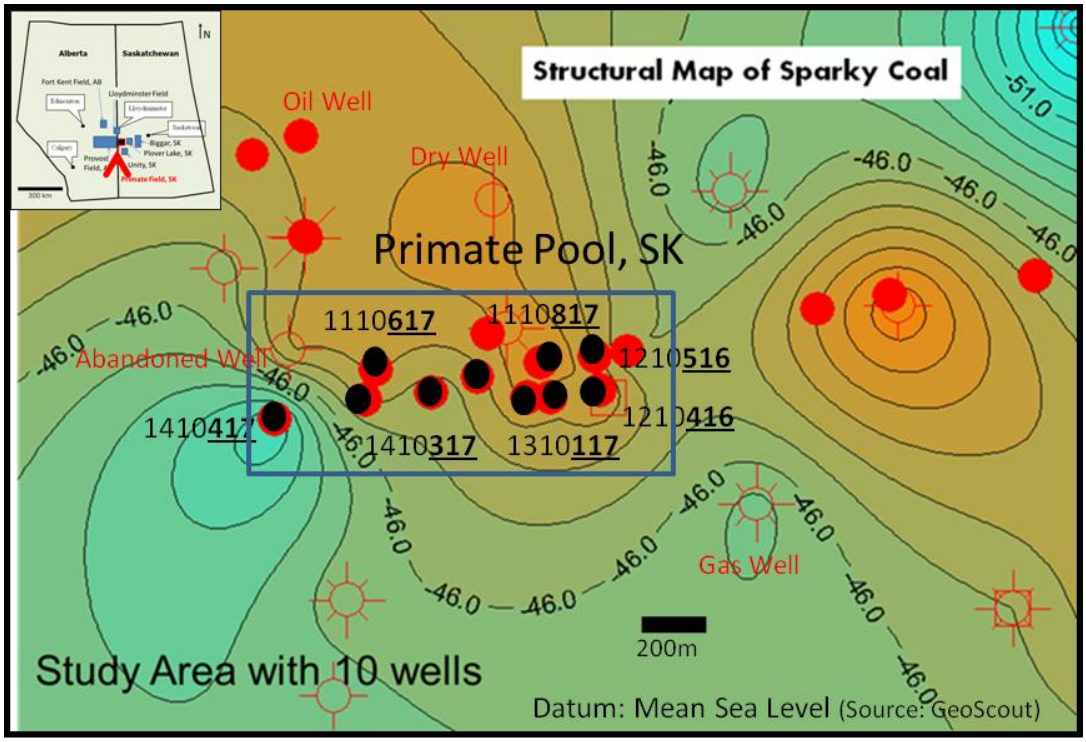

Figure 3-7: Subsurface Structural Map of Sparky Coal represents the structural trend of the overlying depositional events from the log control.

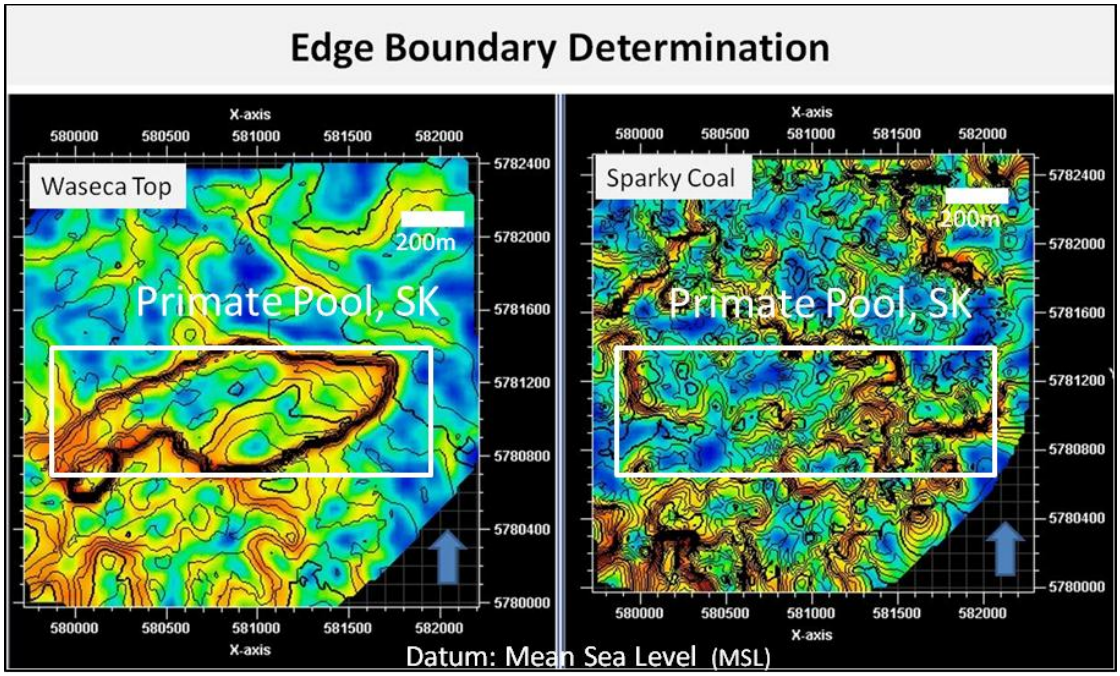

Figure 3-8: Edge boundary determination from the amplitude anomaly that reflects the subsurface structural configuration from the seismic data (hot color key, higher the anomaly reddish/darker the color).

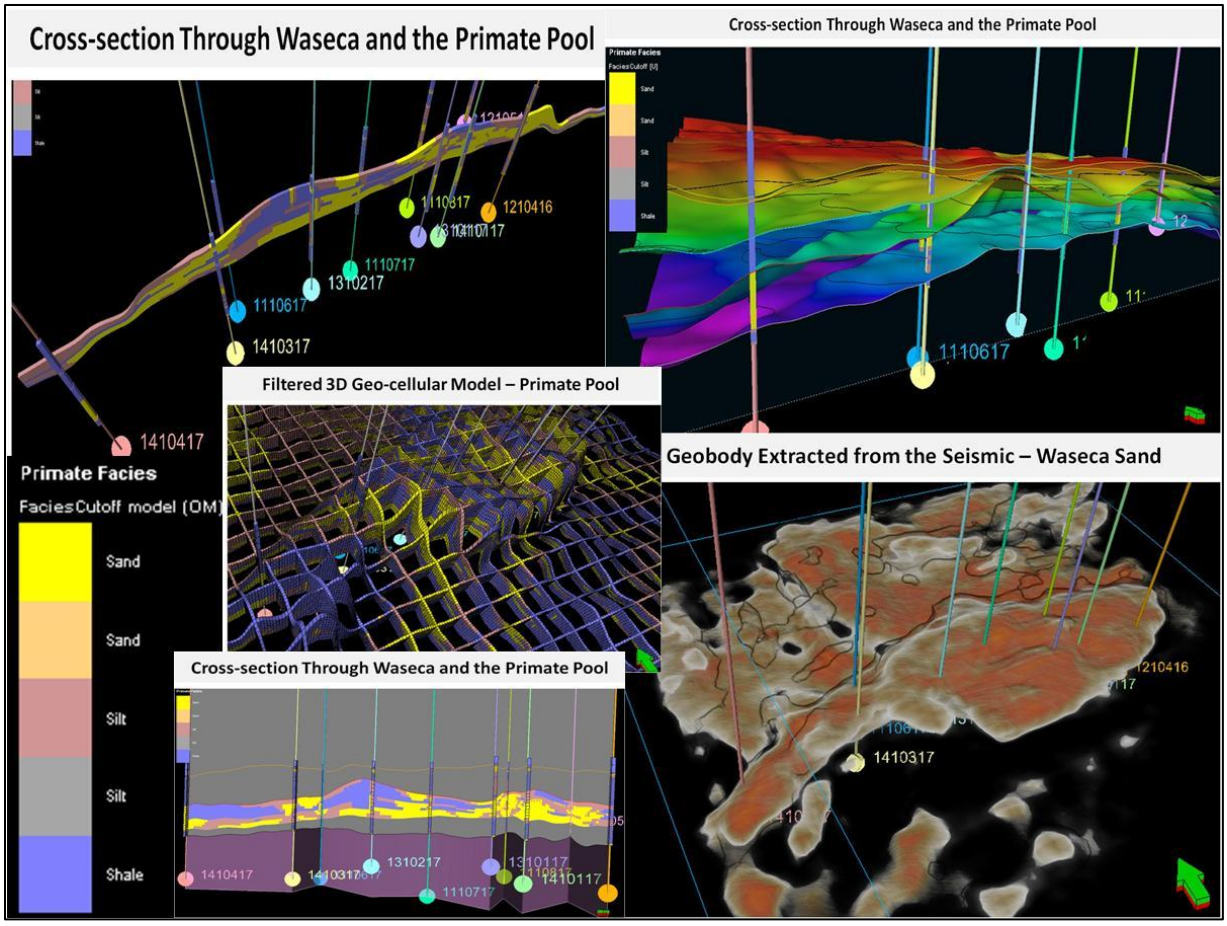

Figure 3-9: Few snapshots of the conventional 3D geological model of the Primate Pool. The top right is the different horizon i.e., McLaren, Waseca and Sparky; right bottom is the extracted geo-body from the seismic; the top left and the front left are slices through reservoir; and the middle center is the grid-cell or faceis distribution in the cells.

3.2 Sedimentary Facies in New model

Sedimentary structures were found in the offset cores and were correlated with the facies associations and facies described earlier. These sedimentary facies have been input into the software SBED's templates (Figure 3-10) based on their physical appearances such as grain size, depositional angles, wave lengths of the laminae, frequency of deposition etc. (Figure 3-11). There are lots of flexibilities in the SBED templates, where changes could be made based on the observation of the cores, which realistically describes the cores in the templates. Shale volume is a factor in the templates that varies depending on the bed-form (sedimentary structure) naturally

and is found in the sedimentary deposits. Based on the shale volume calculation from the observed cores and their log responses, sedimentary facies on the templates have been assigned for the wells that have no cores (Figure 3-11). In this case, shale volume curves became the indicators of the representative sedimentary facies for those wells in the modeling. All the electric facies were translated into sedimentary facies and were stacked individually using the templates to illustrate the near borehole images (Figure 3-16, Appendix VII and VIII). Upscaling these sedimentary features from wellbore scale to reservoir scale, a stochastic facies model for the whole reservoir was built (Figure 3-18). This new model contains the detailed sedimentary facies association related to sedimentary current structures presented in the reservoir. These facies distribution and their characteristics in the model represent the practical and robust approach in reservoir simulation process, which quantitatively estimates the reservoir permeability barriers or heterogeneity volumetrically to evaluate the reservoir performance.

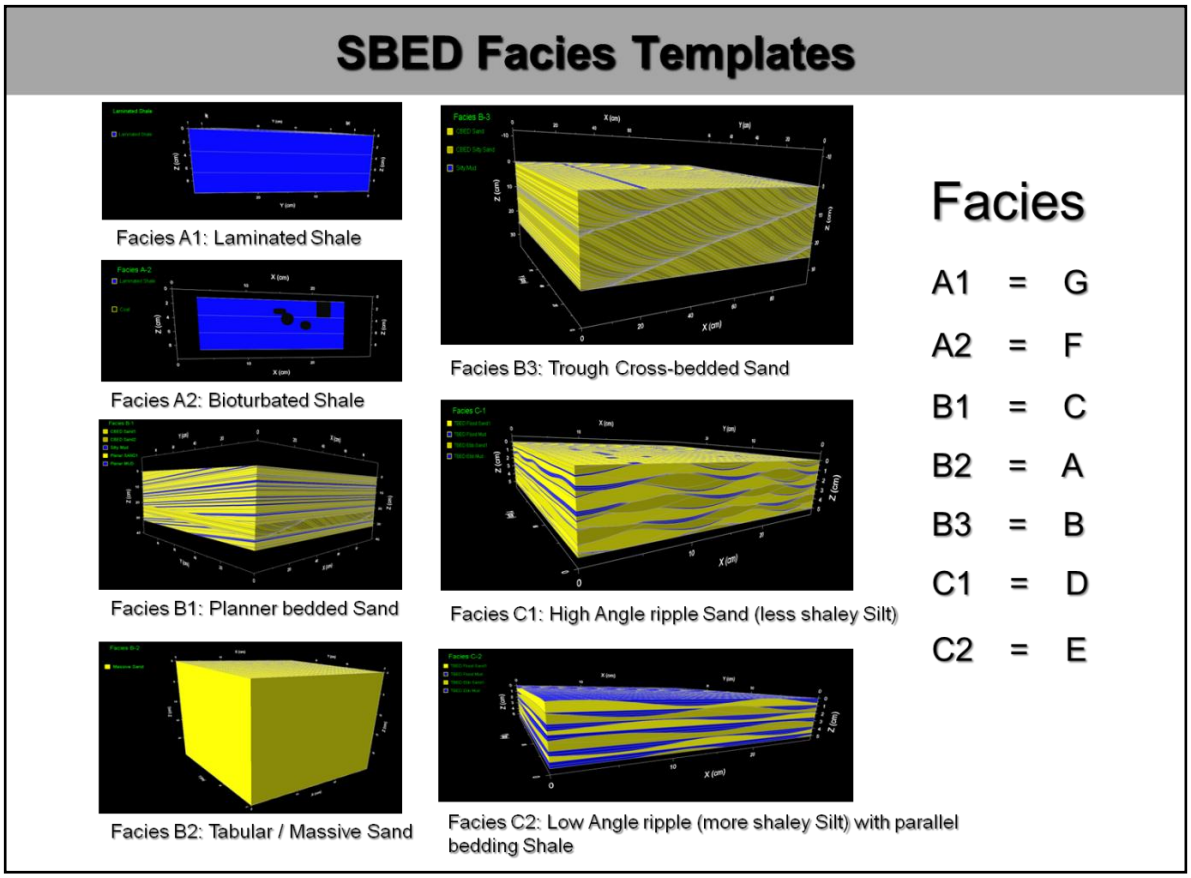

Figure 3-10: Sedimentary structures have been put in SBED templates for the reservoir modeling.

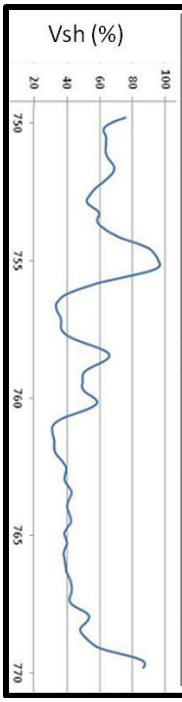

Facies Stacking (The well 1110617)

Depth Interval	Facies Type	Lithology
749.0 – 750.0	Facies A2	Bioturbated / organic Shale
750.0 – 751.5	Facies C2	Silty sand (more sandy)
751.5 – 752.0	Facies C1	Silty sand (more silty)
752.0 – 754.0	Facies C2	Silty sand (more sandy)
754.0 – 756.0	Facies A1	Massive shale
756.0 – 758.0	Facies B2	Massive sand
758.0 – 759.0	Facies C1	Silty sand (more silty)
759.0 – 760.0	Facies C2	Silty sand (more sandy)
760.0 – 760.7	Facies C1	Silty sand (more silty)
760.7 – 763.0	Facies B2	Massive sand
763.0 – 765.0	Facies B3	Sand (low angled lamina- more shaley)
765.0 – 767.0	Facies B1	Sand (high angled lamina – less shaley)
765.0 – 767.0	Facies B1	Sand (high angled lamina – less shaley)
765.0 – 767.0	Facies B1	Sand (high angled lamina – less shaley)
767.0 – 768.0	Facies B3	Sand (low angled lamina- more shaley)
768.0 – 769.0	Facies C2	Silty sand (more sandy)
769.0 – 770.0	Facies A1	Massive shale

Figure 3-11: Sedimentary facies have been translated from the Vsh curve to the well that has no core data, i.e., well 1110617.

3.2.1 High Resolution Up-Scaling

The sedimentary process-oriented modeling enabled the SBED software to generate the geological models by mimicking the physical processes behind sedimentary bedding, such as bedform migration, erosion and deposition (X. H. Wen et al., 1998). The approach formulates the deterministic geological processes in a stochastic framework for further geostatistical analysis, thus combining advantages of both the deterministic and stochastic modeling methods. This is the reason that the SBED models are so geologically realistic over the conventional geostatistical approaches, which are either object-based or cell-based (Jonoud et. al., 2008). The modeling algorithms in SBED software capture the heterogeneity at different spatial scales and for specific sedimentary environments, such as fluvial, shore face and a deep-water environment, which is significant in terms of reservoir characterization (Figure 3-12). Most importantly, the process oriented modeling approach is flexible and is able to reproduce any stratigraphic geometry in 3D as long as a conceptual model is available.

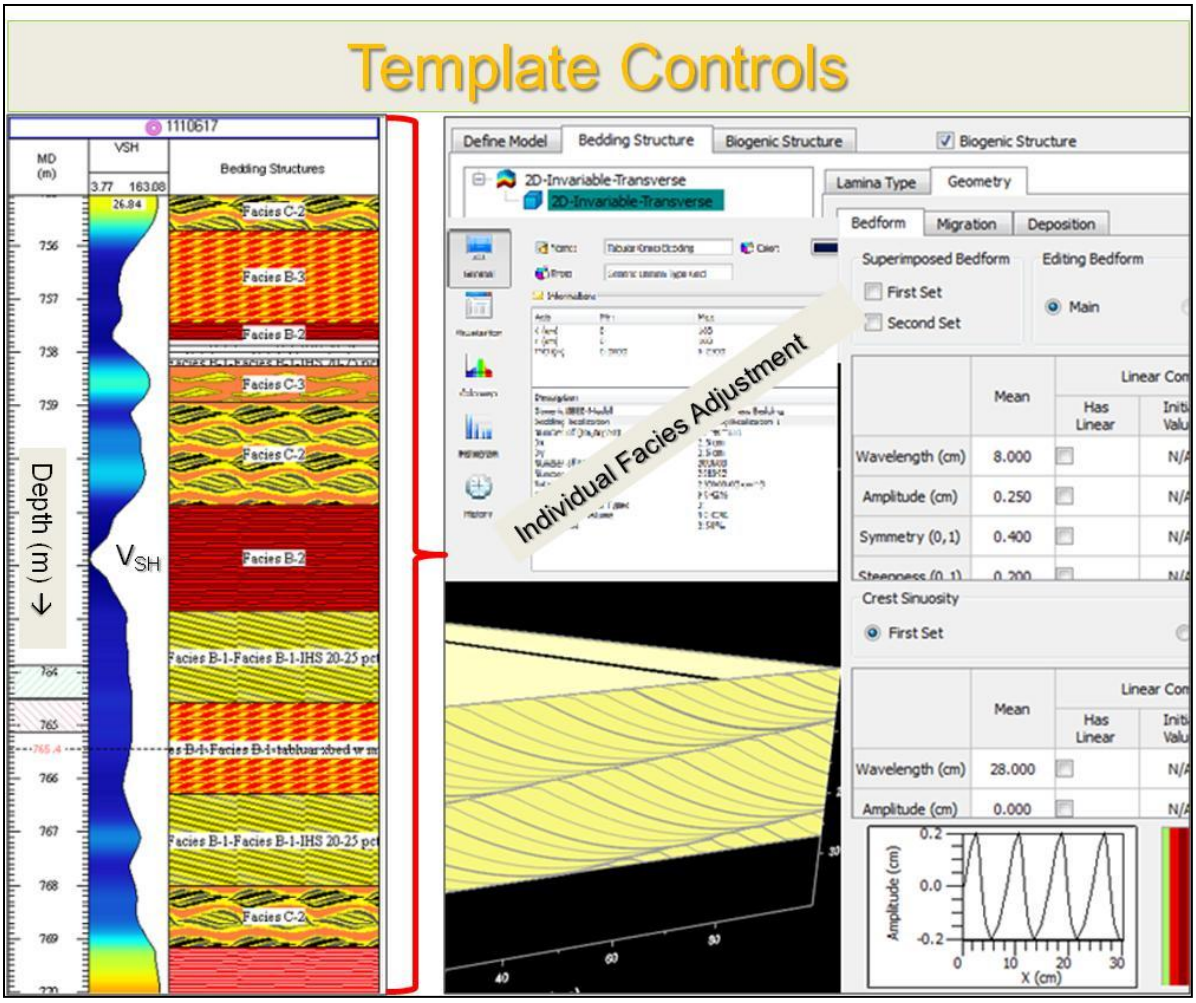

Figure 3-12: Showing the relationship of shale volume and the sedimentary facies for an individual well. An example of SBED controls is shown at the right side in brief.

In the process of up-scaling the Primate data, 'SBED Reservoir Geomodeling' conditioning feature allowed to select the reservoir grid i.e. Primate grid, well data that intersect the reservoir grid, log responses and averaging method where 'Arithmetic' averaging was used in this study. SBED then averaged every well log sample i.e., Vsh positioned in relation to the corresponding Primate grid-cell intersected by the well. Each grid-cell contained one value representing the arithmetic average of Vsh sample points found in that Primate grid-cell. The next step was to create an SBED facies stack model, whereby SBED facies of specified Vsh were positioned relative to the up-scaled Vsh representing the extrapolated expected sedimentary features. The unique single phase 'flow simulation based' permeability upscaling mechanisms are illustrated in the Figure 3-13 and Figure 3-14. Pickup (2000) showed the detail of this new method of upscaling using effective phase tensors mechanism. She also proved the case of

arbitrary viscous/capillary or viscous/gravity ratios and how the models work for cross-bedded systems (Pickup et. al., 1996).

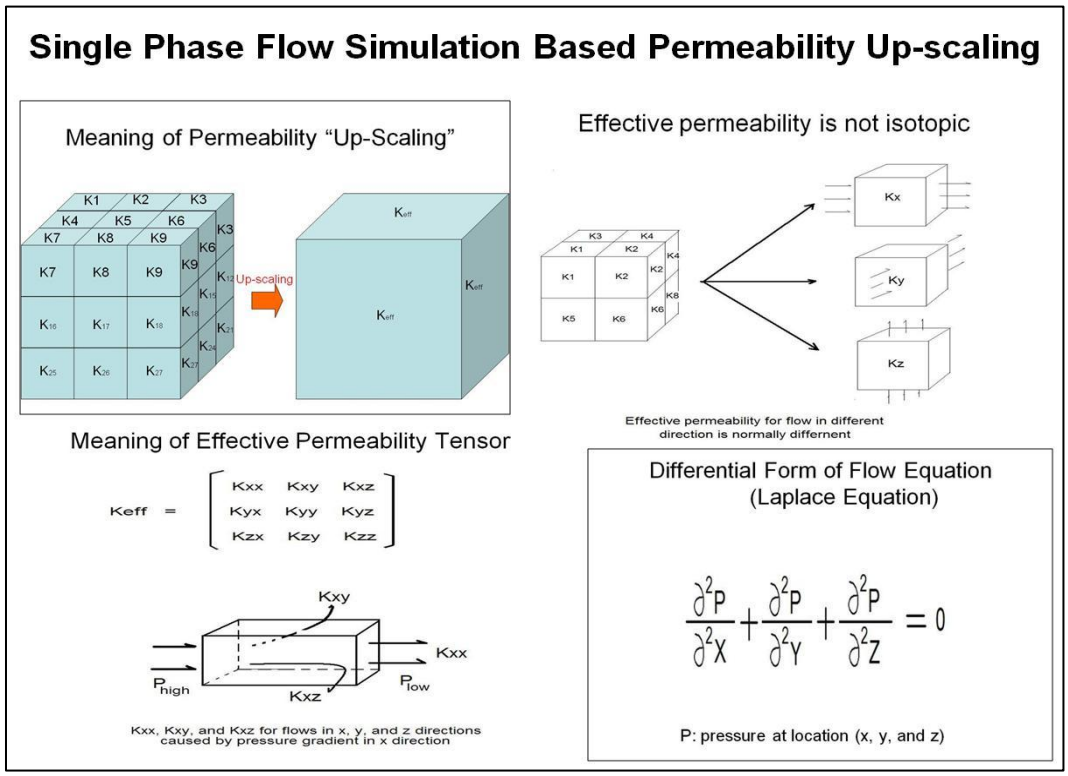

Figure 3-13: SBED's single phase flow simulation based up-scaling is shown in the diagram (Pickup 2000).

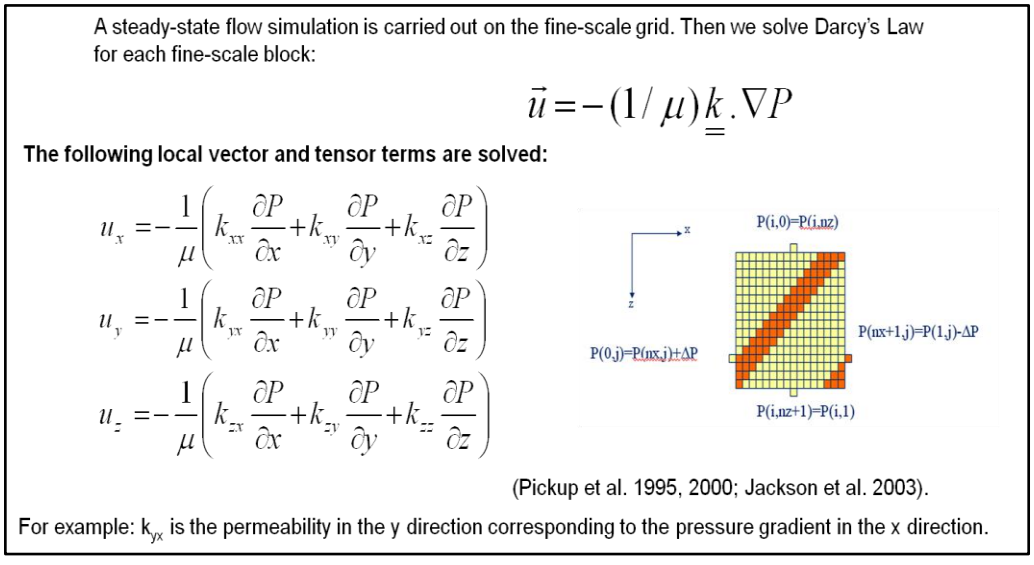

Figure 3-14: SBED's tensor based up-scaling calculation for permeability is shown in the diagram (Pickup et. al., 1996).

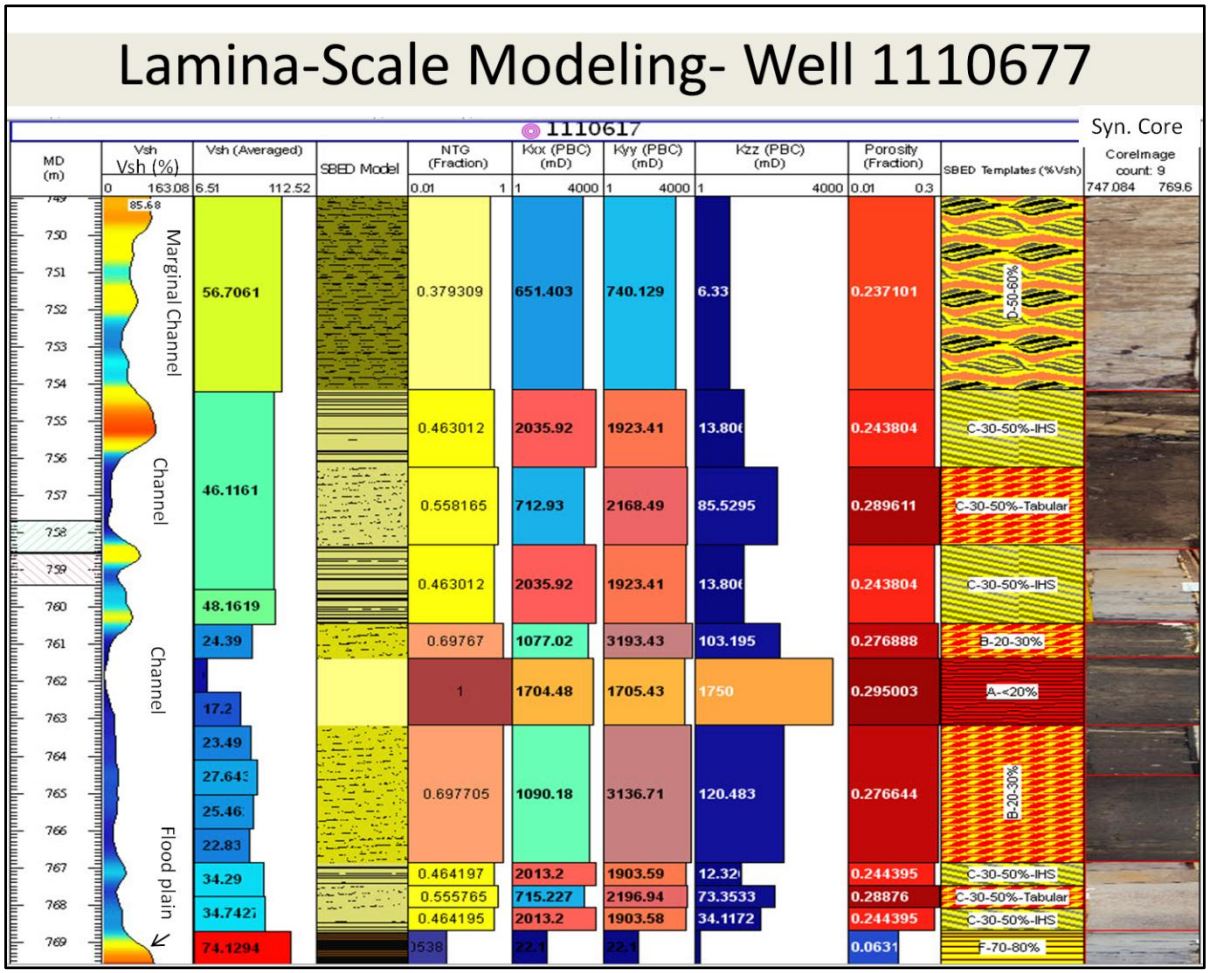

Figure 3-15: Up-scaled reservoir properties (Por, Perm) based on the detailed facies classification and building a synthetic core.

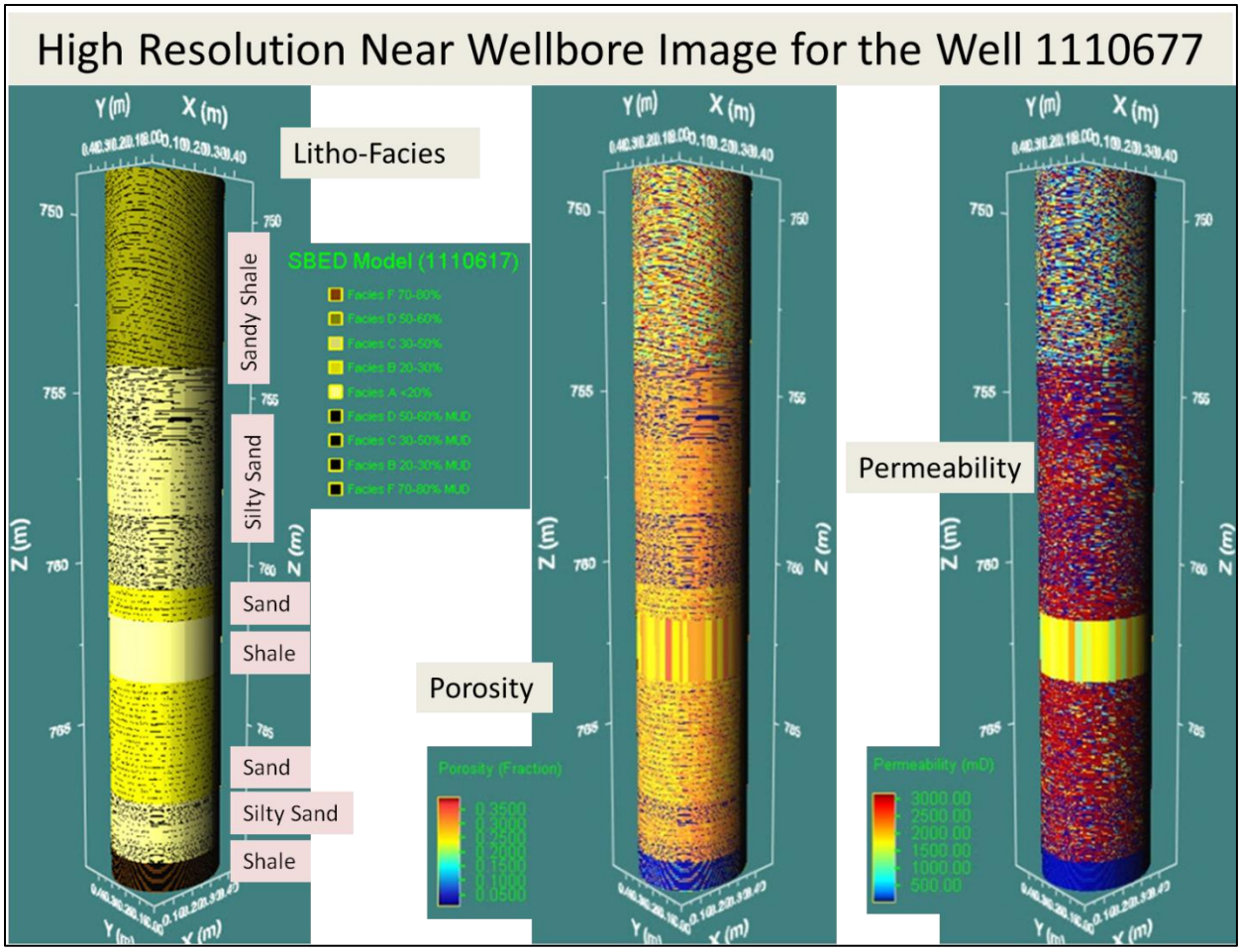

Figure 3-16: High resolution (cm-level) near wellbore image shows reservoir properties (Por, Perm).

Using the 'in-built' SBED up-scaling, all the 10 wells have been up-scaled (Appendix VI) and the facies are stacked in the wellbore scale that reflects all the detail of the sedimentary facies and facies associations (Figure 3-15) and preserves the reservoir attributes in its original state in the near wellbore environment. All the 10 wells were then up-scaled to the reservoir scale from SBED model to Petrel Model framework (Figure 3-17), where the 3D geo-cellular model represents the entire reservoir attributes and their distributions in the reservoir for the simulation and volumetric calculations (Figure 3-18, 3-19 and 3-20).

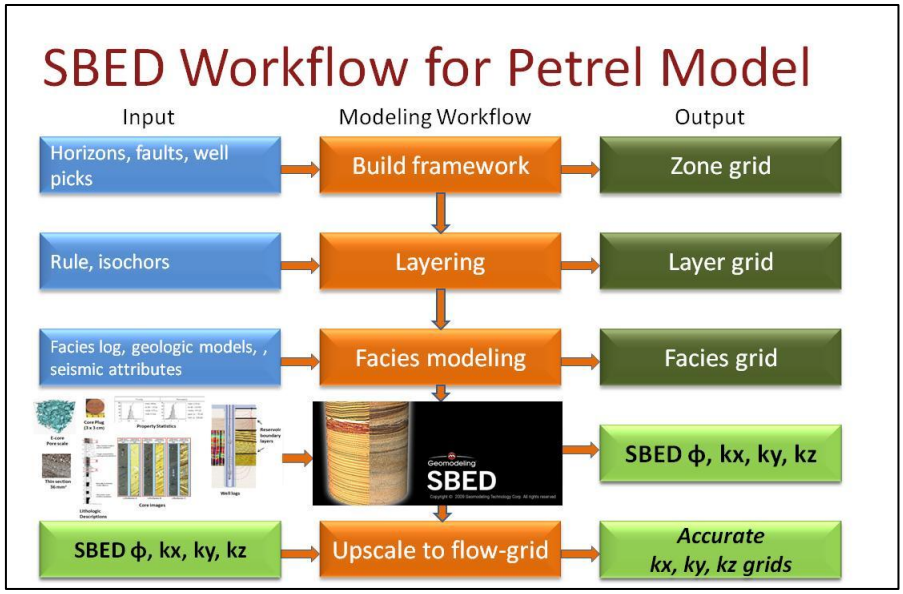

Figure 3-17: Flow chart of transferring SBED properties to Petrel Model (Source: Geomodeling Technology Inc.).

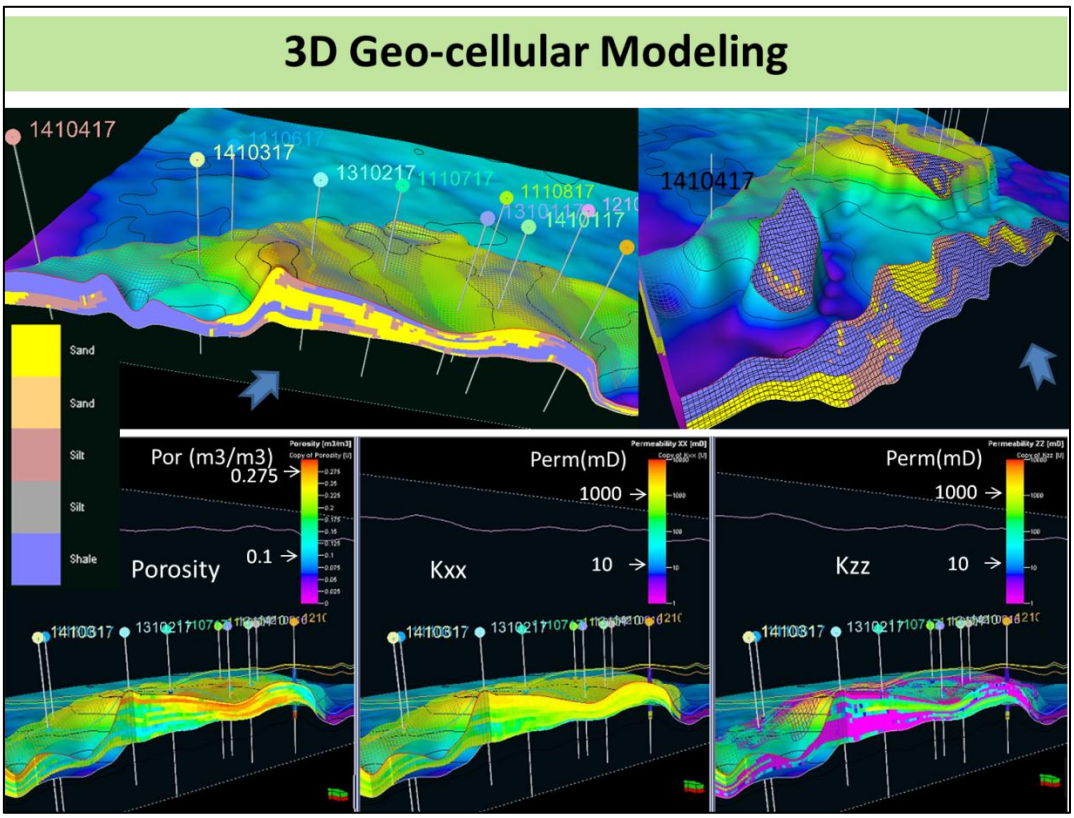

Figure 3-18: New model shows the property distributions in different sections; the top two are slices from different angles, the bottom left is porosity distribution, bottom middle is horizontal permeability distribution (Kxx) and the bottom right is vertical permeability (Kzz) distribution over the Primate Pool in a 3D geo-cellular Model to be used for reservoir simulator.

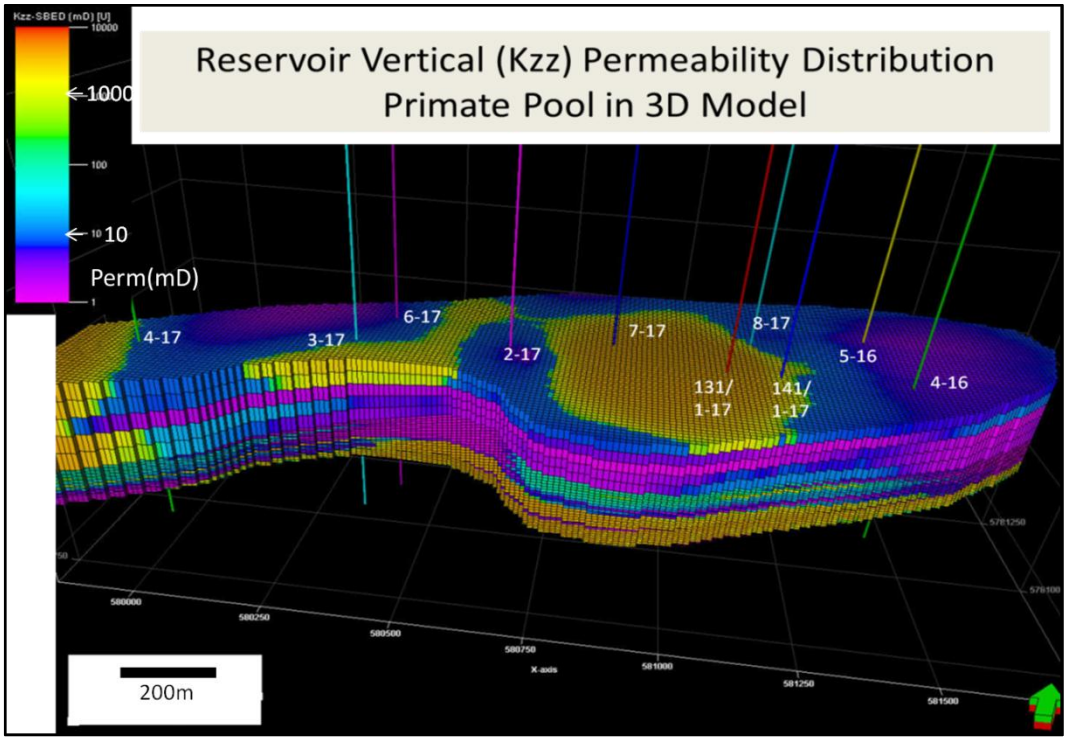

Figure 3-19: Reservoir property i.e., Vertical permeability distribution in the production footprint area of the Primate Pool in a 3D geo-cellular Model.

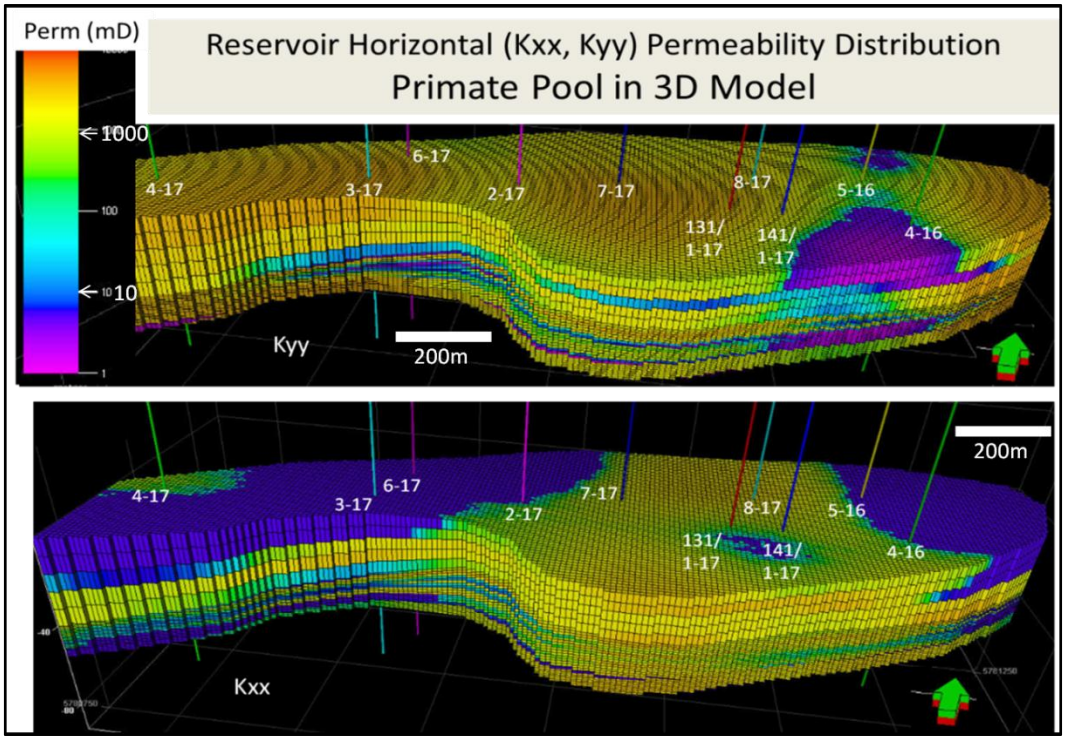

Figure 3-20: Reservoir property i.e., Horizontal permeability (Kxx and Kyy) distribution in the production footprint area of the Primate Pool in a 3D geo-cellular Model.

3.3 Production History Matching

The Primate CHOPS field was first discovered in 2005 and was developed to date with 12 vertical wells using CHOPS as a production mechanism. Ten wells (Table 1-1) were taken into consideration for this current study. The production profile is given in the Figure 3-21. A comparison of the production history of the individual wells and the theoretical estimated production based on the reservoir properties are listed in the Table (3-1). The calculation was done based on the reservoir properties given in the Appendix IX. This comparison reflects the accuracy of the reservoir properties used in the estimation and the reliability of the geological model. This matching between the production history and the results also reflects the complexity of the reservoir, such as the net pay thickness and the oil production are not conformably related, which means that the reservoir has heterogeneity. The gross sand thicknesses of the wells and the amplitude attributes from both the 3D and 4D surveys were plotted (Figure 3-22) and compared with the individual production with the gross sand in the Figure (3-23) and Table (3-2).

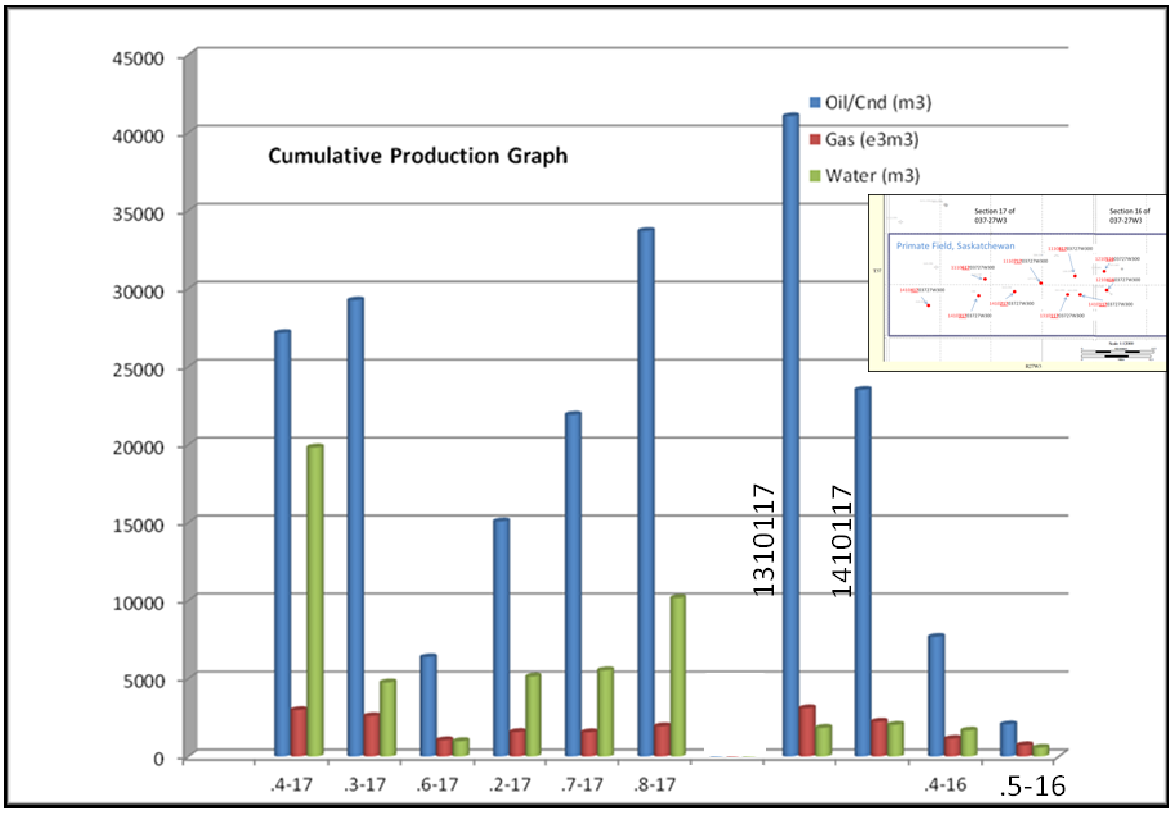

Figure 3-21: Cumulative Production History of the Primate Heavy Oil Pool from 2005. The inset map refers to the Figure 1-2.

Table 3-1: Comparison of the Cumulative oil production by individual well and the estimated recoverable oil production from the conventional method based on the reservoir properties. The format of the well name is corrected in table 3-2.

Production History Matching by Individual Well						
Well Name	Gross Sand (m)	Net Sand (m)	Net/Gross	Oil Prod (m3) in Real	Oil/Cnd (m3) in Estimation	Difference (%)
.4-17	20	7	0.35	26667	27161	1.82%
.3-17	10	5	0.50	16340	29252	44.14%
.6-17	14	7	0.50	18737	6364	-194.42%
.2-17	12	8	0.67	18228	15078	-20.89%
.7-17	18	15	0.83	28159	21911	-28.52%
.8-17	15	12	0.80	20690	33693	38.59%
.1c-17	13	7	0.54	20723	41044	49.51%
.1d-17	21	14	0.67	23085	23506	1.79%
.4-16	5	4	0.80	6908	7669	9.93%
.5a-16	20	8	0.40	10362	2059	-403.23%

3.3.1 Volumetric Estimation and OOIP Calculation

The OOIP (Original Oil in Place) was calculated for each well individually, taking into account the unique drainage areas, porosity thicknesses, S_W values (Appendix IX). All other properties (pressure, compressibility, formation factor etc.) were thought to be equivalent for all included wells (Appendix IX). Usually the average porosity of the producing zone and its associated net pay thickness is multiplied together to create phi-h maps for the upper and the lower sands. In this case, considering the CHOPS mechanism, the porosity is considerably uniform for the unconsolidated sands and the variation only happens for the shalyness and the lithologic heterogeneity. Values for the shape correction were assumed based on the drainage (in this case wormhole) radius usually around 100 to 150 meters. The calculated OOIP was then multiplied by a recovery factor of 0.06 to 0.07 yielding the producible oil (Appendix IX). This is a primary estimation to validate the reservoir properties and the model, and the way to calculate the remaining oil in the Primate pool with additional wells to be drilled.

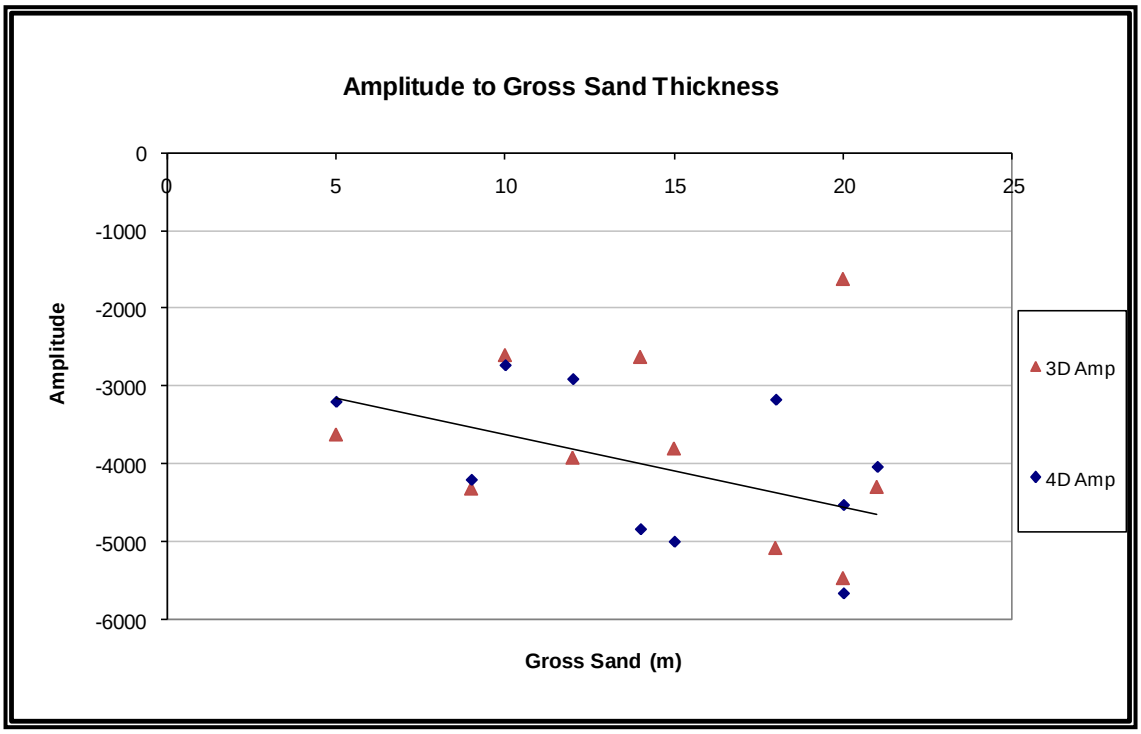

Figure 3-22: Illustrates the relationship of amplitude and gross sands where amplitude increases with the increasing gross thickness. The exceptions are the reflection of heterogeneity that was not counted in proper net to gross estimation.

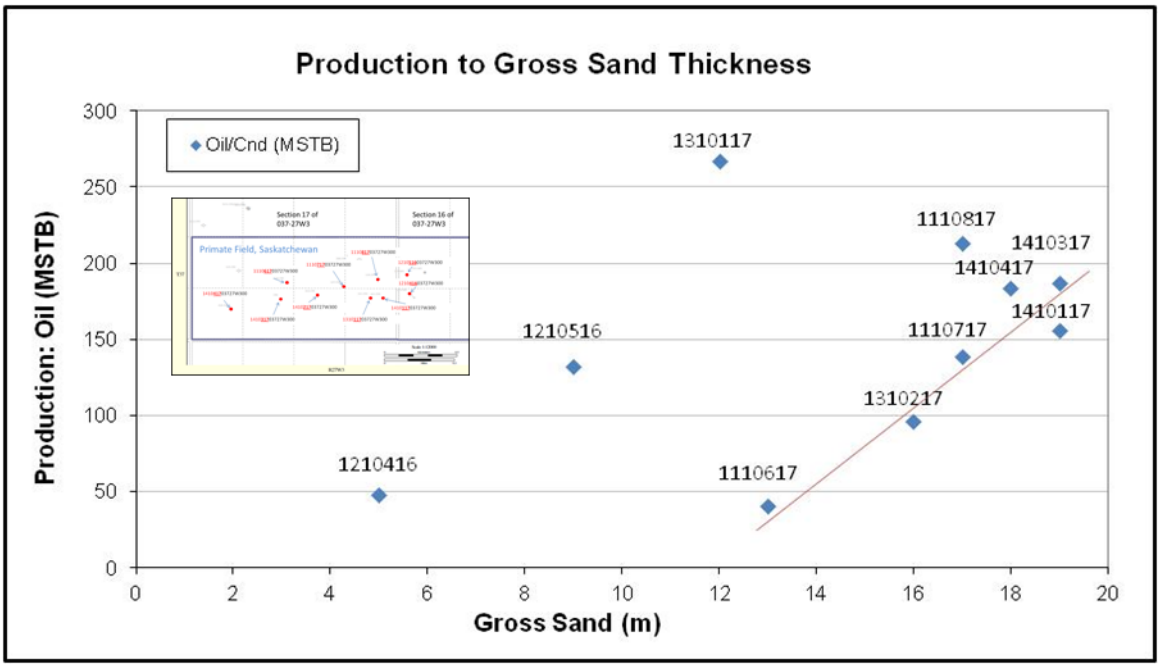

Figure 3-23: Relationship of the cumulative production and the gross sands of the ten wells of the Primate pool. The map refers to the Figure 1-2.

However useful, this method of calculating OOIP was found to be limited and likely less accurate than production analysis. Uncertainty in properties like $S_{W,}$ the sand volume from the production and recovery factors could have large sources of error.

Table 3-2: Reservoir attributes and the production summary of the ten wells.

Reservoir Attributes					Cum. Production		
Well Name	Gross Sand (m)	3D Amp	4D Amp	Corrected Well Name	Oil/Cnd (MSTB)	Gas (MMCF)	Water (MSTB)
.4-17	18	-1623	-4530	1410**417**	184.1	111.61	125.6
.3-17	19	-2598	-2733	1410**317**	186.84	95.26	30.37
.6-17	13	-2622	-4841	1110**617**	40.2	38.02	6.59
.2-17	16	-3912	-2911	1410**217**	95.89	58.41	32.49
.7-17	17	-5069	-3176	1110**717**	138.54	57.71	34.95
.1c-17	12	-4792	-4044	1310**117**	266.79	114.68	12.51
.8-17	17	-3794	-5002	1110**817**	212.81	70.61	64.7
.1d-17	19	-4287	-4040	1410**117**	155.54	83.79	14.05
.5a-16	9	-5455	-5666	1210**516**	131.78	74.1	49.13
.4-16	5	-3615	-3203	1210**416**	48.26	40.53	11.26

DISCUSSIONS AND LIMITATIONS

In finding the relationships of the sedimentary facies and the wireline log responses, many efforts have been taken with the invention of wireline logging tools. Modern logging tools such as Dipmeter and FMI (Formation Micro-Imager) provide enormous information about the bedding structures near the borehole. These tools are expensive and are not commonly used in most cases. Without these, no other tool can directly indicate the sedimentary bed-form patterns from the conventional logging yet. The petrophysical characterization of heterolithic reservoirs is still a very demanding and challenging task, as the very thin alternations of sandstones, siltstones and shales cannot be truly resolved by conventional wireline logs. Even core data from laminated shaly sandstone reservoirs can be misleading as it's subject to interpretation. The significance of clay or shale volume and distribution on a reservoir rock's 'flow and storage' properties has long been recognized. Sometimes laminated shale may have little effect on the intrinsic reservoir properties. However, the use of improper models in many cases may result in underestimation or overestimation of reservoir potential and hydrocarbon reserves.

4.1 Data Integration and Multi-scale Resolution:

Data integration and resolution are the key factors that affect reservoir optimization, along with many unknown factors. Reservoir attributes from geophysical and geological data are used in flow simulation and production history matching where the low resolution factor limits the best possibility. Different data acquisition methods have different resolution limits and are compared in the Figure 1-10. Multi-scale data resolution is a problem in lateral and vertical distribution of the reservoir properties, especially where seismic data of mega-bin (30mx30m) acquisition is difficult to correlate with higher resolution wireline log data (Figure 4-1). From the wireline log data, many visible events in vertical distribution were also discarded in the reservoir simulation process, such as small scale impermeable baffles (Figure 4-2). Figure (4-2) shows part of the cross section of the Primate pool where the reservoir sand porosity is over 30% and resistivity is over 30 ohm-m representing a good quality producing zone. In modeling and simulation these cut-off values are taken in block or net to gross calculations, which don't represent the proper characters of these baffles in the reservoir performances.

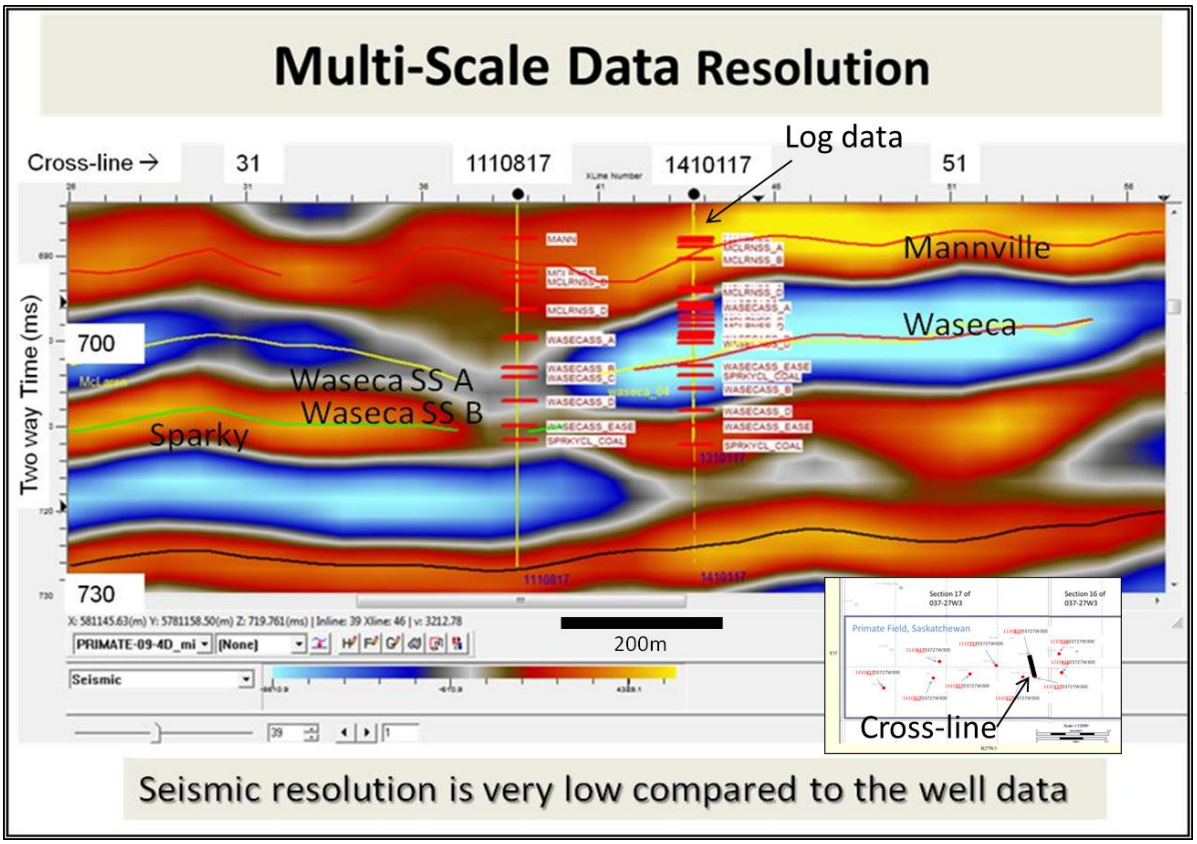

Figure 4-1: Comparison of the wire-line log data resolution to the seismic data (inset map refers to Figure 1-2).

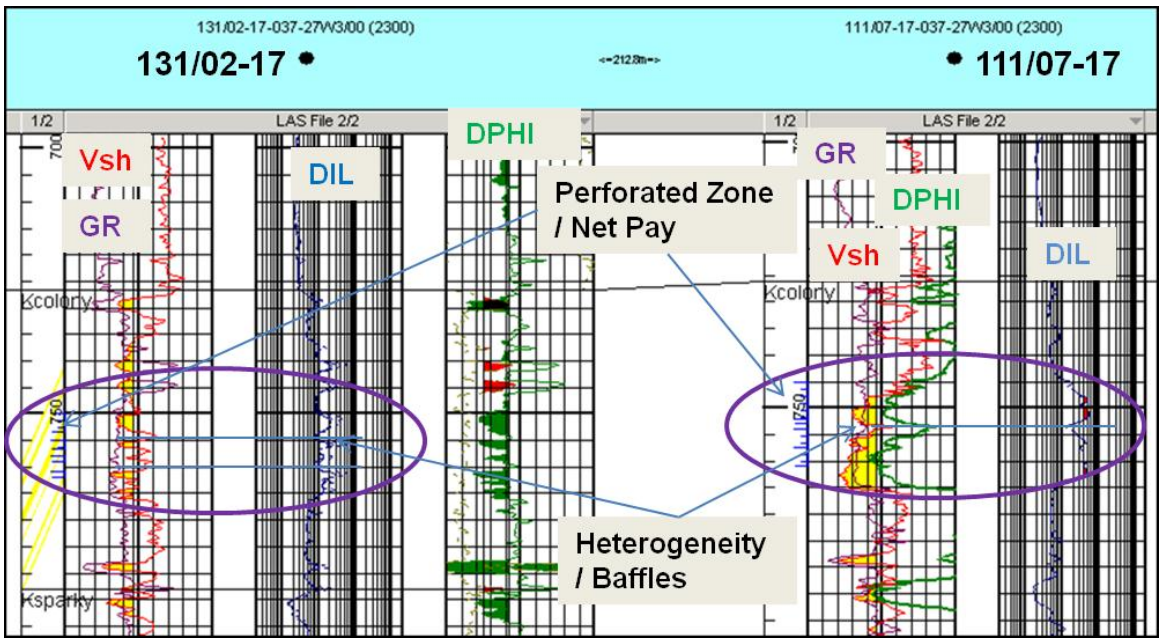

Figure 4-2: Log responses from the perforated intervals show the visible reservoir heterogeneity, which are not considered in the traditional reservoir simulation.

In characterizing the reservoir quality and the reservoir rocks, density data is plotted against the slowness of the sonic data (Figure 4-3) to identify a clear bi-modal nature of distribution over the pool area. This is an indication of the amalgamation of different types of reservoir sands, i.e., incised-channel. The depositional environments of the channel sands are well recognized for the current study. The characteristic features of a fining upward sequence and the vertical sequence of sedimentary facies can be interpreted as a lateral accretion within a point bar. Tidal influence within the meandering fluvial system can produce sandstone and mudstone couplets on the lateral accretion surfaces. In reconstructing the palaeo-environment, all these features were correlated with reservoir properties to illustrate the high resolution (cm-scale) near wellbore model for this project derived from offset cores. The near wellbore models were created using SBED software, which models core to bedset-scale sedimentary and petrophysical heterogeneity.

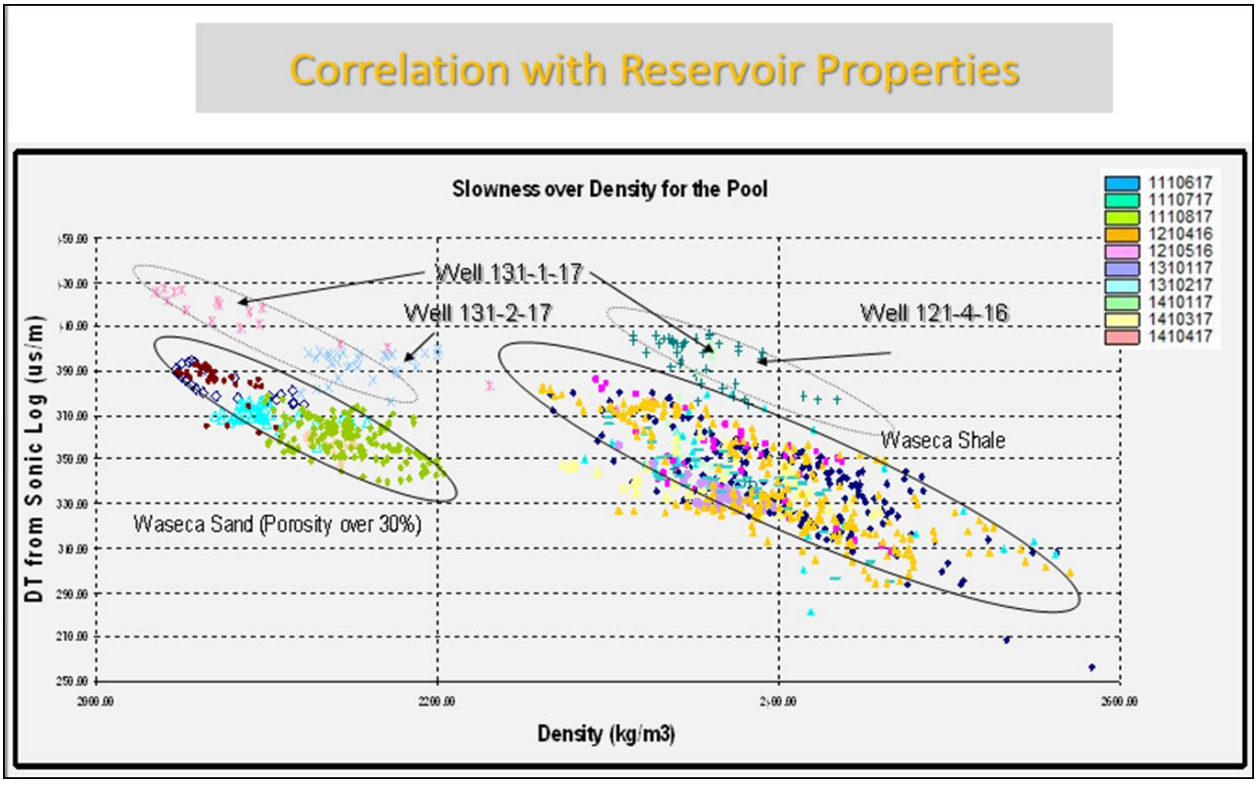

Figure 4-3: The reservoir attributes density and sonic slowness of net pay zones show two distinct characteristics of the reservoir sand and shale in the Primate Pool.

SBED software is a process-oriented modeling (POM) approach that reproduces sedimentary bed-forms to provide up-scaled petrophysical properties i.e., porosity and directional permeability from core plug, mini-permeameter and pore-network scale analyses. There is a missing step in the conventional practice of reservoir modeling using geostatistics that starts from the core-plug data to geostatistical simulation grid. Two fundamental statistics of reservoir properties: 'mean' and 'standard deviation' of porosity and permeability are used from core-plug data into the simulator, where geostatistical simulation grid is on a meter to tens of meter scale and the core-plug data is from a centimeter scale. SBED makes the bridge of this gap (Wen et al, 2008) among core plug data, geostatistical simulation grid, and the flow simulation grid to represent the reservoir attributes in their best resolution with data integrity (Figure 4-4). The output 3D model of this current study is the unique example of a CHOPS field, where small scale (cm-level) reservoir heterogeneity estimation as permeability barriers will play a very important role in reservoir performances.

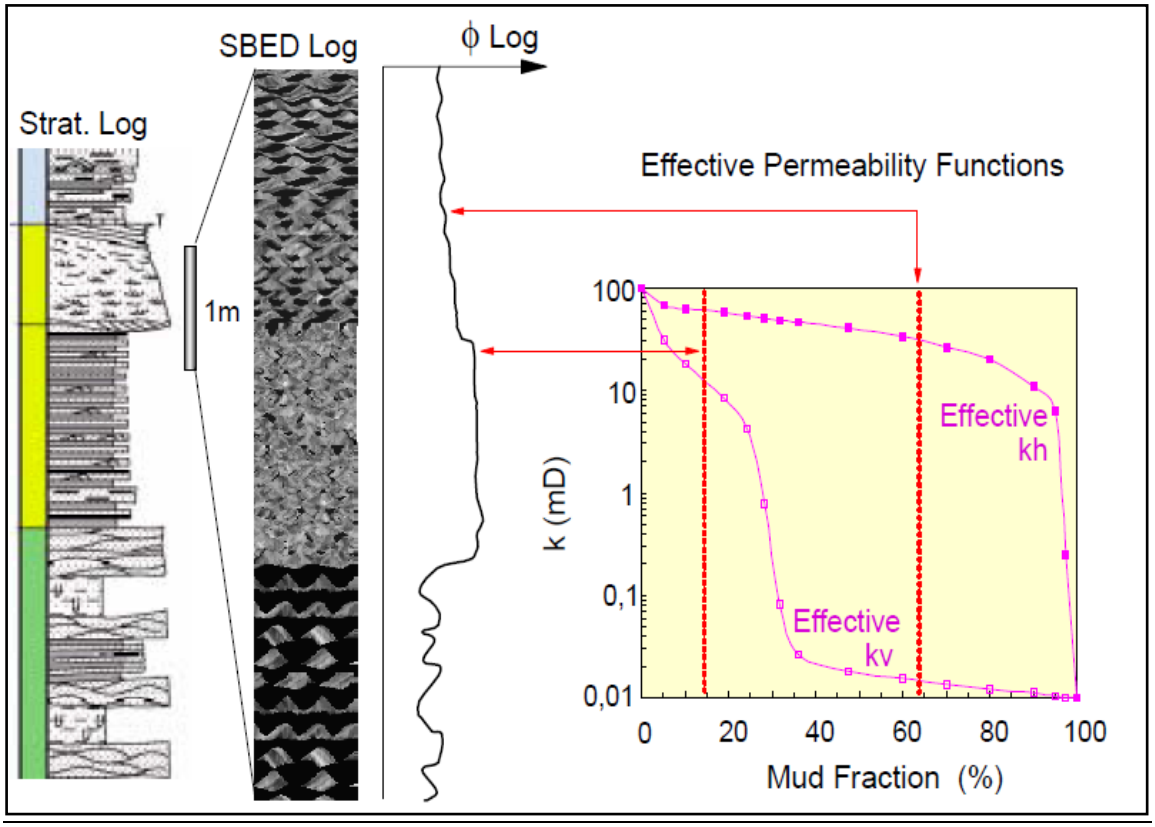

Figure 4-4: Transformation of a litho-stratigraphic log via the SBED model into a set of permeability flow function (Wen et.al., 2008).

4.2 Production Footprints or Wormholes:

Amplitude anomalies from the time-lapse seismic interpretations (Figure 4-5) along with Vp/Vs ratio maps (Figure 2-6) clearly show the gas or foamy oil affected area due to the production footprints of CHOPS mechanism. This production footprint or 'wormhole' area needs to be carefully avoided for any infill or additional drilling in the reservoir. Wormholes are zones of high permeability conduits in CHOPS pool and cannot be interpreted from the conventional seismic data due to its resolution limit. Though the reservoir volume of the Primate pool has been attempted to extract from the acoustic impedance (Figure 4-6), which was constraint to further analyses of reservoir attributes due to its vertical resolution limit. Using high resolution near wellbore imaging and flow based up-scaling of porosity and permeability in the simulation grid resulted in a high resolution directional permeability distribution grids (Figure 3-19 and 3-20). The highly permeable horizontal permeability axes (Kx and Ky) are interpreted as the potential wormhole's direction of propagation (Vasheghani et.al., 2008) (Figure 4-7). This potential direction and the 4D production footprint together can provide better knowledge about the potential wormhole distribution throughout the Primate pool in the reservoir simulator.

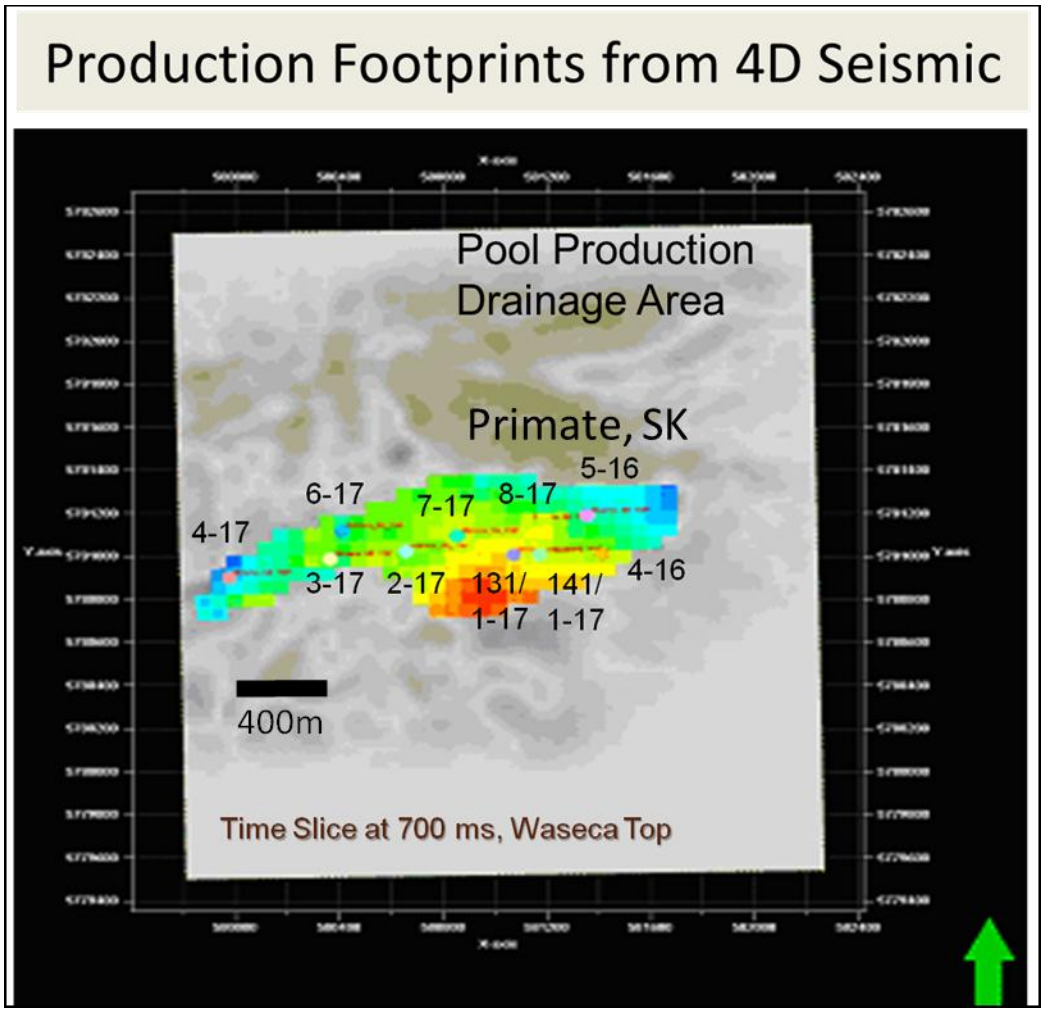

Figure 4-5: Amplitude anomaly between time-lapse seismic 3D interpretation of the surveys 2004 (base) and 2009 (monitor) in Petrel.

` The grid-block permeability is usually influenced by the boundary conditions require in the flow equations and the size of the grid-blocks. Wu et. al. (2002) showed that the up-scaling errors due to both effects are obvious as the quality between the small physical scales of the media and the artificial size of the grid blocks. An accurate computation for a better solution often requires a tremendous amount of computer memory and CPU time, which can easily exceed the limit of today's computer resources. In this study, 1.6 million grid cells were counted from the conventional model and the numbers jumped to 7.5 million in the high resolution near wellbore facies model. Using the maximum efficiency of today's computing power, averaged Vsh value from the continuous log was used to create the grid boundaries and an example is shown in the Figure (4-8).

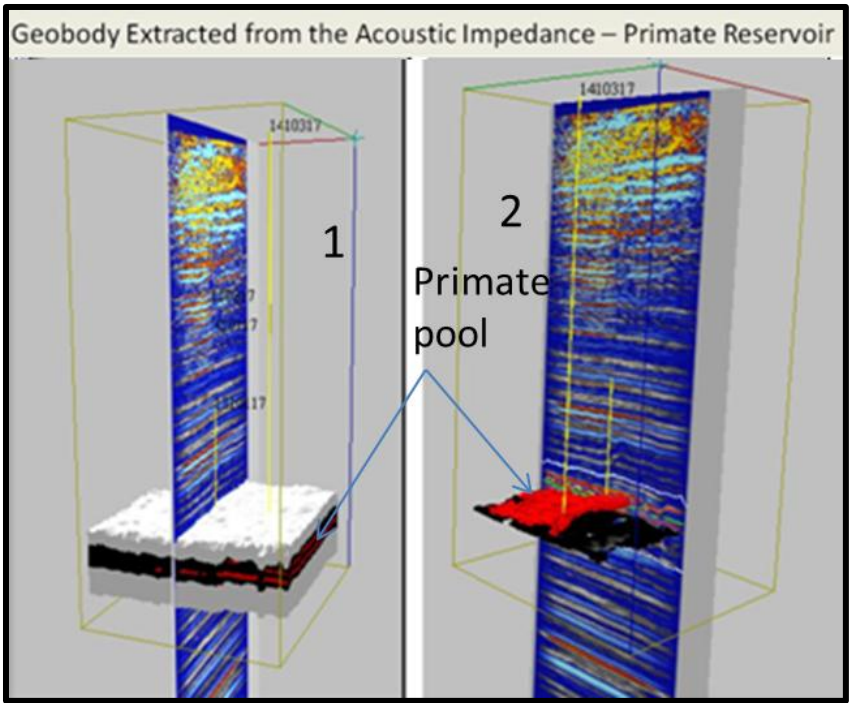

Figure 4-6: Overview the Primate reservoir (McLaren – Waseca) from the seismic interpretation. The extracted geobody was shown in Figure 3-9.

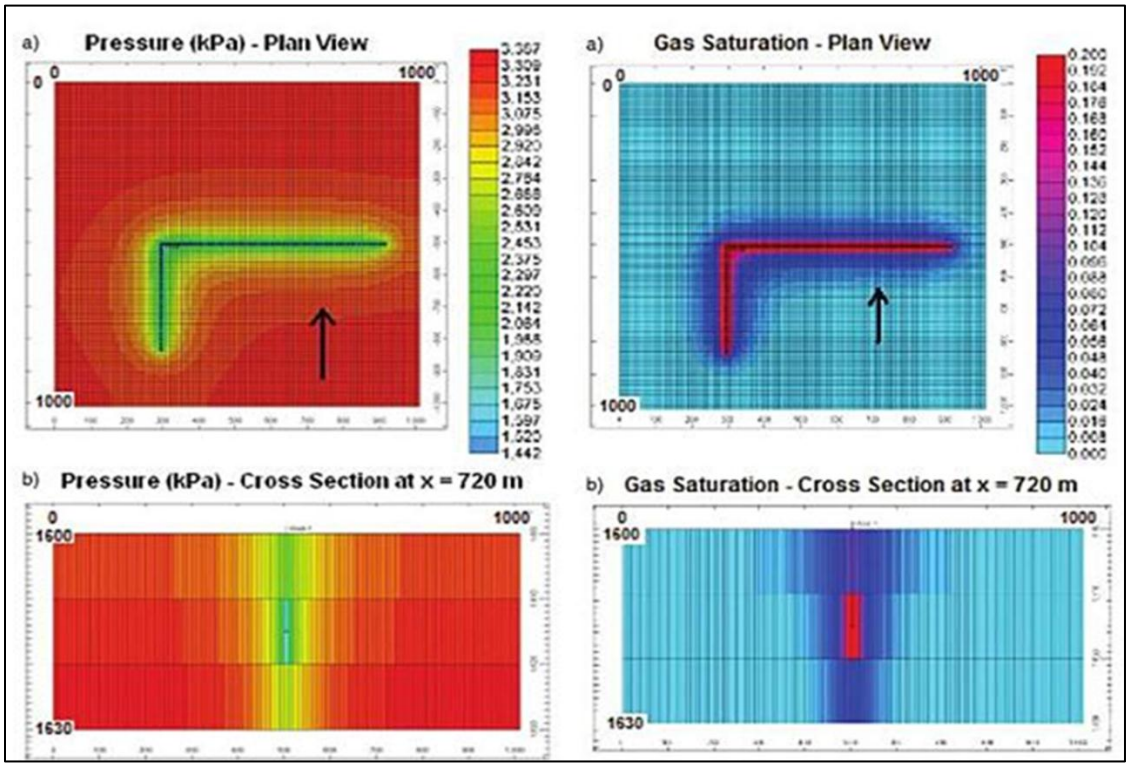

Figure 4-7: Direction of the wormholes and foamy oil extent in between kxx and kyy (Vasheghani, 2008).

4.3 Estimation of Reservoir Heterogeneity:

Thomas-Steiber's (1975) method, which outlines the effect of clay distribution on log responses, was used in this study to confirm the presence of dispersed and laminated shale in the reservoir (Figure 2-8 and 2-9). In this study the log-facies determinations were validated with the Thomas-Steiber's cross plots as one of the criteria. The laminar shale and dispersed shale in the channel sands were examined by comparing the Thomas-Steiber's graph with the offset core data of neighbouring wells in the similar geological settings (Figure 2-12 and 2-13) and used in correlation of the petrophysical data. The core data from the neighbouring wells practically reflected the heterogeneity and was respected accordingly.

The lithological meaning of the log-based facies was interpreted from a sedimentological perspective and defined a link with the sedimentological-depositional model. The seven (from A to G) log-based facies described the reservoir variation in term of sedimentary facies (Table 2-1). Three major sedimentological types broadly cover the seven facies classes. The lithology varies from massive sands (channel deposits), cross-bedded sand and silt (marginal channel or channel fill), wavy ripples of silt and shale to thin laminated shale (non-channel or flood plain). The lithological trend highlighted by the V_{SH} is recognizable in the variation of the log-based facies and the link with the depositional model of the fluvial channel system can be confirmed (Figure 2-15 and 3-6) as mentioned in literatures (Christopher, 2002).

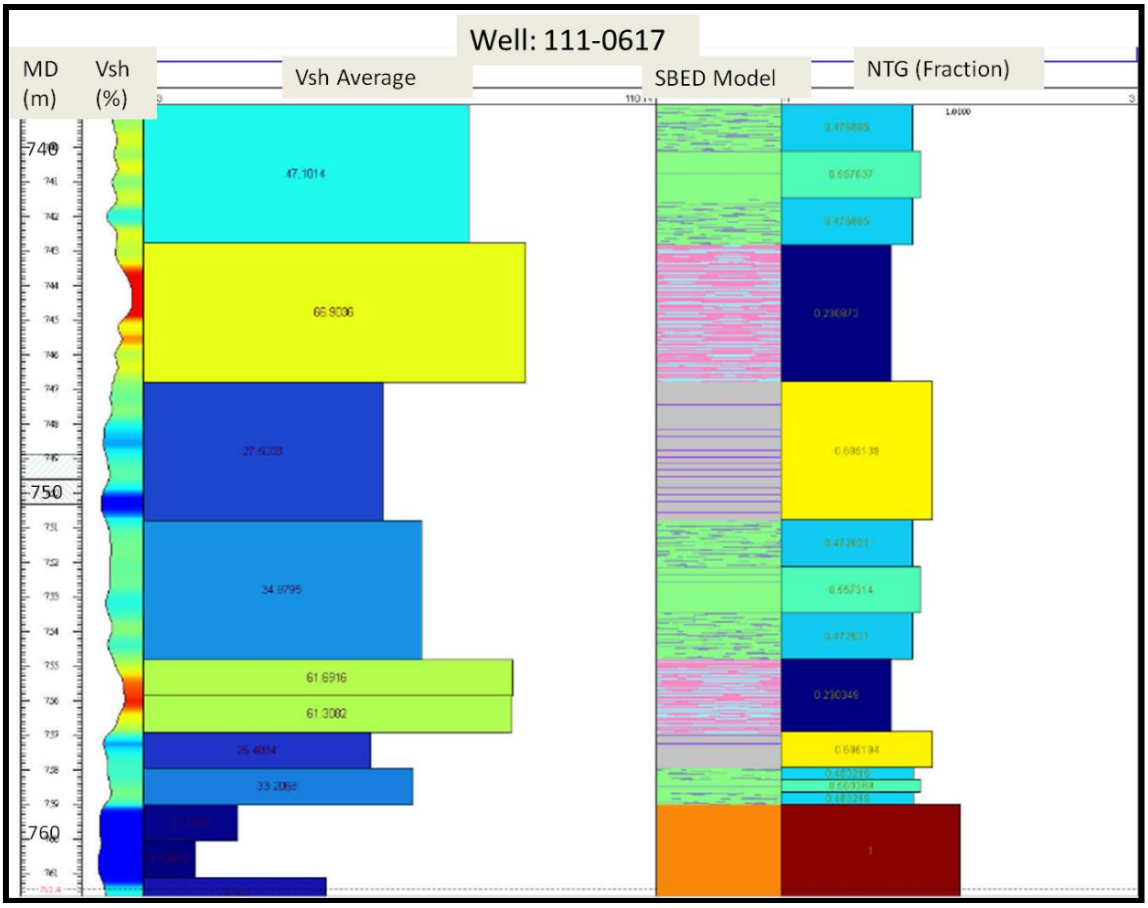

Figure 4-8: Averaged Vsh value from the continuous log is used to create the grid boundaries as shown for the well 111-0617.

The high resolution reservoir properties in near wellbore model finally transferred to full scale reservoir model in Petrel and the flow diagram is shown in the Figure 3-17. A detail volumetric calculation in the reservoir simulator from this model will enable better prediction of reservoir performance (Figure 4-9). Based on this model, precise changes in the reservoir attributes such as porosity and directional permeabilities, as shown in the Figures (4-10, 4-11 and 4-12) can affect the reservoir performances at the pool-scale. A quantitative estimation of the mean permeability distribution along with directional permeabilities was compared for an individual well, i.e., 1110617 and is shown in the Figure 4-10 and 4-11. The results (Figure 4-11 and 4-12) show that the horizontal permeability of the laboratory data and the model data do not differ that much with few exceptions (unconsolidated part is shown on the left graph of the Figure 4-12), whereas the permeability distribution to the vertical direction differ greatly. This effect of the vertical permeability barrier is the reservoir heterogeneity and needs to be properly considered in

reservoir simulation in order to achieve the most practical output. Horizontal permeability barriers will also be considered in the simulator as litho-facies changes laterally.

4.4 Reservoir Performances and Prediction:

All the petrophysical modeling is based on litho-facies. The geometric distributions are determined by the geologic knowledge of the facies deposition, and the flow units controlling the production of a reservoir are generated directly from these facies and facies distributions. The challenge lies in producing a reliable 3D facies model to guide the field development plans and strategies. One common reason for this challenge is the lack of integration of all available data, such as core, logs and seismic.

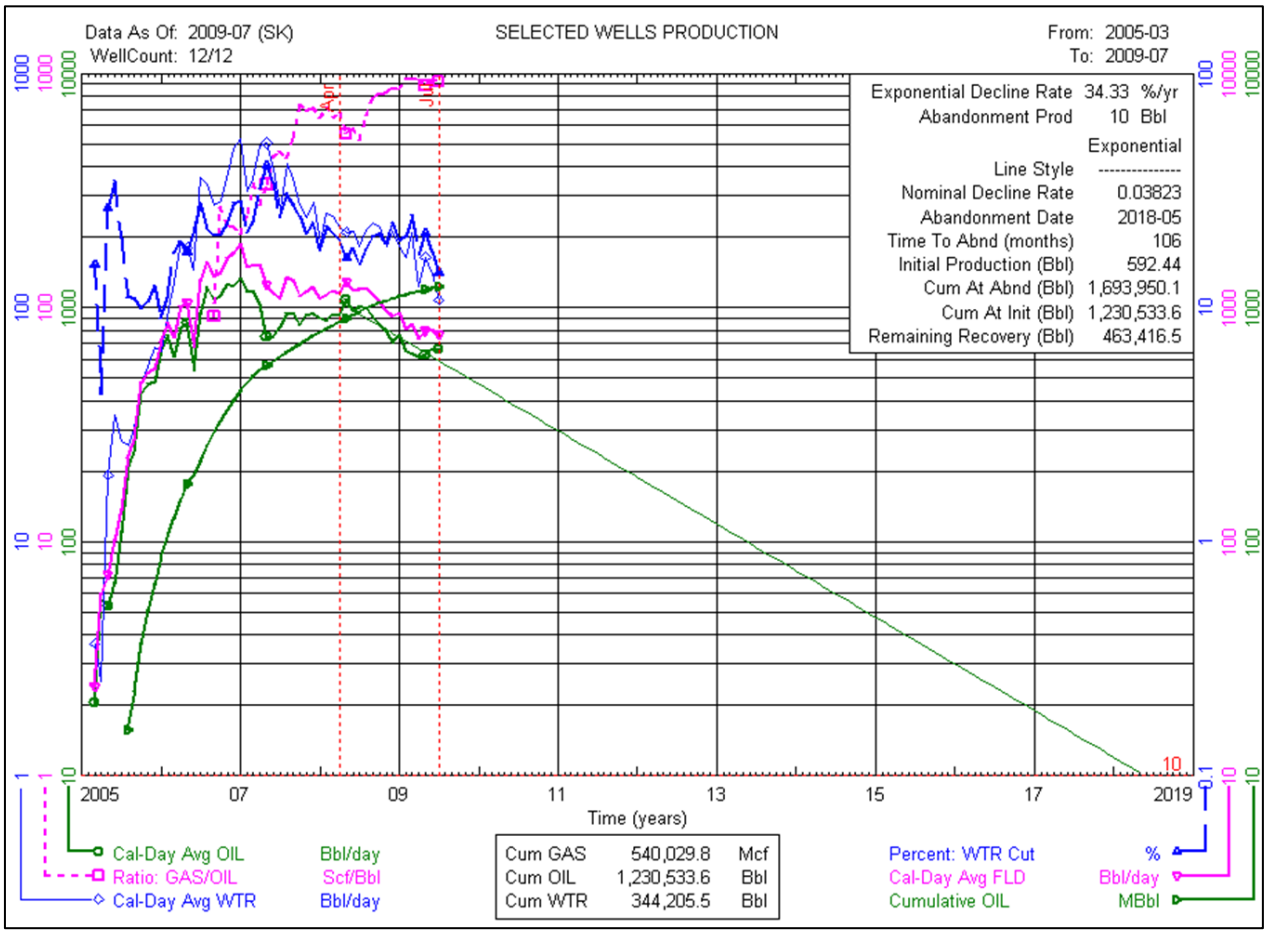

Figure 4-9: Primate Production decline curve for the data from March 2005 to July, 2009.

Primate production decline curve (Figure 4-9); the analysis was done in 2009 by the oil company (Enterra Energy) and compared with the data of Dec, 2011 (latest in March 2012). In reservoir heterogeneity estimation and pool evaluation, it was found that the reservoir was underestimated at 2009 and there is an excellent opportunity to enhance the oil recovery by additional drilling. The additional five wells (Figure 4-13) with the previous production rate of other wells should provide decent revenue for the stakeholders. Since this is an active commercial field; this current study did not want to publish any dollar amount that could effect on the stakeholders based on the reservoir performances. Conclusion based on the performances is that the reservoir was under-estimated and still prospective for EOR.

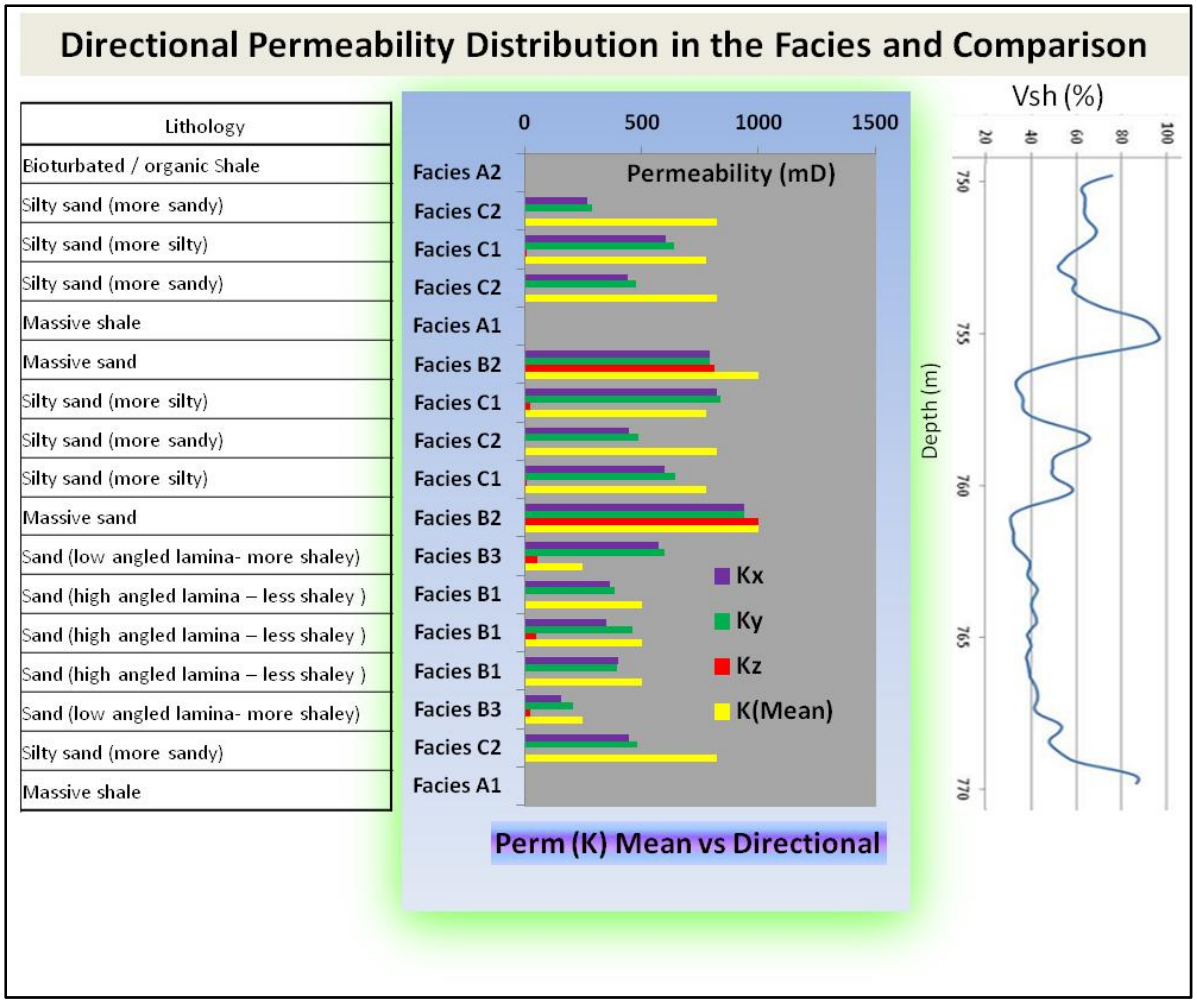

Figure 4-10: Comparison of directional permeabilities (Kx, Ky and Kz) values in the facies distribution of the Primate pool. The permeability barrier represents the reservoir heterogeneity and counted in reservoir simulation process.

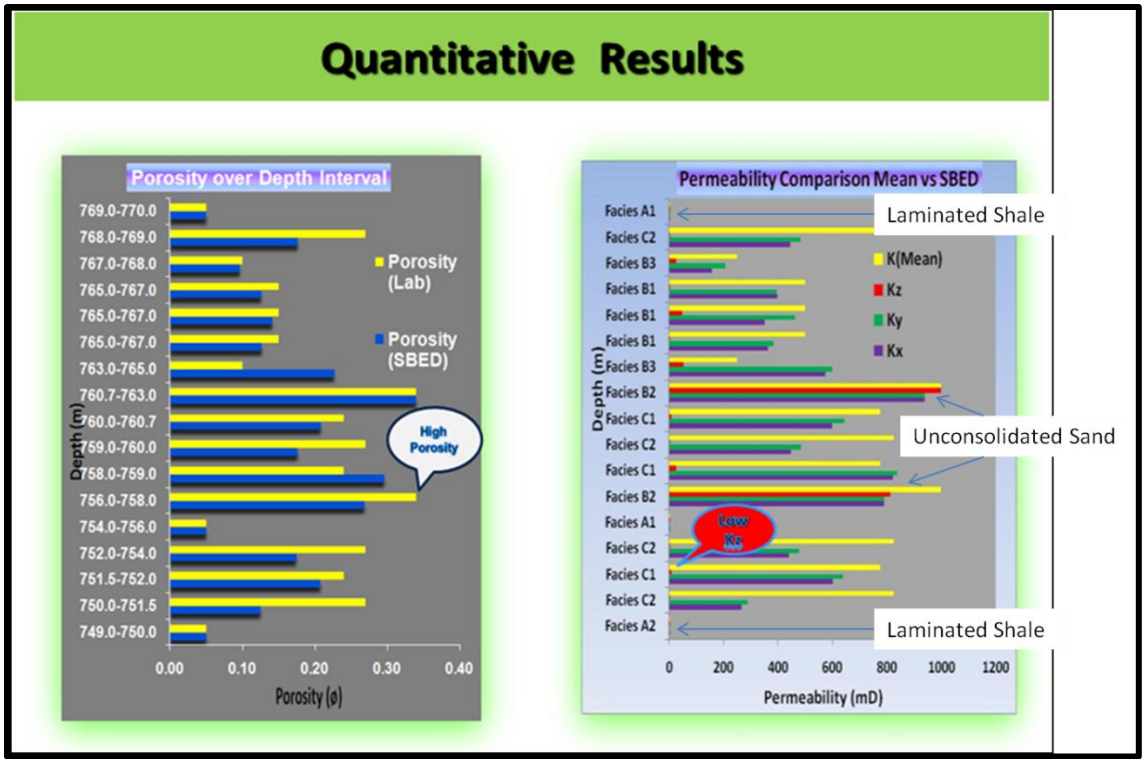

Figure 4-11: Comparison of directional permeabilities (Kx, Ky and Kz) in contrast to laboratory porosity values and the litho-facies (facies at right represent the same depth intervals at the left).

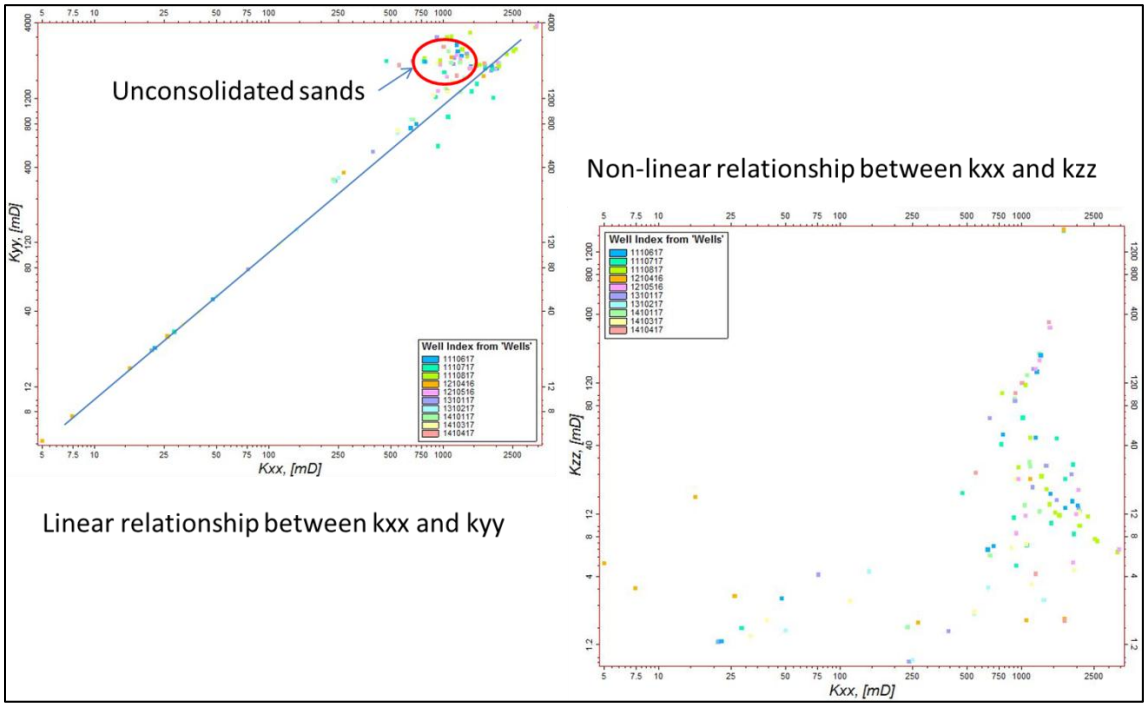

Figure 4-12: Relationship of horizontal (kxx, kyy) permeability versus vertical permeability (kzz) in the Primate pool.

Better Understanding on fluid migration from the seismic data based on the relationships of the velocity data and fluid properties in the form of fluid substitution formulas are commonly based on Gassmann's (1951) equations. Later it was modified by Berryman (1999) introducing the pressure data with the equations. Fluid viscosity quality factor was correlated with permeability by Vasheghani (2011). The Biot's mechanism and squirt flow (BISQ) equations showed that the seismic response is not only sensitive to the parameters in Gassmann's relations and viscosity, but also its relationship to the permeability of the rock; therefore porovisco-elastic theories can be used to predict permeability from seismic attributes as well (Vasheghni, 2011). These types of sensitivity require a very high resolution (small scale) geological model and the current project should be a useful. Without a high performance geological model, all the achievements in other sectors will not be benefited, especially in a reservoir simulation phase where the decisions are made.

The current study focused on the heavy oil reservoir characterization processes and enhanced oil recovery by potential infill or additional drilling. In completing the current study the importance of a 3D geocellular model using high resolution geological data as an input to reservoir simulation was realized. The heavy oil pool has multi-phase reservoir attributes that need more detail information in evaluation of reservoir performances and production history matching. Gassmann's equations for the property modeling or Gaussian distribution (single-phase up-scaling) are not enough for the heavy oil attribute simulation. Since the specific gravity of heavy oil and water are almost similar, it needs more fundamental study to establish more relationships among the reservoir properties and the seismic and geological properties.

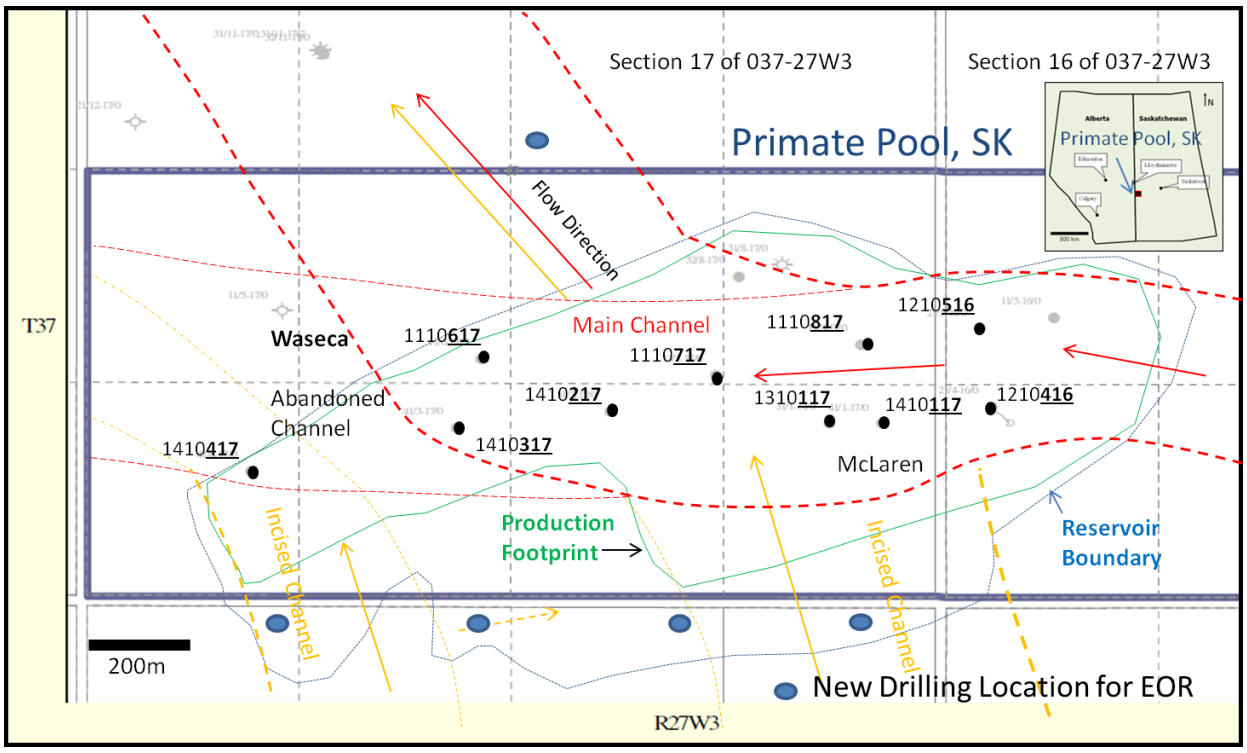

Figure 4-13: Infill or additional drilling locations for enhanced oil recovery are shown on the map.

4.5 Limitations of the Study:

There were several limitations; the most notable was the lack of core plug data. To overcome this limitation, a neighboring field, Provost was used as an analogue. Another limitation that presented a major challenge in defining the high resolution vertical distribution of reservoir properties was the access to only conventional logs like Gamma, Sonic, Neutron, Density and Resistivity for petrophysical interpretation. Advanced logs like dipole sonic, FMI or dip-meter log could have provided better information and integration among the reservoir properties of seismic and the well data. For instance, dipole sonic data could provide shear-velocity information of the reservoir rocks and could have been used to compare the compressional and shear properties of the seismic data; which is a very good discriminator of reservoir and non-reservoir properties.

Time lapsed 3D seismic data was acquired and processed using mega-bins (30mx30m) and the dominant frequency ranged from 30 Hz to 45 Hz, which allows about 15m of vertical resolution. The average net pay zone is about 11 m thick and was not sufficient for the vertical correlation between log data and the seismic data.

Among other limitations, sand production from this CHOPS pool was not recorded and there was no current pressure data available for the simulation grids. All the geological records were collected from the neighbouring fields and the geology was inferred from them. There was no geological study available for this Primate Field. In SBED, averaged Vsh value from the continuous log was used to create the grid boundaries due to computational limitation of today's technology. The SBED software is still in development stage and the output still depend on other software like Petrel, especially for the volumetric calculations.

CONCLUSION AND FUTURE WORKS

Conclusion:

The study was taken from the Primate CHOPS pool that belongs to the Upper Mannville Group (Albian) whose rocks were deposited in an estuarine influenced fluvial environment within a foreland basin. The objective of this study was to estimate the reservoir heterogeneity in reservoir characterization process for the evaluation of reservoir performances and to enhance the oil recovery by infill or additional drilling. In reservoir characterization process, time-lapse 3D seismic, wire-line logs and offset core data were used in building a 3D geo-cellular model. A major challenge in 3-D geo-cellular reservoir modeling was to incorporate the distribution of permeability barriers, particularly with up-scaling factors. Seismic interpretation delineated the reservoir production footprints and lateral extension of the reservoir boundary. Wire-line logs interpretation provided the vertical distributions of the reservoir properties and the offset core data allowed interpretation of the high resolution (cm-scale) sedimentary facies distribution to the wellbores. Petrophysical properties were derived from both the log and offset core data. A detailed log-facies classification and its vertical distribution were modeled in centimetre level scale preserving all the reservoir attributes honouring all the impermeable baffles in apparently homogenous reservoir. This high resolution near wellbore imagery enabled the 3D geo-cellular model to calculate the influence of permeability barriers as reservoir heterogeneity for the reservoir simulation process in evaluating the reservoir performances.

In this study, sedimentary facies were categorized by the Shale Volume factors from the conventional wire-line log interpretation and a Rule-based relationship was established among the Log-facies representing the different sedimentary current structures observed from the cores. Based on acquired information, process-oriented stochastic facies models at the centimetre-scale were created and assigned to 3-D near well-bore geological models. Flow simulation was applied to 3-D near well-bore models to calculate up-scaled directional effective permeability for use in determining realistic volumes of the reservoir. Since the Shale Volume factor provided a unique relationship between the sedimentary bed-forms and their contributing porosity and permeability estimation, it was applied to wells that did not have core data. This modeling approach can be

used to provide a realistic quantitative volumetric assumption of the production prediction and be used to improve Enhanced Oil Recovery (EOR) processes.

Future Works:

Any infill or additional drilling from this field should extract the cores for the validation of the current 3D geo-cellular model with multi-phase reservoir attributes. Detailed AVO and inversion of seismic data along with spectral decomposition could provide better information about the reservoir seismic attributes and could be correlated with the rock physics of the core data to better understand the cold heavy oil reservoir. Detail fluid properties study will also reveal the nature of ambiguous cold heavy oil properties. Correlation of rock physics properties with seismic, geological facies, formation fluid and produced sand will benefit to properly evaluate the reservoir performances for the enhanced oil recovery and effective strategies.

Co-kriging with seismic for Vp/Vs or density distribution in relation to the model's porosity and permeability distribution data could lead to further investigation a greater spatial coverage. Another iteration of this reservoir modeling could incorporate the geological core data from the Primate reservoir with reservoir simulation being done upon drilling in the proposed new locations.

REFERENCES

1. Aki, K. and Richards, P.G., 1980, Quantitative Seismology, Theory and Methods: 2nd Edition, Freeman, San Francisco, CA., 700p.

2. Allen, J. R. L., 1970, A quantitative model of grain size and sedimentary structures in lateral deposits: Geological Journal, Vol. 7, Issue 1, p.129-146.

3. Bardon, C. and Pied, B., 1969, Formation Water Saturation in Shaly Sands, Transactions SPWLA 10th Annual Logging Symposium, Paper Z, 1969.

4. Bauer, D., Hubbard, S., Leckie, D., and Dolby, G., 2009, Delineation of a sandstone-filled incised valley in the Lower Cretaceous Dina-Cummings interval: implications for development of the Winter Pool, west-central Saskatchewan. Bulletin of Canadian Petroleum Geology, Vol-57, No.4, December 2009, P.409-429.

5. Benns, G.W. & O'Connell, Shaun, 1988, The Geology of the Mid Mannville Subgroup in the West-Central Lloydminster Heavy Oil Trend, Alberta: Alberta Geological Survey, 1988, Open File Report, OFR1988-01.

6. Berryman, J. G., 1999, Tutorial - Origin of Gassmann's equations: Geophysics, Vol. 64, No- 5, September-October, 1999, P.1627–1629.

7. Caldwell, W. G. E., 1984, Early Cretaceous transgressions and regressions in the Southern interior plains, In: Stott, D. F. and Glass, D. J. (Eds), Mesozoic of Middle North America: Canadian Society of Petroleum Geologists, Memoir 9. P. 173-204.

8. Cant, D. J., 1996, Sedimentological and sequence stratigraphic organization of a foreland clastic wedge, Mannville Group, Western Canada Basin: Journal of Sedimentary Research. Vol. 66. No. 6. P 1137-1147.

9. Cant, D., J., 1995, Sequence stratigraphic analysis of individual depositionnal succession: effects of marine/nonmarine sediment partitioning and longitudinal sediment transport, Mannville Group, Alberta foreland basin, Canada: AAPG bulletin, V. 79, No 5 , P.749-762.

10. Chen, S., Lines, L., Embleton, J., Daley, P. F., and Mayo, L., 2003, Seismic detection of cold production footprints of heavy oil in Lloydminster field: CSEG convention, June, Calgary, Alberta, Canada.

11. Chen, S., Lines L., Daley, P.F., 2004, Foamy Oil and Wormhole Footprints in a Heavy Oil Cold Production Reservoir, Western Canada: CSEG Recorder, October 49-53.

12. Chiles, J. P. and Delfiner, P., 1999, Geostatistics: Modeling Spatial Uncertainty, John Wiley & Sons, Inc., New York City, USA.

13. Christopher, J. E., 1980, The Lower Cretaceous Mannville Group of Saskatchewan in Lloydminster and Beyond: Geology of Mannville Hydrocarbon Reservoirs, Saskatchewan Geological Society, Special Publ. Number 5.

14. Christopher, J.E., 2002, The heavy oil-productive Lower Cretaceous Mannville sandstones of the Unity-Biggar district, west-central Saskatchewan: in Summary of Investigations 2002, Volume 1, Saskatchewan Geological Survey, Sask. Industry and Resources, Misc. Rep., 2002-4.1, p107-117.

15. Christopher, J.E., 2001, The Lower Cretaceous Mannville Meadow Lake Basin and its Temporal Counterparts, West-Central Saskatchewan: In Summary of Investigations 2001, Volume 1, Saskatchewan Geological Survey, Saskatchewan Energy and Mines. Report 2001-4.1, p.94-105.

16. Christopher, J.E., Kent, D.M., Simpson, F., 1971, Hydrocarbon Potential of Saskatchewan: Saskatchewan Energy and Mines Report 157, 47p.

17. Coates, George R., Xiao, Lizhi and Prammer, Manfred G., 1999, NMR Logging Principles and Applications, Halliburton Energy Services, 1999.

18. Deschamps, R., Euzen, T. and Pruden, D., 2008, The Upper Mannville Incised Valleys of Central Alberta: An Example of Subtle Gas Traps, Back to Exploration. 2008 - CSPG CSEG CWLS Convention, 2008, Calgary, Alberta.

19. Dumitrescu, C. C. and Lines, L., 2010b, Integrated characterization of heavy oil reservoir using Vp/Vs ratio and neural network analysis: Journal of Seismic Exploration, 19, 231-247.

20. Glass, D. J., 1990, Lexicon of Canadian Stratigraphy, Western Canada, Including Eastern British Columbia, Alberta, Saskatchewan and Southern Manitoba, Canadian Society of Petroleum Geologists, V.4, 772p.

21. Goovaerts, P., 1997, Geostatistics for Natural Resources Evaluation, Oxford Press, N. Y., USA.

22. Harris, J., 2002, Crosswell seismic profiling: The Decade Ahead: Fall 2002 SEG Distinguished Lecture.

23. Jonoud, S. and Jackson, M.D., 2008, Validity of Steady-State Upscaling Techniques, SPE Res Eval & Eng 11 (2): 405-416.

24. Journel, A. G., 2002, Combining Knowledge from Diverse Sources: An alternative to Traditional Data Independence Hypotheses, Mathematical Geology, 34, No.5, 573.

25. Journel, A. G., 1974, Geostatistics for Conditional Simulation of Orebodies: Economic Geology (1974) 69, No.3, p.445.

26. Journel, A. G., 1986, Geostatistics: Models and Tools for the Earth Sciences, Mathematical Geology (1986) 18, No.1, 119.

27. Keith, D. A. W., Wightman, D. M., Pemberton, S. G. MacGillivray, J. R., Berezniuk, T., and Berhane, H. 1988, Sedimentology of the McMurray Formation and Wabiskaw Member (Clearwater Formation), Lower Cretaceous, in the Central Region of the Athabasca Oil Sand Area, Northeastern Alberta, In: Sequences, Stratigraphy, Sedimentology: Surface and Subsurface. D. P. James and D. A. Leckie (eds.). Canadian Society of Petroleum Geologists, Memoir 15, p.309-324.

28. Knox, P. R. and Barton, M. D., 1999, Predicting interwell heterogeneity in fluvial-deltaic reservoir; effects of progressive architecture variation through a depositional cycle from outcrop and subsurface observations, In: Reservoir Characterization-Recent Advances. R. Schatzinger and J. Jordan (eds.), American Association of Petroleum Geologists, Memoir 71, p.57-72.

29. Kramers, J. W., 1984, Introduction, In: Oil Sands Geology Studies of the Alberta Research Council, Internal Report. p. 1-17.

30. Kramers, J. W., Bachu, S., Cuthiell, D., Lytviak, A.T., Hasiuk, J. E., Olic, J. J., Prentice, M. E, and Yuan, L. P., 1993, The Provost Upper Mannville B Pool; An Integrated Reservoir Analysis: Fourth Unitar/UNDP Conference on Heavy Crude and Tar Sands, Volume 60, p. 1-18

31. Krige, Daniel G., 1951, A statistical approach to some basic mine valuation problems on the Witwatersrand, J. of the Chem., Metal. and Mining Soc. of South Africa, 52 (6), p.119–139.

32. Lines, L. R. et. al., 2008, Collaborative Methods in Enhanced Cold Heavy Oil Production: The Leading Edge, September 2008, v-27, no-9, p. 1152-1156.

33. Lines, L. R., Daley, P. F., Embleton, J. E. and Bording, R. P., 2008, The Resolution and Detection of "Subseismic" High-Permeability Zones in Petroleum Reservoirs: The Leading Edge, pp.664-669.

34. Lines, R. L., Ying Zou, and Joan Embleton, 2005, Reservoir Characterization and Heavy Oil Production: CSEG Recorder, January 2005, p.27-29.

35. Lines, L., F. Vasheghani and S. Treitel, 2008, Reflections on Q: CSEG Recorder, 33, 36-38.

36. Matheron, G., 1973, The Intrinsic Random Functions and their Application: Advances in Applied Probability, v-5, p.439.

37. Mathison, J.E., 1988, Upper Mannville Tidal Creek and Incised Fluvial Channel Reservoirs at the Fort Kent Thermal Project of East-central Alberta. Sequences, Stratigraphy, Sedimentology: Surface and subsurface. Canadian Society of Petroleum Geologists, Memoir 15, p. 331-350.

38. McNeil, D.H. and Zonneveld, J-P., 2004, Foraminiferal evidence of the Early Albian Moosebar/Clearwater Seaway in Mannville Group strata, Fort à la Corne kimberlite field, east-central Saskatchewan: In Summary of Investigations 2004, Volume 1, Saskatchewan Geological Survey, Sask. Industry Resources, Misc. Rep. 2004-4.1, CD-ROM, Paper A-15, 9p.

39. Mezzatesta, A. G., Rodriguez, E. F., Mollison, R. A. and Frost, E., 2002, Laminated Shaley Sand Reservoirs - An Interpretation Model Incorporating New Measurements: SPWLA, 43rd Annual Logging Symposium, June 2-5.

40. Miall A.D., 1985, Architectural-element analysis: a new method of facies analysis applied to fluvial deposits: Earth Sci. Rev., 22, p. 261-308.

41. Miall, A. D., 1977, A Review of the Braided-river depositional environment: Earth Sci. Rev., 13, p.1-62.

42. Miall, A.D., 1978, Lithofacies types and vertical profile models in braided river deposits, A summary, In: Fluvial Sedimentology (Ed. Miall, A. D.). Can. Soc. Petrol. Geol., Calgary, Memoir 5, p.597-604.

43. Middleton, L. T & Trujillo, A. P., 1984: Sedimentology and depositional setting of the Upper Proterozoic Scanlan Conglomerate, Central Alberta.

44. Mossop, G.D. and Shetsen, I (Compilers), 1994, Geological Atlas of the Western Canada Sedimentary Basin, On-line version: http://www.ags.gov.ab.ca/ags_pub/Atlas_www/Atlas.htm (1998, 12, 09), Alberta Geological Survey.

45. Nur, A., C. Tosaya, and D. Vo-Thanh, 1984, Seismic monitoring of thermal enhanced oil recovery processes: 54th Annual International Meeting: SEG Expanded Abstracts, 3, 337-340.

46. O'Connell, S. C., 1985, The geology and resource characterization of the Lower and Mid Mannville Formations of the South Lloydminster heavy oil trend, Alberta: Alberta Research Council, Geological Survey Department, Consultant Report to AOSTRA, 190 p.

47. OFR 1988-1, Alberta Geological Survey, Revised January 11, 2011: http://www.ags.gov.ab.ca/publications/abstracts/OFR_1988_01.html

48. Pickup, G.E., 2000, Steady-State Upscaling: From Lamina-Scale to Full-Field Model, SPE Journal 5 (2): 208–217.

49. Pickup, G.E. and Kenneth S. S., 1996, The Scaleup of Two-Phase Flow in Porous Media Using Phase Permeability Tensors, SPE Journal 1996: 369-381.

50. Reineck, H. E. and Singh, I. B., 1980, Depositional sedimentary environments with reference to terrigenous clastics: 2nd edition, Springer – Verlag. 549p.

51. Ruvo, L., Doyle, J., Cozzi, M., Riva, S., Scaglioni, P. and Serafini G., 2008, Multi-Scale Data Integration in Characterizing and Modeling A Deep-Water Turbidite Reservoir: SPE, Annual Technical Conference and Exhibition held in Denver, Colorado, USA, September 21-24.

52. Sawatzky, R.P., Lillico, D.A., London, M.J., Tremblay, B.R. and Coates, R.M., 2002, Tracking cold production footprints: CIPC conference, Calgary, Alberta, Canada.

53. SBED Manual, 2010, Geomodeling Research Corporation, 300,840 - 6th avenue, S. W., T2P 3E5, Calgary, AB, Canada.

54. Selley, R. C, 1996, Ancient Sedimentary Environments and their sub-surface diagnosis: 4th Edition (1996), Chapman & Hall, London, UK.

55. Simandoux, P., 1965, Measures Dielectriques en Milieu Poreaux, Application a Mesure des Saturations en Eau, Etude du Comportement des Massifs Revue de lInstitut Francais du Petrole: Issue Supplementaire, pp. 193-215, 19.

56. Smith, D.G. 1988, Modern point bar deposits analogous to the Athabasca Oil Sands, Alberta, Canada: in P.L de Boer, A. van Gelder and S.D. Nio eds., Tide-Influenced Sedimentary Environments and Facies, Reidel Publishing Company, p.417-432.

57. Strebelle, S., 2002, Conditional Simulation of Complex Geological Structures Using Multiple-Point Statistics, Mathematical Geology, 34, No.1, 1.

58. Thomas, E. C. & Steiber, S. J., 1975, The distribution of shale in sandstone and its effect upon porosity: 16th Annual SPWLA Logging Symposium, June 4-7.

59. Toksöz, M. N., C. H. Cheng, and A. Timur, 1976, Velocities of seismic waves in porous rocks: Geophysics, 41, 621-645.

60. Vasheghani, F. F., 2011, Estimating Heavy Oil Viscosity from Seismic Data: Ph. D Thesis, University of Calgary, Alberta, February, 2011.

61. Vasheghani, F. and Embleton J., 2008. The effects of cold production on seismic response. The Leading Edge 27: 1148

62. Visher, G.S., 1965, Published in: Primary Sedimentary Structures and Their Hydrodynamic Interpretation, Edited by Gerard V. Middleton, Vol. 12. 1965. P.116-132.

63. Watson, I.A., Lines, L.R., and Brittle, K.F., 2002, Heavy-oil reservoir characterization using elastic wave properties: The Leading Edge, 21 (8), 736-739.

64. Weber, K. J., 1986. How heterogeneity affects oil recovery, In: J. L. W. Lake and H. B. Carroll, (eds.) Reservoir Characterization: Academic Press Inc. Orlando, Florida, p. 487-544.

65. Wen, R., Martinius, A. W., Naess, A. and Ringrose, P., 2008, Three-Dimensional Simulation of Small-scale Heterogeneity in Tidal Deposit - A Process-based Stochastic Simulation Method, Geomodeling Research Corporation, 300,840 - 6th avenue, S. W., T2P 3E5, Calgary, AB, Canada.

66. Wen, X. H. and G´omez-Hern´andez, J. J., 1998, Upscaling hydraulic conductivities in cross-bedded formations: Mathematical Geology, 30, p.181–211.

67. Worthington, P. F., 2008, Quality-Assured Evaluation of Effective Porosity using Fit-for-Purpose Estimates of Shale Volume Fraction: Society of Petrophysicists and Well Log Analysts (SPWLA) 49th Annual Logging Symposium, May 25-28.

68. Wu, X. H., Efendiev, Y. and Hou, T. Y., 2002, Analysis of Upscaling Absolute Permeability, Discrete and Continuous Dynamical Systems – Series B, Vol-2, Number 2, May 2002, pp. 185-204.

69. Xu, Yong, 2012, Rock physics and seismic methods for characterizing the heterogeneity of oil sands reservoirs in the Western Canadian Sedimentary Basin: Ph. D Thesis, University of Calgary, Alberta, January, 2012.

APPENDICES

Appendix I: Core description of the offset well 100/14-29-037-01W4/0

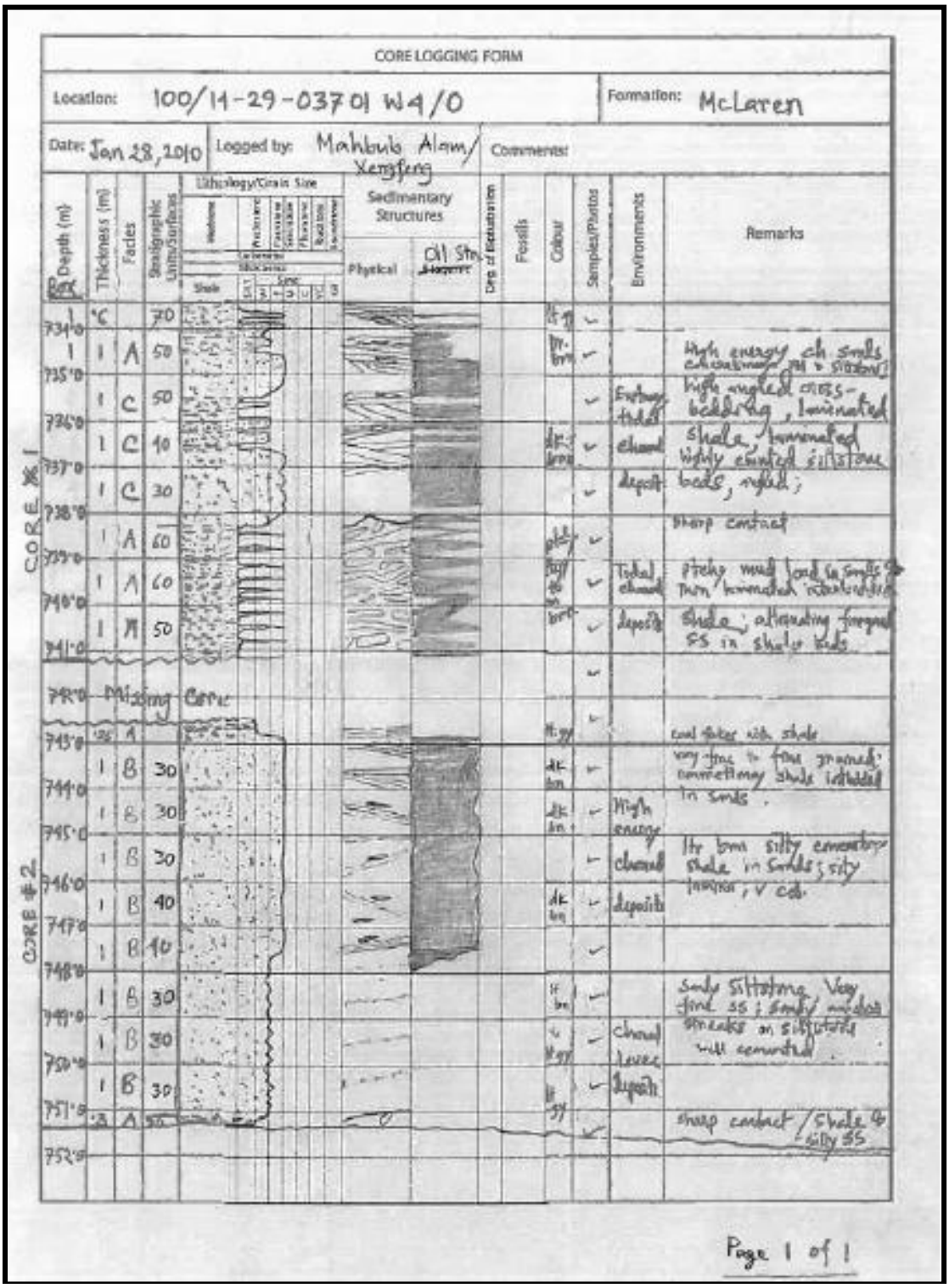

Appendix II: Core description of the offset well 100/05-20-037-01W4/0

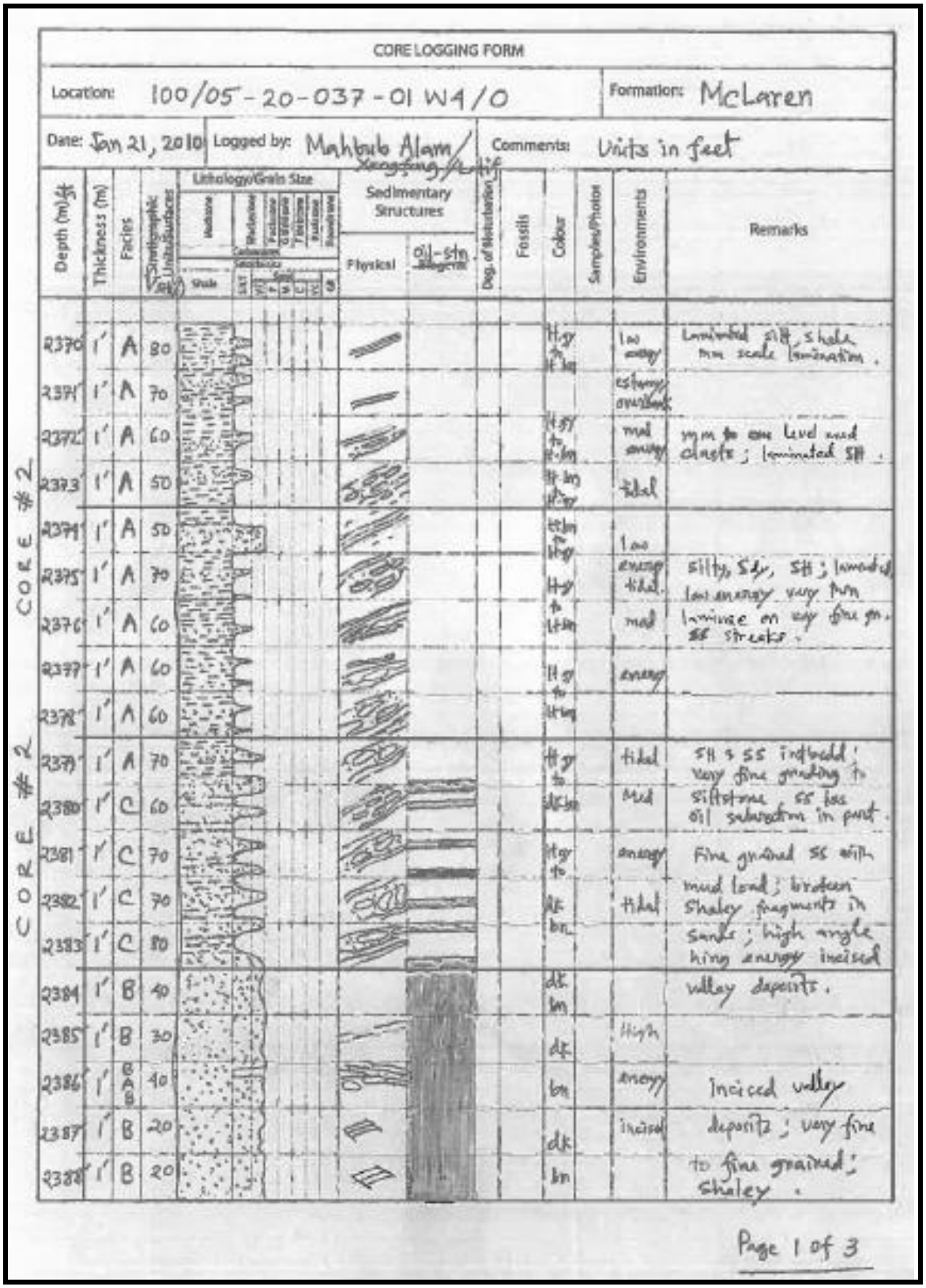

CORE LOGGING FORM

Location: 100/05-20-037-01W4/0 Formation: McLaren

Date: Jan 21, 2010 Logged by: Mahbub Alam / Xiaojing Liu Comments: Units in feet

CORE #2

Depth (m)/ft	Thickness (m)	Facies	Stratigraphic Units/Surfaces	Lithology/Grain Size	Sedimentary Structures	Deg. of Bioturbation	Fossils	Colour	Samples/Photos	Environments	Remarks
2370	1'	A	80					H.gy to lt.brn		low energy	Laminated silt, shale mm scale lamination.
2371	1'	A	70							estuary overbank	
2372	1'	A	60					H.gy to lt.brn		mod energy	mm to cm bed mud clasts; laminated Slt.
2373	1'	A	50					lt brn to lt.gy		tidal	
2374	1'	A	50					lt.brn to brn.gy		low	
2375	1'	A	70					brn.gy		energy tidal	silty, Sdy, Slt; laminated
2376	1'	A	60					H.gy to lt.brn		mod	low energy very fine gr. laminae on cm scale ss streaks.
2377	1'	A	60					H.gy to lt.brn		energy	
2378	1'	A	60								
2379	1'	A	70					H.gy to dk.brn		tidal	Slt & SS interbedd; very fine grading to
2380	1'	C	60							Mud	Siltstone SS has oil saturation in part.
2381	1'	C	70					H.gy to dk brn		energy	Fine grained SS with
2382	1'	C	70							tidal	mud lend; broken Shaley fragments in
2383	1'	C	80								sands; high angle hing energy incised
2384	1'	B	40					dk brn			valley deposits.
2385	1'	B	30					dk		High	
2386	1'	B A B	40					brn		energy	Incised valley
2387	1'	B	20					dk		incised	deposits; very fine
2388	1'	B	20					brn			to fine grained; Shaley.

Page 1 of 3

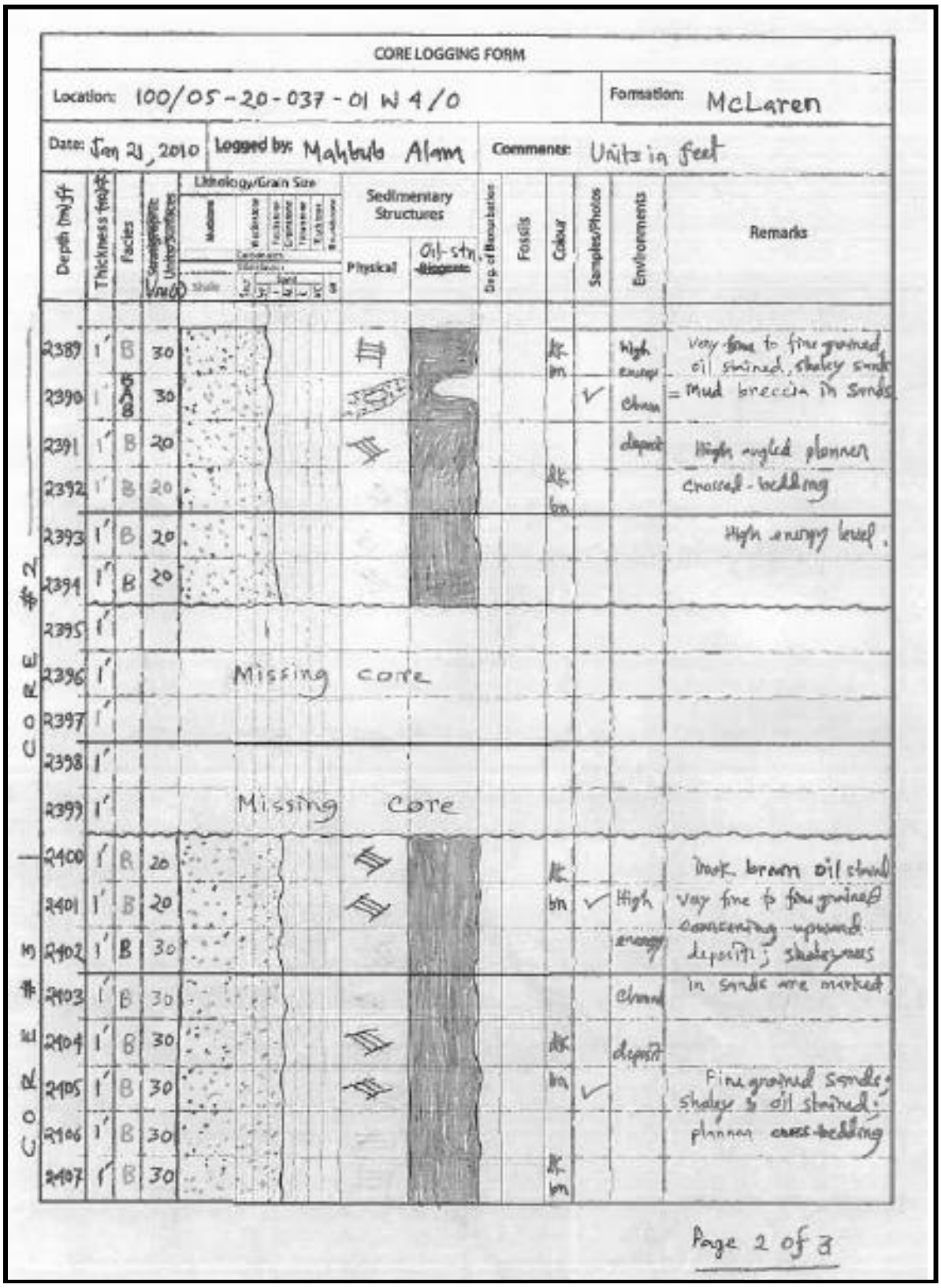

CORE LOGGING FORM

Location: 100/05-20-037-01 W 4/0 | Formation: McLaren

Date: Jan 21, 2010 | Logged by: Mahbub Alam | Commenter: Units in feet

CORE #2

Depth (m)/ft	Thickness (m)/ft	Facies	Stratigraphic Units/Surfaces	Lithology/Grain Size	Sedimentary Structures: Physical	Sedimentary Structures: Oil-stn/Biogenic	Dep. of Bioturbation	Fossils	Colour	Samples/Photos	Environments	Remarks
2389	1'	B	30						lt. brn		High energy	Very fine to fine grained, oil stained, shaley sands = Mud breccia in Sands
2390	1'	B	30						brn	✓	Channel deposit	
2391	1'	B	20									High angled planner cross-bedding
2392	1'	B	20						dk brn			
2393	1'	B	20									High energy level.
2394	1'	B	20									
2395	1'											
2396	1'			Missing core								
2397	1'											
2398	1'											
2399	1'			Missing core								
2400	1'	B	20						lt. brn			Mod. brown oil stained
2401	1'	B	20						brn	✓	High energy	very fine to fine grained coarsening upward deposits; shale-mms in sands are marked
2402	1'	B	30									
2403	1'	B	30								Channel deposit	
2404	1'	B	30						dk brn			
2405	1'	B	30						brn	✓		Fine grained sands, shales & oil stained; planner cross-bedding
2406	1'	B	30									
2407	1'	B	30						lt. brn			

Page 2 of 3

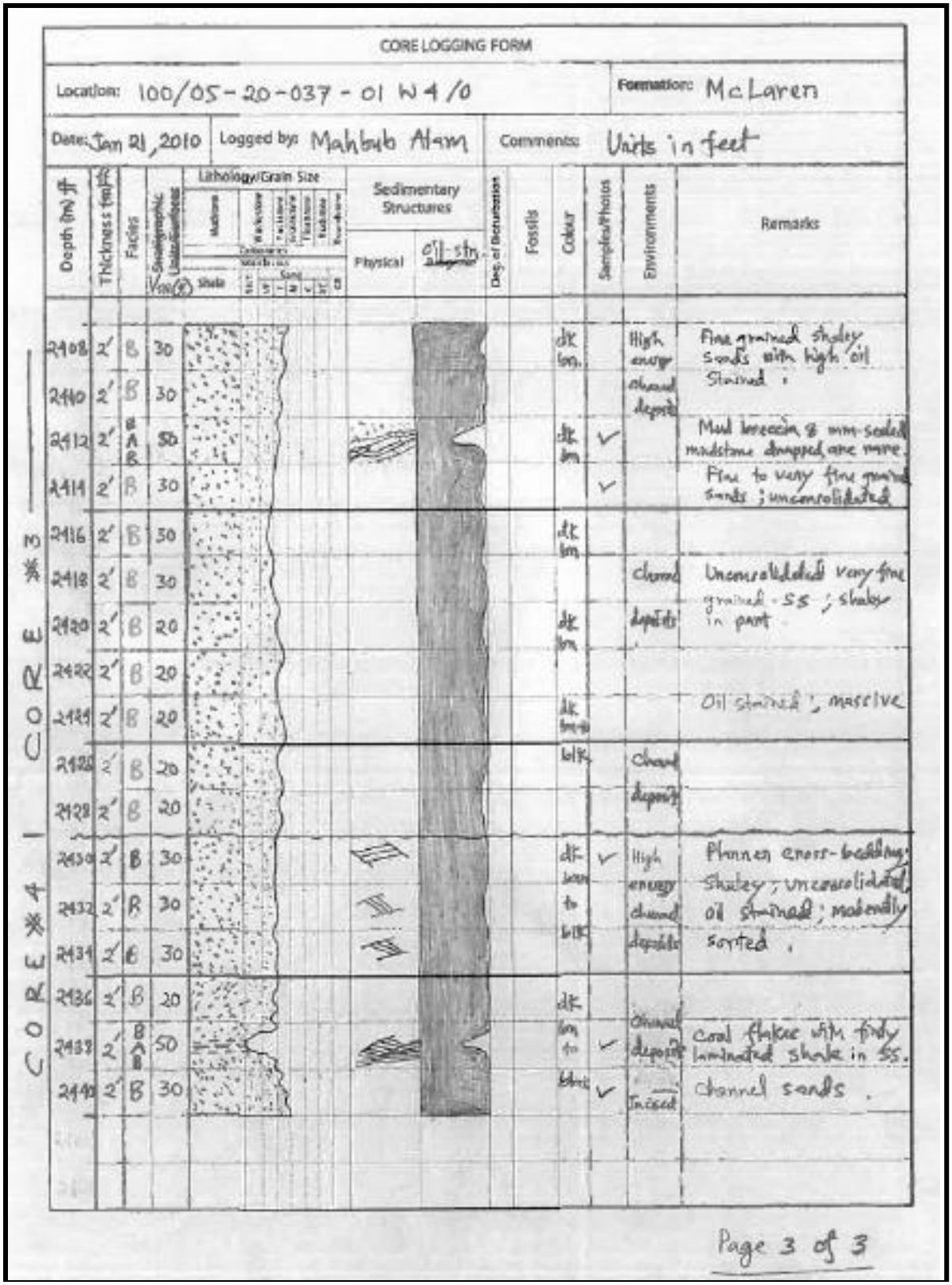

CORE LOGGING FORM

Location: 100/05-20-037-01 W4/0 — Formation: McLaren

Date: Jan 21, 2010 — Logged by: Mahbub Alam — Comments: Units in feet

CORE #3 — CORE #4

Depth (m) ft	Thickness (m) ft	Facies	Sedimentary Structures	Colour	Samples/Photos	Environments	Remarks
2408	2'	B	30	dk brn		High energy channel deposits	Fine grained shaley sands with high oil Stained.
2410	2'	B	30				
2412	2'	B A B	50	dk brn	✓		Mud breccia & mm-scaled mudstone draped ripple mire.
2414	2'	B	30		✓		Fine to very fine grained sands; unconsolidated
2416	2'	B	30	dk brn			
2418	2'	B	30			channel deposits	Unconsolidated very fine grained SS; shaley in part
2420	2'	B	20	dk brn			
2422	2'	B	20				
2424	2'	B	20	dk brn			Oil stained, massive
2426	2'	B	20	blk		channel deposits	
2428	2'	B	20				
2430	2'	B	30	dk brn to blk	✓	High energy channel deposits	Planner cross-bedding; Shaley; unconsolidated, oil stained; modestly sorted.
2432	2'	B	30				
2434	2'	B	30				
2436	2'	B	20	dk brn to blk		channel deposits	
2438	2'	B A B	50		✓		Coal flakes with finly laminated shale in SS.
2440	2'	B	30	blk	✓	Incised	Channel sands.

Page 3 of 3

Appendix III: Core description of the offset well 100/11-16-038-01W4/0

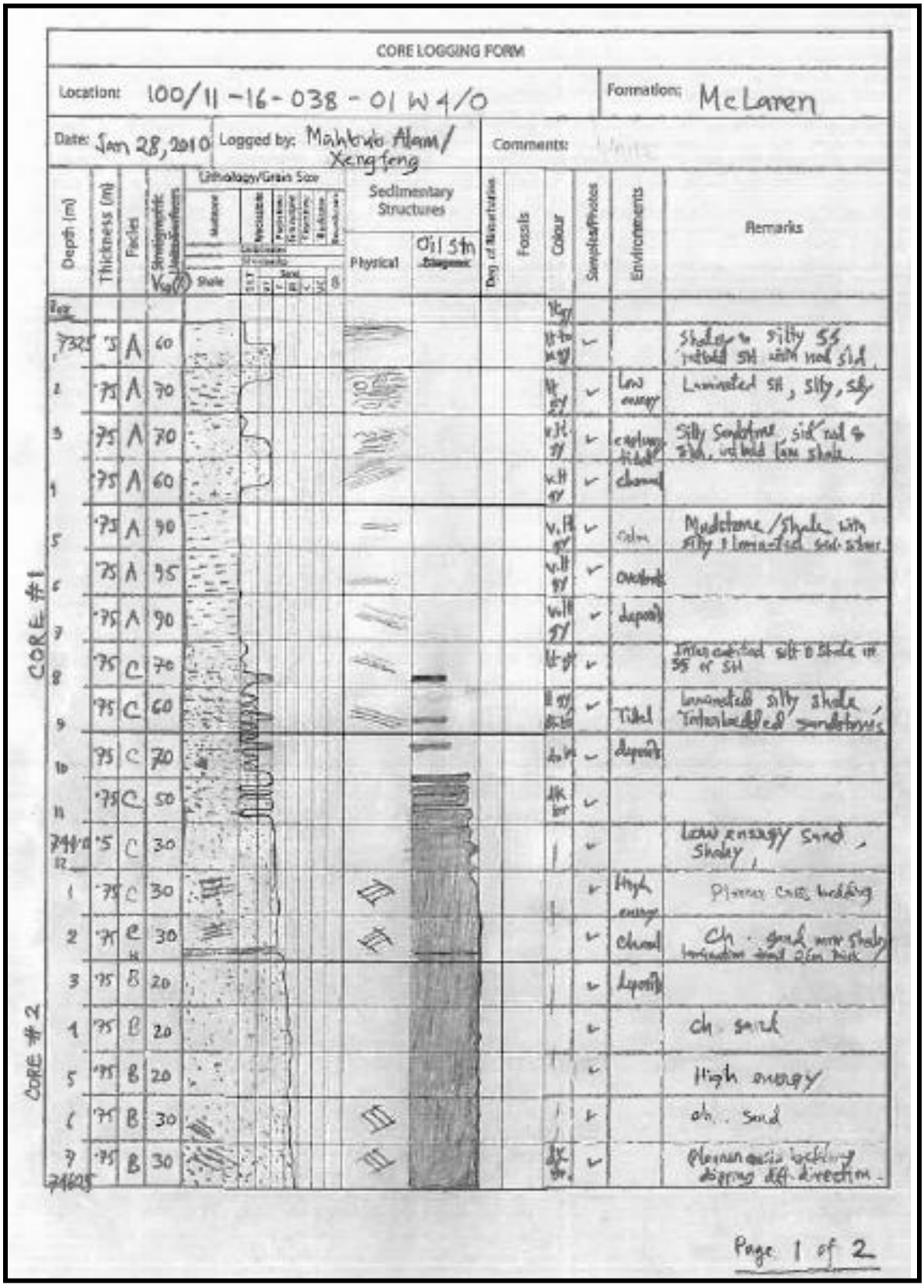

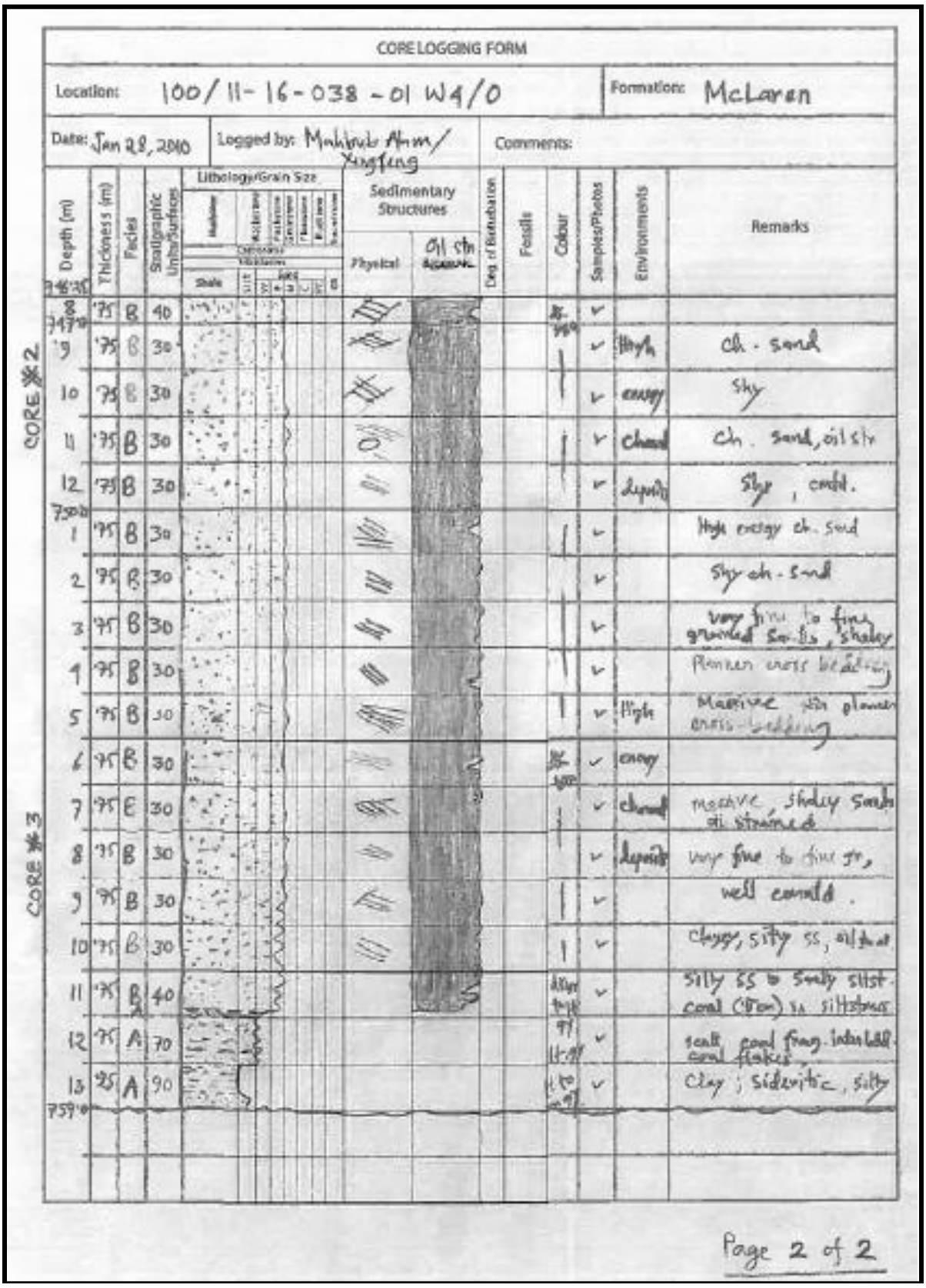

CORE LOGGING FORM

Location: 100/11-16-038-01 W4/0

Formation: McLaren

Date: Jan 28, 2010

Logged by: Mahbub Alam / Yingfeng

Comments:

Depth (m)	Thickness (m)	Facies	Stratigraphic Units/Surfaces	Lithology/Grain Size	Sedimentary Structures	Deg of Bioturbation	Fossils	Colour	Samples/Photos	Environments	Remarks
7479											
9	75	B	40						✓		
10	75	B	30						✓	High energy	ch. sand
11	75	B	30						✓	channel	Sltv
12	75	B	30						✓	deposits	ch. sand, oil stn
7500											Sltv, cmtd.
1	75	B	30						✓		High energy ch. sand
2	75	B	30						✓		Sltv ch. sand
3	75	B	30						✓		very fine to fine grained ss, shaley
4	75	B	30						✓		Planar cross bedding
5	75	B	30						✓	High	Massive str planar cross-bedding
6	75	B	30						✓	energy	
7	75	B	30						✓	channel	massive, shaley sand str stromed
8	75	B	30						✓	deposits	very fine to fine gr,
9	75	B	30						✓		well consld.
10	75	B	30						✓		clayey, silty ss, oil stn
11	75	B	40						✓		silty ss to sandy siltst. coal (10cm) in siltstone
12	75	A	70						✓		sandy coal frag. interbed coal flakes
13	25	A	90						✓		clay; sideritic, silty
7590											

CORE #2

CORE #3

Page 2 of 2

Appendix IV: Offset logs of three wells (only the intervals of interests)

100/14-29-037-01W4/0

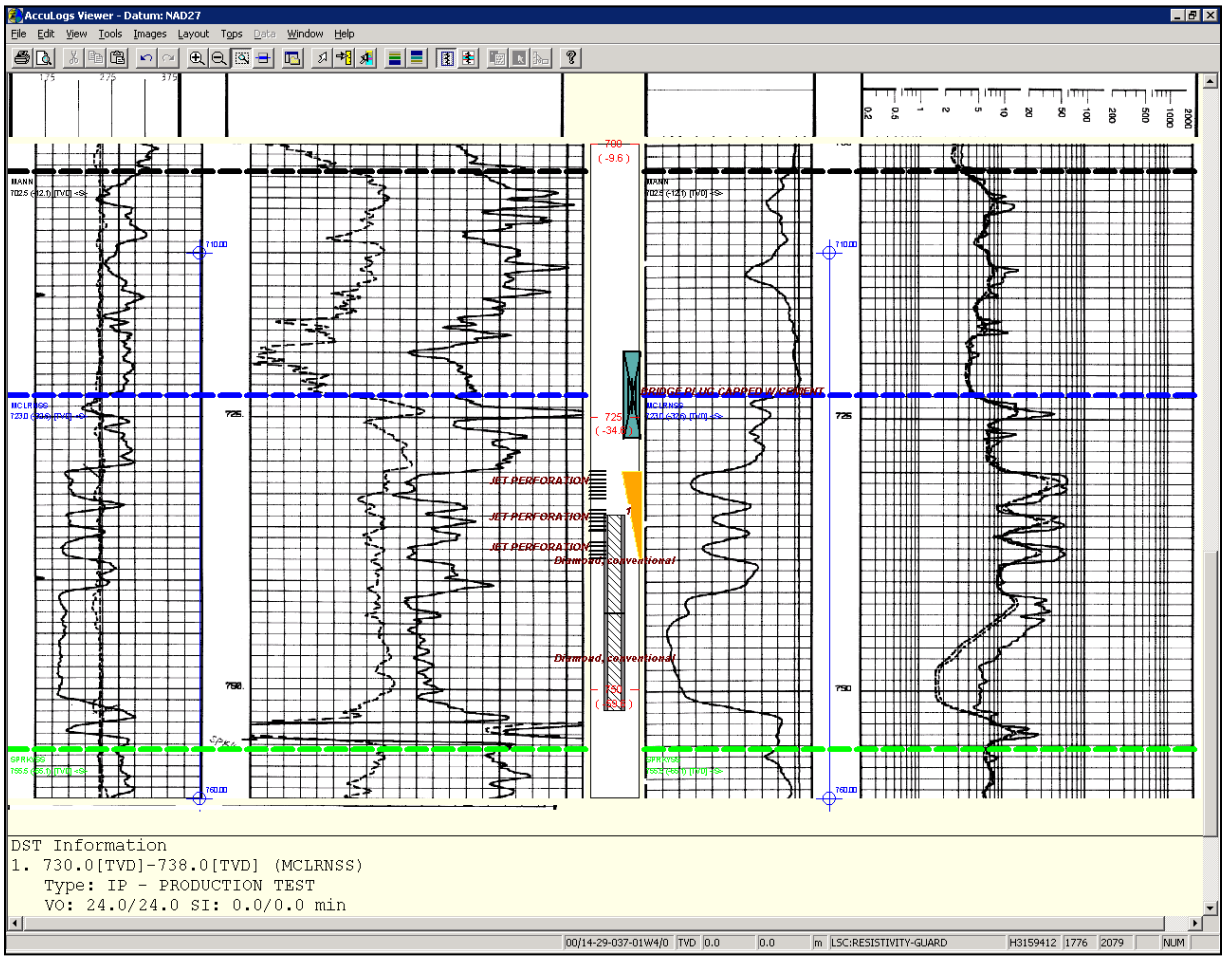

100/5-20-037-01W4/0

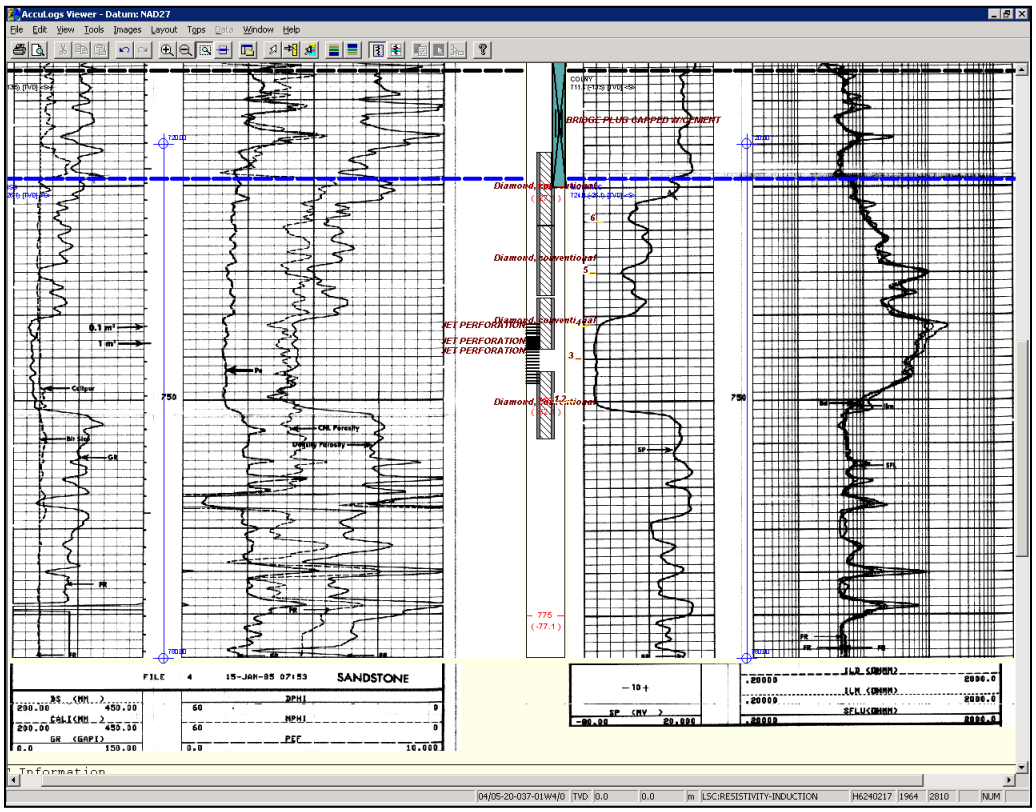

100/11-16-038-01W4/0

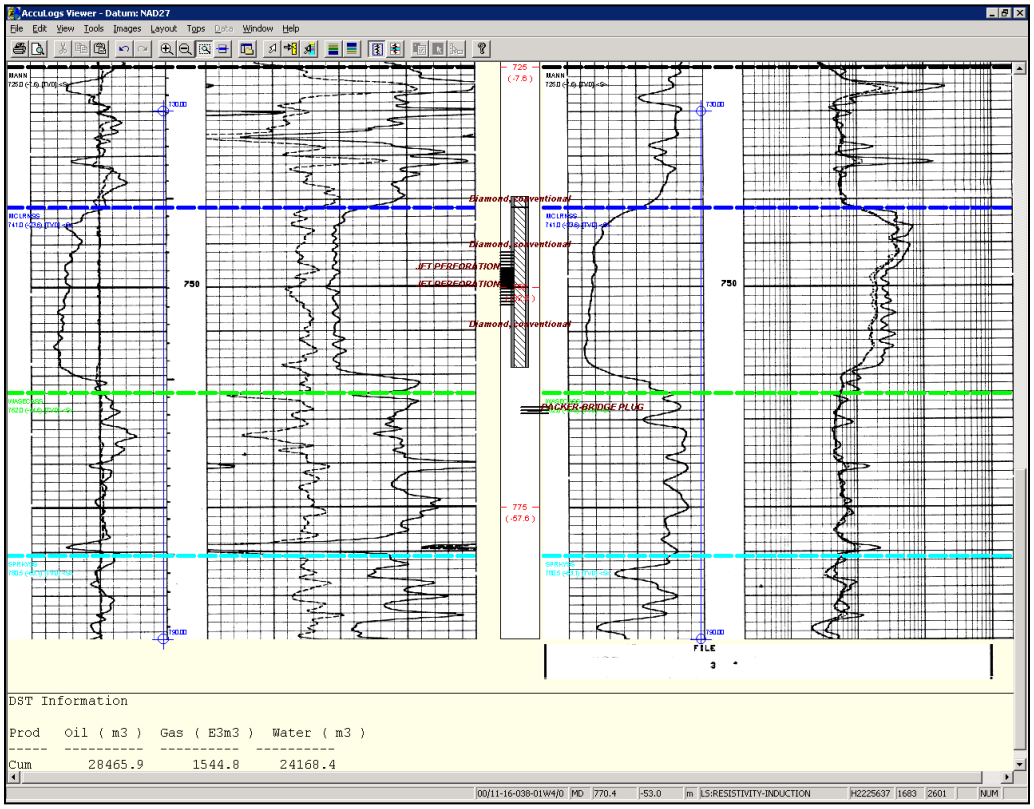

Appendix V: Vsh Curves for the Offset three wells.

Vsh curve for the well 100/14-29-37-1W4/0

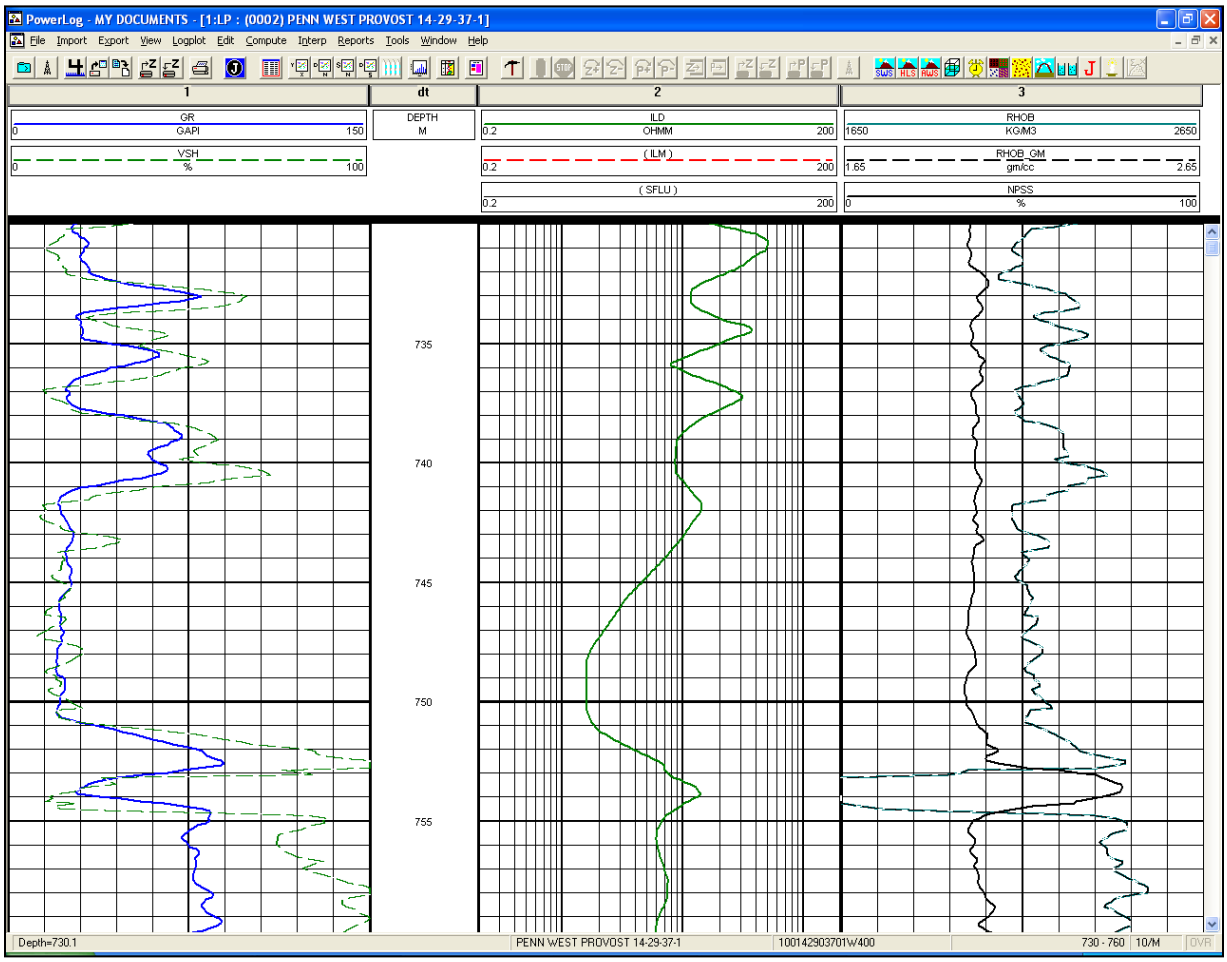

Vsh curve for the well 100/5-20-037-1W4/0

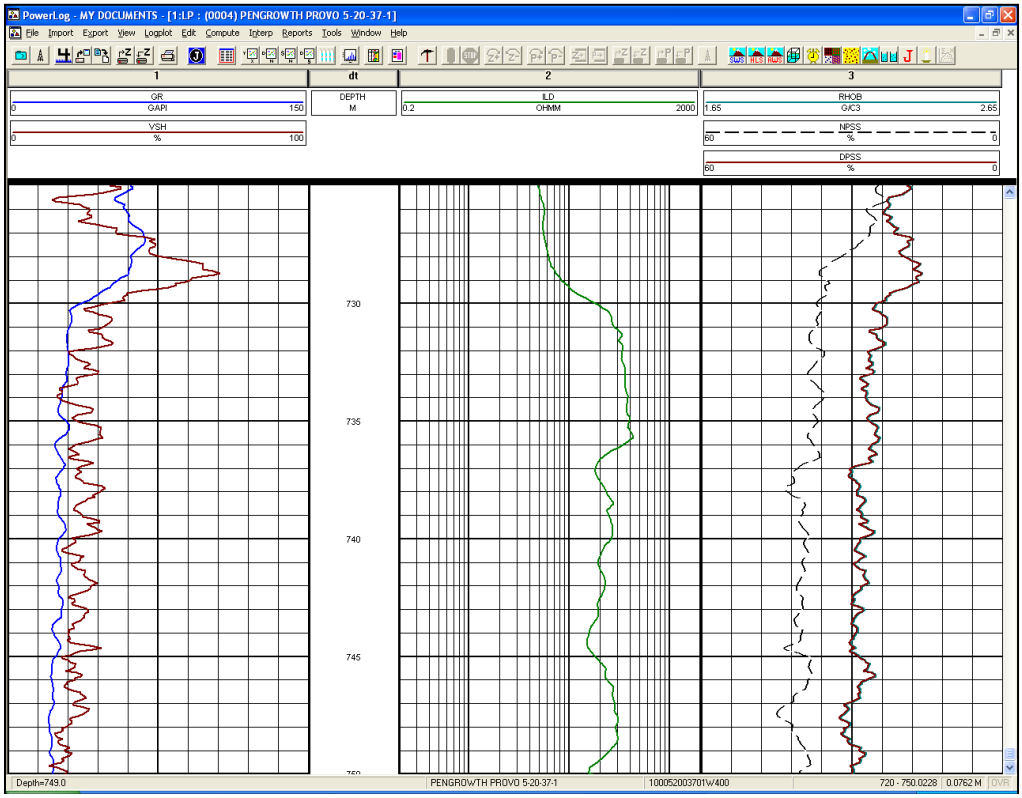

Vsh curve for the well 100/11-16-038-1W4/0

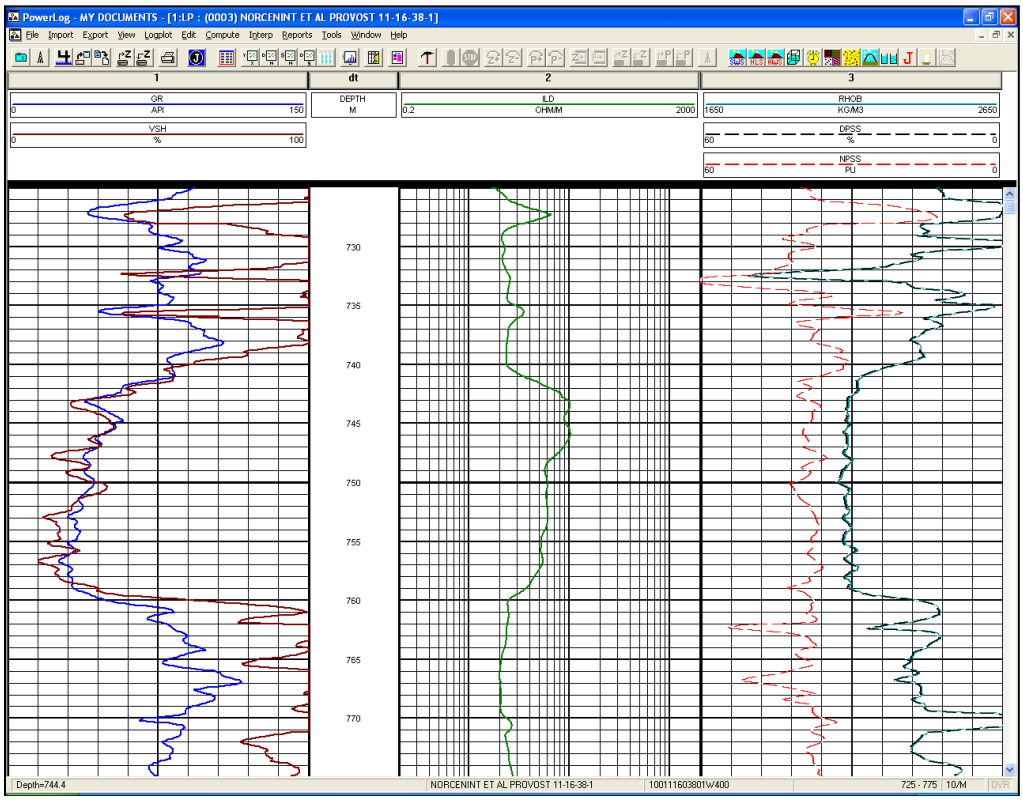

Appendix VI: Up-scaled Results from SBED showing the porosity (in fraction) and the directional permeability (in mD) distribution for all the wells in the reservoir intervals (depths units in meter).

Well 1110617					
Depth	**Kxx**	**Kyy**	**Kzz**	**Porosity**	**NTG**
748.88	651.40	740.13	6.34	0.24	0.38
754.14	2035.92	1923.41	13.81	0.24	0.46
756.24	712.93	2168.49	85.53	0.29	0.56
758.33	2035.92	1923.41	13.81	0.24	0.46
760.42	1077.02	3193.43	103.19	0.28	0.70
761.35	1704.48	1705.43	1750.00	0.30	1.00
763.17	1090.18	3136.71	120.48	0.28	0.70
766.85	2013.20	1903.59	12.33	0.24	0.46
767.47	715.23	2196.94	73.35	0.29	0.56
768.08	2013.20	1903.58	34.12	0.24	0.46
768.70	22.19	22.19	1.27	0.06	0.05
769.60	22.19	22.19	1.27	0.06	0.05
1110717					
Depth	**Kxx**	**Kyy**	**Kzz**	**Porosity**	**NTG**
743.28	21.27	21.30	1.25	0.06	0.21
747.60	1938.02	1202.88	8.35	0.23	0.73
750.49	774.23	2147.89	40.40	0.29	0.92
753.39	1067.35	885.05	6.83	0.18	0.57
756.28	1703.79	1705.92	1722.41	0.30	1.00
757.30	365.63	2431.98	12.27	0.22	0.72
759.37	1703.11	1705.23	1723.00	0.30	1.00
764.52	2017.74	1981.38	20.38	0.26	0.81
764.86	883.06	2097.43	44.51	0.29	0.92
765.20	950.26	470.02	3.90	0.17	0.50
765.54	950.26	470.02	3.90	0.17	0.50
1110817					
Depth	**Kxx**	**Kyy**	**Kzz**	**Porosity**	**NTG**
738.74	2081.04	1988.70	9.79	0.25	0.48
740.09	781.42	2255.17	99.09	0.29	0.56
741.45	2081.04	1988.70	9.79	0.25	0.48
742.81	3381.88	3707.18	6.08	0.20	0.23
746.76	1052.45	3152.99	114.54	0.28	0.70
750.78	2087.30	1995.29	9.66	0.25	0.47
752.12	787.56	2254.96	98.12	0.29	0.56
753.46	2087.29	1995.29	9.66	0.25	0.47
754.79	3371.44	3695.94	6.05	0.20	0.23
756.90	1032.44	3226.96	108.21	0.28	0.70
757.94	2140.65	2124.69	10.93	0.25	0.48
758.29	813.12	2244.49	139.93	0.29	0.56
758.64	2140.65	2124.69	10.93	0.25	0.48
758.99	1706.31	1704.79	1750.00	0.30	1.00
764.24	3379.40	3711.65	6.11	0.20	0.23
765.32	3379.40	3711.65	6.11	0.20	0.23

1210416					
Depth	**Kxx**	**Kyy**	**Kzz**	**Porosity**	**NTG**
733.96	5.00	5.00	5.00	0.07	0.00
760.86	1725.58	2073.19	1.88	0.12	0.13
762.60	245.12	323.11	1.54	0.14	0.21
763.49	871.44	3127.10	74.14	0.28	0.70
764.35	1832.14	1733.37	11.44	0.23	0.43
764.64	783.31	2143.31	51.72	0.29	0.56
764.93	1092.45	1038.33	5.88	0.19	0.35
765.22	246.24	324.60	1.55	0.14	0.21
766.10	5.00	5.00	5.00	0.07	0.00
777.52	1703.82	1705.04	1750.00	0.30	1.00
778.48	1703.82	1705.04	1750.00	0.30	1.00

1210516					
Depth	**Kxx**	**Kyy**	**Kzz**	**Porosity**	**NTG**
747.47	1725.58	2073.19	1.88	0.12	0.13
752.74	1998.87	1899.84	11.84	0.24	0.45
754.49	752.86	2120.11	40.62	0.29	0.55
756.25	1115.92	1070.98	5.54	0.19	0.35
758.00	1005.28	3181.72	95.64	0.28	0.70
758.97	1702.67	1704.23	1750.00	0.30	1.00
761.77	1005.28	3181.72	95.64	0.28	0.70
762.73	1702.67	1704.23	1750.00	0.30	1.00
765.57	3432.64	3767.83	6.33	0.21	0.23
766.48	3432.64	3767.83	6.33	0.21	0.23

1310117					
Depth	**Kxx**	**Kyy**	**Kzz**	**Porosity**	**NTG**
743.80	1725.58	2073.19	1.88	0.14	0.21
748.39	2053.47	1997.04	13.24	0.24	0.46
749.93	668.92	2155.33	64.06	0.29	0.56
751.46	2053.47	1997.04	13.28	0.24	0.46
753.00	1702.83	1706.17	1750.00	0.30	1.00
761.08	921.27	3146.40	86.77	0.28	0.70
762.84	2156.68	2072.51	18.32	0.25	0.48
763.13	603.41	2128.22	66.23	0.29	0.56
763.42	2141.88	2049.41	17.10	0.25	0.47
763.71	21.39	21.39	1.26	0.06	0.05
764.59	21.39	21.39	1.26	0.06	0.05

1310217					
Depth	**Kxx**	**Kyy**	**Kzz**	**Porosity**	**NTG**
743.83	1733.88	2079.90	1.85	0.12	0.13
747.61	239.98	319.09	0.88	0.14	0.21
751.39	1986.76	1923.76	8.23	0.24	0.46
751.87	785.80	2139.22	40.96	0.29	0.56
752.34	991.14	827.39	2.96	0.17	0.31
752.81	1729.34	2076.09	1.83	0.12	0.13
755.59	1966.36	1905.92	7.90	0.24	0.46
756.05	757.96	2135.01	40.37	0.29	0.56
756.51	1005.02	865.29	3.10	0.17	0.32
756.97	21.62	21.62	1.26	0.06	0.05
759.74	1726.11	2068.11	1.83	0.12	0.13
761.14	1966.36	1905.90	7.90	0.24	0.46
761.60	757.96	2135.06	40.38	0.29	0.56
762.06	1005.03	865.29	3.10	0.17	0.32
762.52	236.01	317.23	1.65	0.14	0.21
765.29	236.01	317.23	1.65	0.14	0.21

1410117					
Depth	**Kxx**	**Kyy**	**Kzz**	**Porosity**	**NTG**
742.45	1735.45	2083.09	1.83	0.12	0.13
746.60	2127.46	2078.90	21.79	0.25	0.48
748.00	836.45	2144.20	38.34	0.29	0.55
749.39	1138.68	1116.62	10.02	0.19	0.35
750.79	2127.46	2078.89	21.80	0.25	0.48
752.19	836.38	2144.17	33.65	0.29	0.55
753.59	1138.68	1116.61	10.01	0.19	0.35
754.98	914.85	3154.37	89.99	0.28	0.70
760.51	1703.76	1704.52	1750.00	0.30	1.00
762.77	931.70	3127.58	98.71	0.27	0.69
763.86	2016.01	1977.48	19.07	0.24	0.46
764.23	843.25	2193.70	39.23	0.29	0.55
764.61	1003.54	612.95	5.82	0.17	0.31
764.99	235.48	325.29	1.62	0.14	0.21
766.11	235.48	325.29	1.62	0.14	0.21

1410417.00					
Depth	**Kxx**	**Kyy**	**Kzz**	**Porosity**	**NTG**
768.19	1705.14	1702.76	1750.00	0.30	1.00
781.88	922.08	3128.10	98.71	0.28	0.70
783.48	1705.14	1702.76	1750.00	0.30	1.00
784.28	288.01	2430.30	12.31	0.22	0.53
785.08	2353.09	2334.23	19.60	0.27	0.51
785.35	661.83	2147.47	53.58	0.29	0.55
785.62	1021.16	979.83	3.56	0.17	0.32
785.88	1722.62	2068.23	1.82	0.12	0.13
786.68	1722.62	2068.23	1.82	0.12	0.13

Appendix VII: SBED Input: Analytical data from the core plugs of the offset wells in the table were used in the Facies Templates of SBED for the Reservoir Wells.

Analytical Data (derived from offset wells)

SBED Facies	Vshale %	PHI (Fraction) (Mean)	PHI (Fraction) StDev	PERM (mD) (Mean)	PERM (mD) StDev
Facies A	<20	29.5	3.6	1750.0	353.6
Facies B	20-30	29.6	2.7	5102.5	4454.7
Facies C	30-50	31.1	1.8	3900.0	4242.6
Facies D	50-60	27.8	7.5	1408.3	1431.9
Facies E	60-70	30.0	5.4	5800.0	100.0
Facies F	70-80	22.0	0.1	100.0	10.0
Facies G	>80	5.0	0.1	5.0	0.1
All MUD	100	0.020	0.010	0.100	0.001

Well Key	
	111603801w4
	142903701w4
	Suggested Data

Permeability

B2	B3	B1	C1	C2	A2	A1
Facies A	Facies B	Facies C	Facies D	Facies E	Facies F	Facies G
1500	175	900	3000	5800	Suggest Data	Suggest Data
2000	1000	6900	225		N/A	N/A
	1200		1000			
	1300					
	10000					
	7500					
	10000					
	10000					
	8800					
	1050					

Porosity

B2	B3	B1	C1	C2	A2	A1
Facies A	Facies B	Facies C	Facies D	Facies E	Facies F	Facies G
30.8	27	32	35	33	22	5
25	29	32	33	32	22	5
33	38	31	38	35	22	5
31.8	30	33	22	34		
25	28	31	25	34		
31.4	28	32.9	18	24.1		
	30.7	31	18	32.3		
	31	27	27	25.3		
	26	30.2	34	20		
	26					
	31.5					
	28.9					
	29.7					
	28.2					
	30.2					
	30.8					
	30					
	30					

Previous Facies Templates

B2 -- A -- <20%
B3 -- B -- 20-30%
B1 -- C -- 30-50%
C1 -- D -- 50-60%
C2 -- E -- 60-70%
A2 -- F -- 70-80%
A1 -- G -- >80%

Appendix VIII: Near Wellbore Images of the Individual Wells.

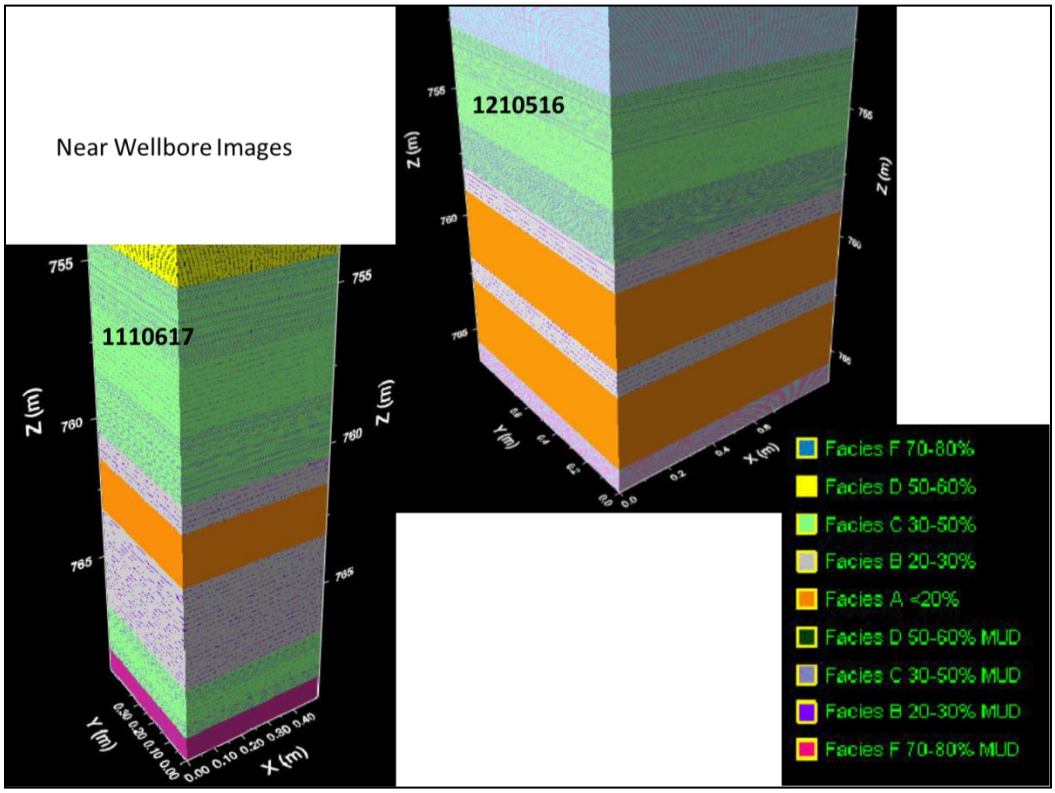

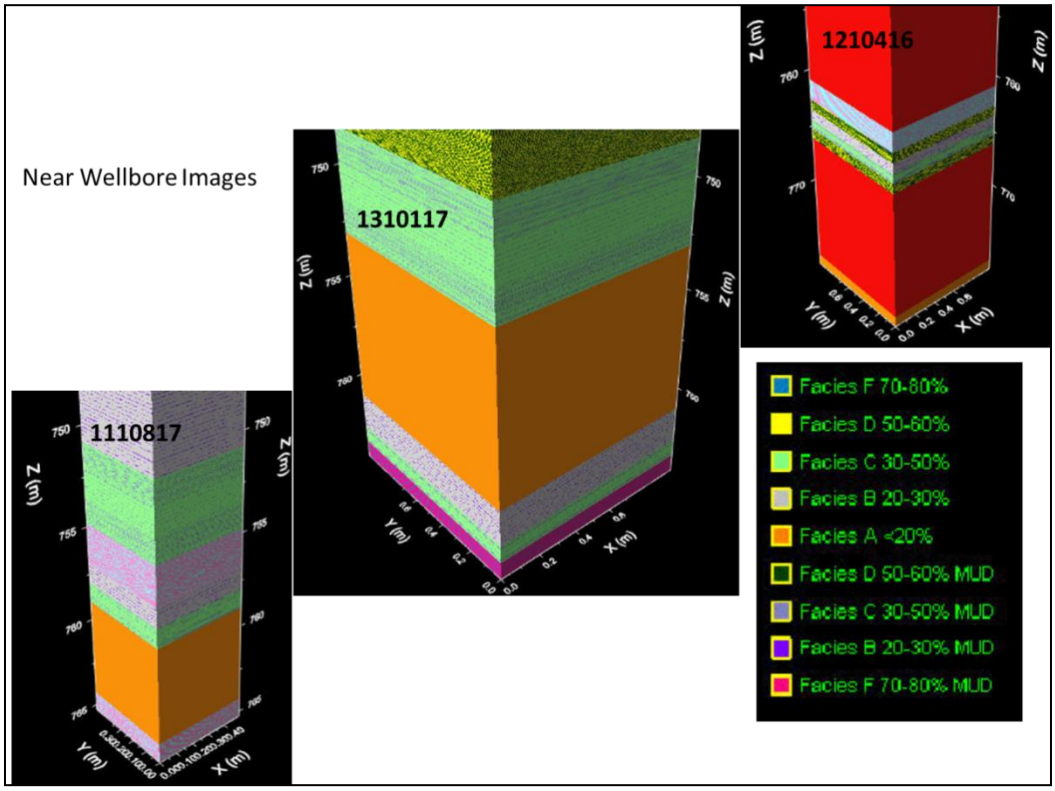

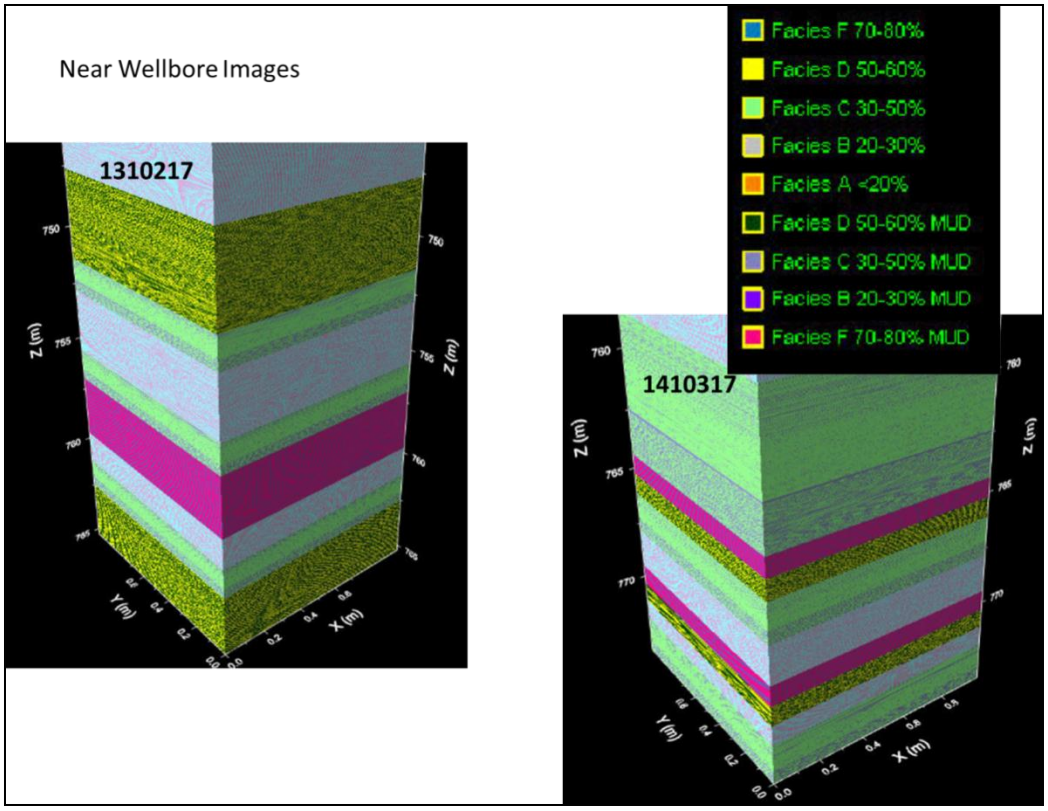
Near Wellbore Images
1310217
1410317
Facies F 70-80%
Facies D 50-60%
Facies C 30-50%
Facies B 20-30%
Facies A <20%
Facies D 50-60% MUD
Facies C 30-50% MUD
Facies B 20-30% MUD
Facies F 70-80% MUD
Z (m)
X (m)
Y (m)

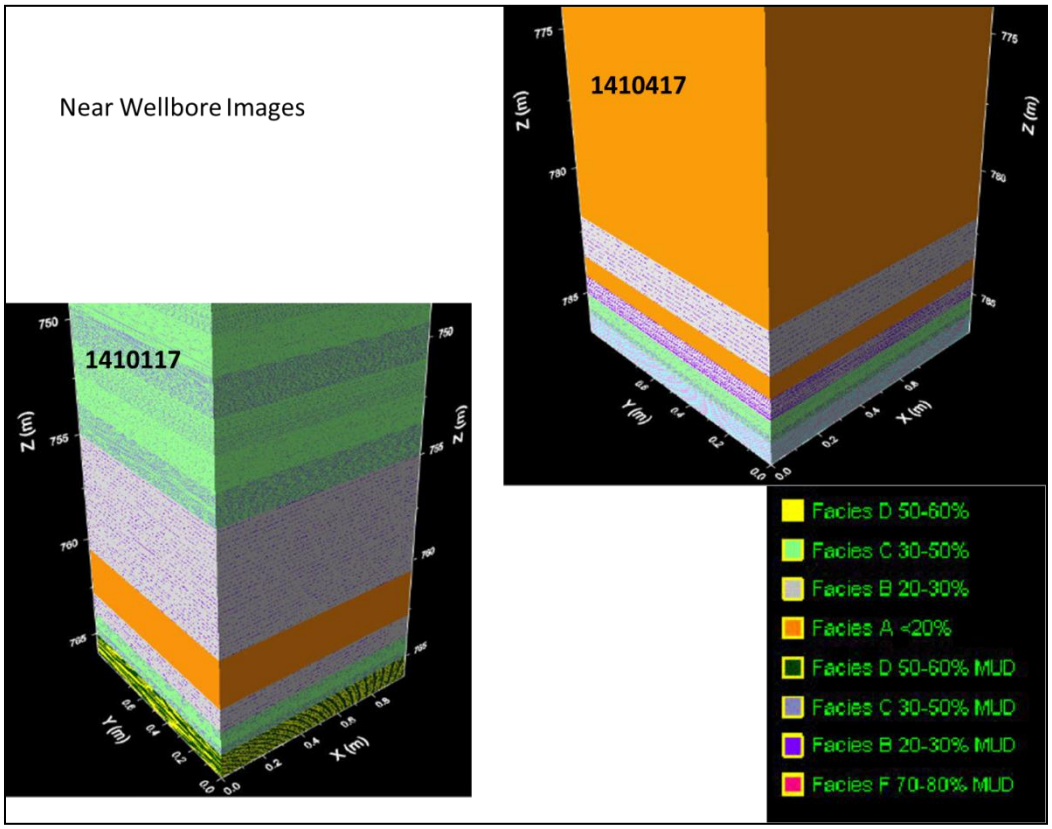
Near Wellbore Images
1410417
1410117
Facies D 50-60%
Facies C 30-50%
Facies B 20-30%
Facies A <20%
Facies D 50-60% MUD
Facies C 30-50% MUD
Facies B 20-30% MUD
Facies F 70-80% MUD
Z (m)
X (m)
Y (m)

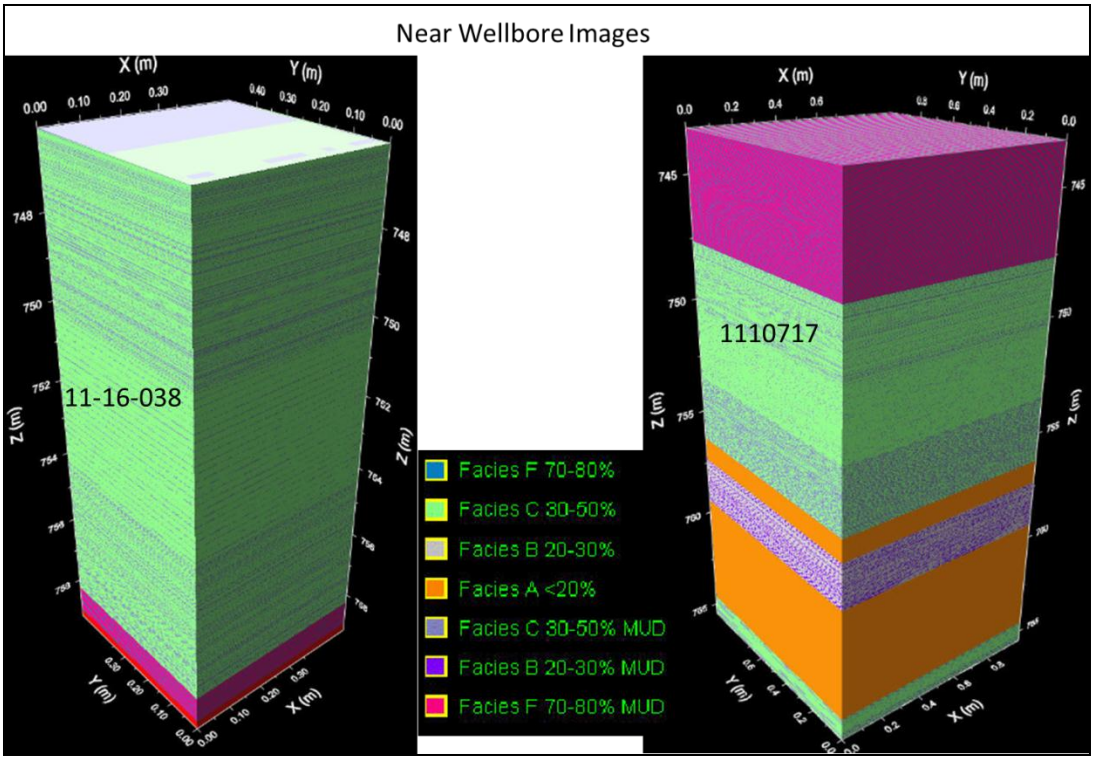
Near Wellbore Images
11-16-038
1110717
Facies F 70-80%
Facies C 30-50%
Facies B 20-30%
Facies A <20%
Facies C 30-50% MUD
Facies B 20-30% MUD
Facies F 70-80% MUD

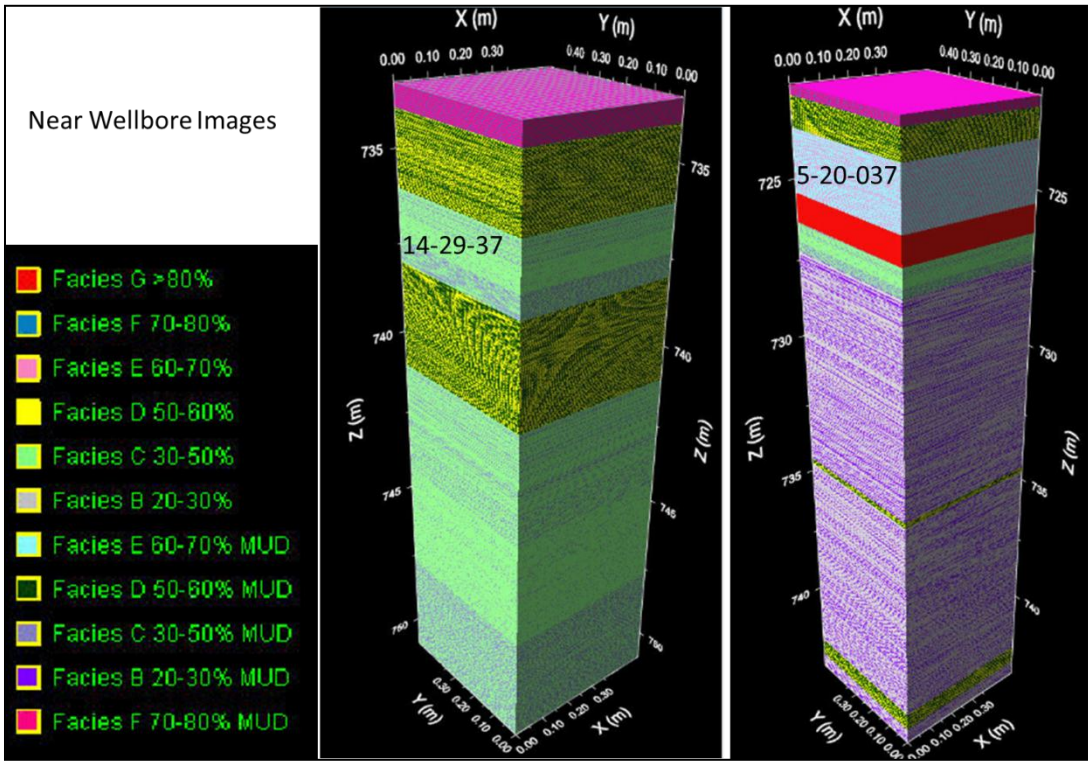
Near Wellbore Images
14-29-37
5-20-037
Facies G >80%
Facies F 70-80%
Facies E 60-70%
Facies D 50-60%
Facies C 30-50%
Facies B 20-30%
Facies E 60-70% MUD
Facies D 50-60% MUD
Facies C 30-50% MUD
Facies B 20-30% MUD
Facies F 70-80% MUD

Appendix IX: The parameters used in the calculation of the Original Oil in Place (OOIP) and Recoverable Oil for the production history matching from the Primate Pool.

Production Evaluation					
			OIL PROSPECT		
	P.90	**P.50**	**P.10**	**Mean**	
AREA	0.01	0.015	0.02	0.02	10*6 sq. metres
PAY	8	10	12	10.00	metres
POROSITY	0.25	0.35	0.4	0.33	decimal value
1-SW	0.8	0.85	0.9	0.85	decimal value
1-SH	0.8	0.9	0.95	0.88	decimal value
SHAPE CORRECTION	0.5	0.8	1	0.77	decimal value
OIL RECOVERY FACTOR	0.065	0.06	0.07	0.07	decimal value
NET:GROSS PAY RATIO	0.40	0.50	0.90	0.60	decimal value
OIL IN PLACE	**0.003**	**0.016**	**0.074**	**0.017**	**10*6 M*3**
	0.016	**0.101**	**0.465**	**0.109**	**10*6 barrels**
RECOVERABLE OIL	**0.000**	**0.001**	**0.005**	**0.001**	**10*6 M*3**
	0.001	**0.006**	**0.032**	**0.007**	**10*6 barrels**
Ref. Red Zed Energy Corp.					
czinkan@shaw.ca					